THREE-DIMENSIONAL PARAMETRIC ANALYSIS OF A TWIN-HULLED, SUBMERGED, FLUID-FILLED STRUCTURE SUBJECTED TO AN EXTERNAL SHOCKWAVE

by

Daniel Pyke

Submitted in partial fulfillment of the requirements
for the degree of Master of Science

at

Dalhousie University
Halifax, Nova Scotia
April 2015

Table of Contents

List of Figures

Abstract

This work takes a three-dimensional approach to examining the problem of an external shockwave interacting with a twin-hulled, submerged, fluid-filled structure. The problem will be examined parametrically by using multiple variables including inner and outer shell thickness, internal fluid composition, external shell composition, and distance between shells. The effect that each variable had on the peak stresses and normal displacements seen within the model were examined independently to provide an overview of the problem for potential design considerations, as well as to highlight the power of the three-dimensional model used. Additionally, to justify the additional computational expense of using a three-dimensional model vs a two-dimensional model, comparisons were done with two-dimensional simulations using the same variables to examine to what degree the two methods diverge.

Acknowledgements

I would like to thank Dr. Serguei Iakovlev for allowing me to be part of this project. It has been a truly amazing experience and has taught me a lot about myself and my strengths. Additional thanks to everyone at the Engineering Mathematics department at Dalhousie University for their guidance and the opportunities they have given me. Finally, I would like to thank everyone who has kept me on task these past couple years, your encouragements have been much appreciated and this wouldn't have been possible without you.

Chapter 1

Introduction

The analysis of interactions between shockwaves and submerged structures is a wide and diverse field that has seen extensive study since the end of World War II. Originating within the field of naval architecture, the work has progressed from simple modal analysis of structures to detailed three-dimensional simulations that can take into account a wide range of different variables. It is, however, still a field with many potential areas of research to be done. The interactions involved are quite complex and as a result there are unresolved issues in just about every branch of research.

The scope of the research has been greatly assisted by new technologies. The earliest studies provided analytic approximations of the systems to allow for easier evaluations, but with advanced computing techniques the research has evolved to be able to analyze a variety of situations; no longer confined to simple structural analysis, the field has evolved to consider everything from acoustics to cavitation to complex hydrodynamic interactions.

The adequacy of the models has similarly improved. The original two-dimensional shells subjected to a plane shock have been expounded upon. The shockwave models have been improved to more accurately simulate real conditions. The interaction models have been improved from simple approximations to much more detailed models that take into account elements such as the diffraction and radiation of the shockwaves. Additionally, the geometries of the systems have become much more complex, evolving from two to three dimensions and adding multiple shells or surface features to more accurately model particular scenarios of interest.

One of the current challenges, and the primary focus of this work, is modeling the full shockwave interactions of a complex shell system in three dimensions. The system in question involves a twin-hulled geometry, where two shells separated by a fluid-filled space are subjected to external shockwaves, which is of particular interest for its application in the design and operation of multi hulled submarines. Understanding

how such a craft responds to shockwaves and how it differs from similar vessels is an important step to ensuring long-term operational viability.

This problem has seen some research in the past, but is still far from being fully understood. The added complexity of the two-shell configuration has meant that it has seen significantly less research than its classical, single shell counterpart, which has been the primary focus in the research to date. Additionally, a full three-dimensional analysis has not yet been performed on such a system, with previous work primarily using a two-dimensional approximation.

1.1 Scope of the Work and Goals

The work herein is a natural progression of that done by Iakovlev[[29]-[38]]. The purpose here is to study the effects of shockwaves on twin-hulled submarines through the use of a three-dimensional mathematical model. The model uses two cylindrical shells in order to represent the submarine. The model was originally utilized to analyze single shell structures[29], but has evolved to take into account more complex geometries [30], up to the point where it has previously been used for two-dimensional analysis of these twin-hulled systems[38]. This work outlines the next step, expanding this previous work into a full three-dimensional study of the twin-hulled system. Two-dimensional approximations have been present within shell-shockwave work since the very beginning. By focusing on a cross section rather than the whole structure, the problem can be greatly reduced in complexity and computational requirements. By removing this simplification, an already complex system, the twin-hulled geometry, becomes even more so. Because of this, it has become important to refer back to what has been learned already in order to direct our investigation and to understand the differences between the current work and the two-dimensional model.

To allow for a detailed comparison between the two and three-dimensional models, this work uses many of the same variables and restrictions used within a previous two-dimensional analysis of the same problem [38]. The study took into account a wide range of variables to demonstrate the capabilities of the model and to analyze how the variables affected the exremeties of the stress-strain state and hydrodynamic field. The first step of the current analysis will be to perform a similar parametric study for the three-dimensional model. The variables used for the three-dimensional parametric

analysis are much the same as those used within the two-dimensional study, with few alterations.

One of the primary variables for the study is the inter-hull clearance, the space between the inner and outer hulls. Previously, a range of values from 10% to 50% of the outer hull radius had been considered. However, from the two-dimensional analysis, it is clear that it is not necessary to model this full range, so instead only the extremes will be analyzed here. Similarly, the previous study also analyzed a wide range of values of shell thicknesses, both of the inner and outer shell. Inner shell thickness varied relative to the radius of the outer shell, and the outer shell thickness varied relative to the thickness of the inner shell. For the three-dimensional study, similar values are used. The inner shell thickness varies between 0.25% and 1% of the radius of the outer shell, and the outer shell thickness varies between 20% and 100% of the inner shell thickness. Finally the study will consider outer shell shell material and the type of fluid in the inter-hull space. Analyses were done using steel and composite materials for the shells, and water and diesel fuel for the internal fluid. This results in three distinct cases for analysis: a steel-water-steel system to act as the baseline, a steel-diesel-steel system to examine the effects of the internal fluid, and a steel-water-composite system to examine the effects of the material used for the outer shell.

In addition to the parametric study, a comparison study will also be included to examine the differences between the two-dimensional and three-dimensional models. Three-dimensional datasets will be matched with the data from their two-dimensional counterparts and direct comparisons made to highlight the variations between the two. The primary focus of this study will be to examine how the stresses and strains vary between the models, and to understand how well the two-dimensional mode approximates the three-dimensional one.

Overall, the three major goals of this work are fairly straightforward. First, the three-dimensional model must be able to execute all of the cases listed above without issue. The results must converge and erroneous values must be kept to a minimum. Second, any notable trends with respect to the different variables should be identified. Not every variable is going to have a major effect on the results, but obvious trends and unexpected results should be made note of. Third, the three-dimensional

results should be compared against the two-dimensional results and how well the two models agree should be noted. Additionally, whether the different variables cause any particular trends in this agreement should be commented on.

1.2 Literature Review

Since the 1950s, the field of shell-shockwave interactions has been continuously evolving. Up until the 1980s, most of the work focused on the structural aspects of the problem and primarily used analytical methods. The shells used were most often evacuated cylinders and a variety of assumptions were used in order to simplify the evaluation process.

In the 1980s, with computational technology evolving, numerical methods became much more practical and analytical methods became less widely used. Complex imaging became possible as well, so experiments were set up to observe the shockwave interactions. Simulating these interactions became much more achievable, and with experiments to compare the results to, such simulations had a reliable means of verification.

Since the 1990s, as numerical methods became even more powerful, the types of problems that were considered became more and more specific. Rather than focus on a general problem, specific applications of shell-shockwave interactions became the norm. These include specific shell configurations, types of hydrodynamic interactions, and, in general, systems that were much more complex than what had been seen previously

1.2.1 Early Period (1950s-1970s)

Early references mention a paper from 1951 written by G. L. Carrier [4] as the first publication to model the shell-shockwave problem in its current form. This report outlined the governing equations of the shell's motion within certain modes. This report, however, did not provide any numerical results, only the governing equations. Following this, in 1953, another report was written on the subject [42], which also included some limited numerical results. However, due to the classified nature of the work it was not mentioned until years later [11].

The first major publication of the problem in its current form was by Mindlin and Bleich in 1953 [46]. The problem outlined involved a shell that was elastic, circular in cross section, homogeneous in material, and infinitely long. The modes of motion allowed were also constrained. The shell was submerged in an acoustic media and the wave was considered to be flat and parallel to the central axis of the shell.

The purpose of the paper was to provide an approximate mathematical solution. The setup allowed the whole problem to be essentially two-dimensional, and the use of a plane wave, which was presented in the form of a step function, further simplified the setup. The equations are developed with major simplifications regarding how the shockwave propagates through the shell over time. Because of this, as stated within the work, the model was only really accurate at the early stages of the interaction, and the closeness of the results to what would be expected fall off greatly over time.

This work was soon revisited by Haywood in 1958 [19]. This new work used much the same setup as Mindlin and Bleich [46] but aimed to address some of the error due to simplifications and allow for a greater range of valid solutions. Haywood's work was focused on providing a practical numerical approximation of the shell deflections, as Carrier's exact solution was deemed far too computationally expensive for practical use. Hence, a number of simplifications were used and compared to a finished result for validation.

As was seen in Mindlin and Bleich's work, the wave was considered to be indefinitely long and parallel to the shell's axis, turning the problem into a two-dimensional one and greatly reducing the complexity of the system [46]. One of Haywood's developments was the use of a wave that was cylindrical in nature. The approximations within the method mostly involved how the shockwave interacts with the shell.

While not exact, the improved model provided valid approximations over a much longer timeframe, with deviations more limited along the full duration of the shell-shockwave interactions. This was unlike Mindlin and Bleich's previous approximations that quickly dropped off in accuracy after the early stages [46]. While not a breakthrough, this new method did provide a means for practical analysis and evaluation. Very much in the spirit of work being done even today, this early work sought to overcome the technological limitations of the time to provide a stepping stone for what would follow.

Work that followed in the early 1960s focused on a variety of different aspects of the shell-shockwave interaction. Bryson and Gross published a study in 1961 in which they photographed shockwave interactions with various shapes, among them solid cylinders [3]. Here the fluid was air and the objects were subjected to shockwaves with mach numbers near 3. While, strictly speaking, not a shell-shockwave interaction, these photos would serve as a helpful tool for researchers in the years to come to make comparisons and validate models.

Peralta and Raynor published a paper in 1963 that focused on the early stage interactions only [52]. The setup was two-dimensional and the shockwave considered to be a plane wave. The inner and outer fluids, however, were one of the areas where changes were made. Multiple cases involving different fluids inside and outside of the shells were considered here. Particular cases included one where both the inner and outer fluids were water, and also one where the inner fluid was gasoline. Different shell response characteristics were also considered. While more limited in scope, this work would mark a departure from a focus wholly on the structural elements of the problem to one where the hydrodynamic response is an important characteristic.

The first of a series of fully analytical solutions was published by Geers in 1969 [11]. The solution used a new approach which was based on the Laplace-Fourier transform technique. The final result of this analysis was an analytical solution in the form of a Fourier Series. The goal of this research was to provide a complete analytic solution for motion in all dimensions. In addition, the work sought to compare this solution to some of the approximate models seen previously. Both Mindlin and Bleichs model [46] and Haywoods model[19] were used for comparison, with Geers findings closely matching those of the original authors within limited timeframes.

Following Geers' publication was one by Huang in 1970, which also used the Laplace-Fourier transform technique to solve the problem [23]. Huang's work took a slightly different approach to the problem, focusing more on presenting the results over longer time periods, rather than focusing on short term interactions. His publication included numerous graphs of the shell-shockwave interactions done over these longer time periods. This highlighted the asymptotic and oscillatory nature of the motion. The results of the work were compared to those of Payton [51] who modeled the early-time response, and refers to the works of Murray [47] and Forrestal [10] who

modeled the exact solutions of the second and first modes of motion, respectively.

At this point, however, both Geers' and Huang's works are still focusing on the two-dimensional model. The major developments were that the new method of solving the problem meant that the approximations were no longer needed to provide solutions. It is also around this time that the more complex three-dimensional loading would begin to be addressed. The beginnings of this came in 1970 when Huang and Wang [24] developed a method similar to the previous, two-dimensional work to solve for a model involving a cylindrical shell subjected to a spherical shockwave, rather than a plane or cylindrical wave. Rather than being completely analytical, it included a numerical procedure to calculate the inverse transforms.

In Huang and Wang's work, the spherical shockwaves were treated as a series of cylindrical waves with infinitely steep wave fronts. However, due to this treatment Gibbs' phenomena was present during the initial interactions, which caused some minor instability at the early stages. In order to correct this issue, the pair would follow this up with another paper in 1971 [25]. Here, only the early time interactions are considered, and the concept of a fictitious Reimann surface was used to overcome the issues caused by the Gibbs phenomena. With this addition, simple expressions for the early time responses were found. These expressions detailed how the curvature of the incoming shockwave affects the bending moments of the shell. Basically, if the source of the shockwave is extremely close to the shell, much higher peak values are seen. This effect decreases as the source is moved farther from the shell.

Up until this point, most of the work had been dedicated to single shelled structures. With the models becoming more complex and considering additional parameters, the issue of more complicated geometry was first considered. Huang's publication in 1979 became the first incidence where multiple shells were considered [27]. As was the case with previous studies, the focus here was primarily on the structural dynamics of the system, and how the addition of an outer shell affected the loading experienced by the inner shell.

In this work, two co-axial shells made of steel were considered, with the outer shell considered to be relatively thin. The motions observed by the inner shell were plotted against a single shell only[23]. In each case the results indicated a slight reduction of the inner shell values. There were similar findings when spherical shells

were examined rather than cylindrical shells[28].

The overall developments of this period focused first on advancing the understanding of the structural elements of the problem and unifying much of the work done thus far. Beyond this, there were also some advances in understanding the hydrodynamics of the system. Up to this point the computational technologies available had been somewhat limited and many simplifications have been used to allow the problems to be solved.

1.2.2 Later Period (1980s-Present)

In the 1980s analysis of shell-shockwave interactions shifted from using primarily analytical methods to using numerical methods.

In 1985 Yang et al. examined the diffraction of strong plane shocks by various curved surfaces, such as cylinders [62], and in 1987 Yang and Liu presented a numerical model to compute the shock wave diffraction on solid cylinders [63]. The model was two-dimensional and used numerical methods to model the Euler's equations of gas dynamics. Using the experimental values, a corresponding simulation was performed and compared to the Bryson and Gross experiment for validation [3]. The agreement between the experiment and the simulation was very good, and captured the important features of the interaction with remarkable accuracy. On a similar note was the work of Glass et al. in 1989 which considered the diffraction of shock waves on a semi-circular cylinder and presented experimental comparisons [18], and the work of Eidelman et al. in 1993, which examined shock wave diffraction of cylinders within dusty flows [9].

With advancing experimental techniques a number of high quality visualizations of shell-shockwave interactions were published. In 1987 a series of such studies appeared, including the work of Takayama, which considered shock wave propagation over a cylinder in a dusty gas flow [59]; Heilig, who addressed aspects of shock wave reflection from a cylinder [21]; and Hermann et al., who studied vortex shedding by a cylinder within a shock flow [22]. In 1989 Sugiyama et al. examined a shock-induced flow past a circular cylinder in a dusty flow, and included numerical results [56], and in 1993 Takayama addressed a shock flow inside and outside a cylinder with a slotted surface [60].

In 1994 an investigation by Geers and Zhang was published that aimed to simplify the modeling of fluid-filled shells [15][16]. In order to do this, equations that approximate how an internal fluid responds to an excited outer fluid were developed. These equations were developed using a technique referred to a doubly asymptotic approximations (DAA), a technique in use since the 1970s to solve similar sorts of problems [12][13][14]. The results were then compared to exact transient response time histories for a fluid-filled submerged spherical shell. The approximations compared favorably, and the simplification deemed well suited for use within numerical investigations to cut down on computation time.

An experimental investigation by Stultz in 1994 examined some different aspects of the twin-hulled geometry [55]. In this experiment, a system consisting of a two-shell arrangement with additional weight rings was used. The model intended to provide a more realistic representation of certain types of industrial systems, and the results were compared with the outcomes of respective numerical simulations. The time-histories of the structural strains and velocities were recorded along with those for the pressure in the inter-shell domain. The work provided insights into the fundamental physics of the shock response of a double-shell configuration. Of specific note was the influence of the outer shell on the structural dynamics of the inner shell.

There also are a considerable number of shock-response studies that, while not directly addressing the double-shell case, are still valuable sources of information about various aspects of the interaction between a shock load and a structurally complex systems. In 1999 Oakley et al. considered the interaction between a shock wave and cylinder placed inside a larger cylindrical confinement [48], and addressed the shock wave reflection patterns occurring in such a system. This was extended by Oakley et al. in 2001 to a system of three cylinders, a more representative model of the reactor system in question [49]. In 1997 Jialing and Hongli considered the reflection on a system of two cylinders of a shock wave propagating in a channel [40], and addressed the shock wave reflection patterns induced during the shock response. The shock interaction with a two-cylinder arrangement was addressed by Heilig in 1999 [20]. Takano et al. examined stresses in elastic cylinders subjected to external shock waves in 1997, and also considered surface-radiated acoustic waves [58]. In 1998 Sun studied shock wave diffraction on bodies of various shapes numerically,

comparing simulations to experimental results [57]. In 1997, Ofengeim and Drikakis [50] and Drikakis et al. [8] numerically examined diffraction of a plane shock wave on a rigid cylinder, considering inviscid and viscous models. Additionally, a system of multiple cylindrical structures placed inside a larger cylindrical confinement filled with fluid was addressed by Sigrist et al. in 2007, with innovations introduced aimed at efficient numerical simulation of such a system [54].

In 2000, Wardlaw and Luton published a study where they consider an explosion inside a double-wall cylinder [61]. This is essentially the 'internal' version of the double-shell problem where the inter-shell clearance is small. They considered both the fluid and structural dynamics of the interaction and particular attention was paid to the effect of shock-induced cavitation, a challenging to model phenomenon. Time-histories of the hydrodynamic pressure and shell surface velocity were presented for the inner and outer shells, highlighting the importance of the shock wave reflection phenomena in both the structural and fluid dynamics of the system. In 1999, Sandusky et al. conducted experiments on fluid-filled aluminum shells subjected to internal explosions, examining plastic deformations, wall velocities, and strain [53]. In 2001 this was expanded as Chamber et al. experimentally examined pressure on the inner surface of a similar shell, presenting comparisons to numerical studies [5].

There have also been a number of studies on the reflection effects in the presence of additional surfaces, structural or otherwise, which have also provided valuable insights into the potential reflection mechanisms: for example, in 2006 Jappinen and Vehvilainen considered an explosion under ice [39], and in 2000 Gitterman and Shapira addressed an explosion in the presence of a free surface [17]. Furthermore, studies where the radiation by elastic structures was addressed are also relevant as they provide the information on the wave structure of the radiated hydrodynamic fields. To that end, in 1998 Ahyi et al. considered the radiation by a single submerged cylindrical shell[1], in 2000 Derbesse et al. [7] and in 2005 Ahyi et al. [2] considered the radiation for more complex shell systems, notably cylindrical shells with spherical endcaps.

In 2002, the first version of our current model for analyzing the shockwave interaction of submerged, fluid-filled shells was published by Iakovlev [29]. It uses a

combined analytical-numerical approach and because of the hybrid nature the respective simulations are relatively computationally inexpensive, and are suitable for carrying out repeated simulations within reasonable timeframes.

Following this there were several additional studies published devoted to the analysis of various aspects of more complex systems. These studies include, in 2004 and 2010, an examination of the shock response of a fluid-filled shell filled containing a rigid co-axial core [30][36], an analysis of the interaction effects of an external shock-wave and a fluid-filled shell in 2006 and 2007 [31][32]. Additional works published in 2008 focus on the acoustic fields induced during the interaction, including comparisons to experimental data [33][34], and another study published in 2009 examines the effects on the fluid-filled shell where the internal and external fluids are not necessarily identical [35]. These studies have served to establish the mathematical framework and to provide information about the shock-structure interaction that will be critical in the context of the double-hull geometry being explored here, this includes the most recent work from 2014 which examines the same problem from a two-dimensional point of view [38].

Chapter 2

Mathematical Formulation

2.1 Initial Setup

The problem, as it is considered here, consists of a circular cylindrical shell of radius r_0 and thickness h_2, with an inner, co-axial shell of radius a and thickness h_1, as shown in Figure 2.1. We assume that the thickness to radius ratios $h_2/r_0 \ll 1$ and $h_1/a \ll 1$; and that the deflections of the shell surfaces are small compared to their thicknesses. Additionally, we assume that the Love-Kirchhoff hypothesis holds true. The density, Poisson's ratio, and Young's modulus are ρ_2, ν_2, and E_2 for the outer shell and ρ_1, ν_1, and E_1 for the inner shell. Additionally, the sound speed in the external and internal shells are c_2 and c_1, respectively. For motion, the longitudinal, transverse, and normal displacements of the middle surface of the shells are u_2, v_2, and w_2 for the external shell and u_1, v_1, and w_1 for the internal shell. The shell is submerged into fluid with the density ρ_e and sound speed c_e which is assumed to be irrotational, inviscid, and linearly compressible. The same assumptions are made for the inter shell fluid, which has density ρ_i and sound speed c_i. The system is subjected to a shock wave with the source located at a distance R from the shell axis. Due to the high frequency nature of these shell shock interactions, it is more convenient to deal with dimensionless variables. As such, all variables are normalized according to r_0, c_e, and ρ_e. The notable exception to normalization is pressure, which is expressed in Pascals. Due to the cylindrical nature of the structure, a polar co-ordinate system (ϱ, θ) is employed.

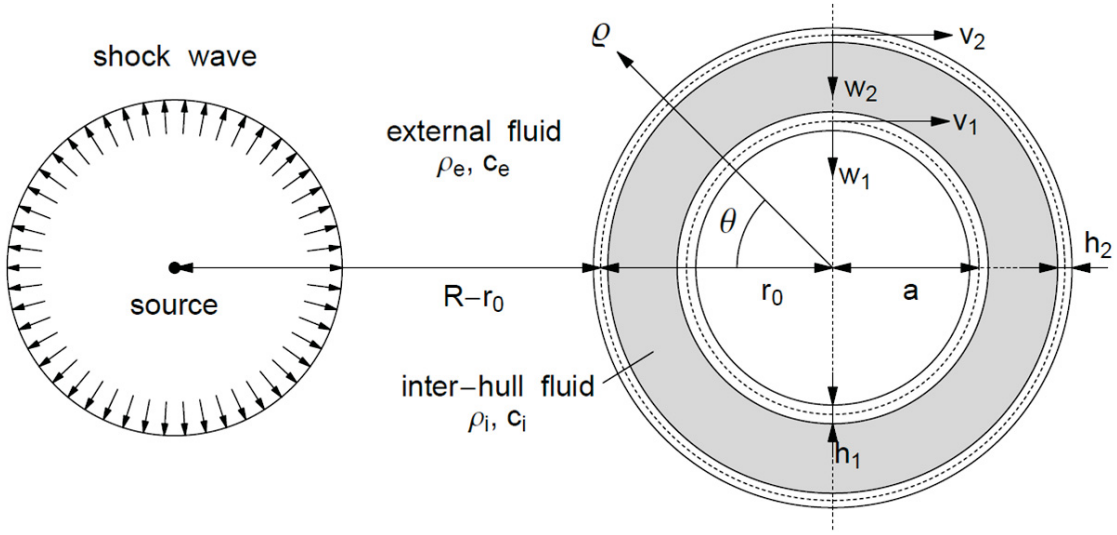

Figure 2.1: Diagram of the double-shell problem

The fluids are governed by the wave equations,

$$\nabla^2\phi_e = \frac{\partial^2\phi_e}{\partial t^2}, \tag{2.1}$$

and

$$\nabla^2\phi_i = \frac{c_e^2}{c_i^2}\frac{\partial^2\phi_i}{\partial t^2}, \tag{2.2}$$

where ϕ_e and ϕ_i are the fluid velocity potentials of the external and internal fluids, and t is time.

The hydrodynamic pressures of the external and internal fluids, p_e and p_i are

$$p_e = -\frac{\partial\phi_e}{\partial t}, \quad \text{and} \quad p_i = -\frac{\rho_i}{\rho_e}\frac{\partial\phi_i}{\partial t}. \tag{2.3}$$

The strain energy per unit area of the external shell E_2^p and the internal shell E_1^p are given by Love in 1927 [43]

$$E_2^p = \frac{E_2 h_2}{2(1-(\nu_2)^2)}\Big\{(\varepsilon_2^1)^2 + (\varepsilon_2^2)^2 + 2\nu_2\varepsilon_1^2\varepsilon_2^2 + \frac{1}{2}(1-\nu_2)(\Omega_2)^2 + (k_2)^2((\kappa_1^2)^2 + (\kappa_2^2)^2 + 2\nu\kappa_2^1\kappa_2^2 + 2(1-\nu_2)(\tau_2)^2)\Big\} \tag{2.4}$$

$$E_1^p = \frac{E_1 h_1}{2(1-(\nu_1)^2)}\Big\{(\varepsilon_1^1)^2 + (\varepsilon_1^2)^2 + 2\nu_1\varepsilon_1^1\varepsilon_1^2 + \frac{1}{2}(1-\nu_1)(\Omega_1)^2 + (k_1)^2((\kappa_1^1)^2 + (\kappa_1^2)^2 + 2\nu\kappa_1^1\kappa_1^2 + 2(1-\nu_1)(\tau_1)^2)\Big\} \tag{2.5}$$

where

$$\varepsilon_2^1 = \frac{\partial u_2}{\partial x}, \qquad \varepsilon_2^2 = \frac{1}{r_0}\left(\frac{\partial v_2}{\partial \theta} - w_2\right), \qquad \Omega_2 = \frac{\partial v_2}{\partial x} + \frac{1}{r_0}\frac{\partial u_2}{\partial \theta},$$
$$\kappa_2^1 = \frac{\partial^2 w_2}{\partial x^2}, \qquad \kappa_2^2 = \frac{1}{(r_0)^2}\left(\frac{\partial^2 w_2}{\partial \theta^2} + \frac{\partial v_2}{\partial \theta}\right), \quad \tau_2 = \frac{1}{r_0}\left(\frac{\partial^2 w_2}{\partial \theta \partial x} + \frac{\partial v_2}{\partial x}\right), \tag{2.6}$$

and $(k_2)^2 = (h_2)^2/12$ for the outer shell and

$$\varepsilon_1^1 = \frac{\partial u_1}{\partial x}, \qquad \varepsilon_1^2 = \frac{1}{a}\left(\frac{\partial v_1}{\partial \theta} - w_1\right), \qquad \Omega_1 = \frac{\partial v_1}{\partial x} + \frac{1}{a}\frac{\partial u_1}{\partial \theta},$$
$$\kappa_1^1 = \frac{\partial^2 w_1}{\partial x^2}, \qquad \kappa_1^2 = \frac{1}{a^2}\left(\frac{\partial^2 w_1}{\partial \theta^2} + \frac{\partial v_1}{\partial \theta}\right), \qquad \tau_1 = \frac{1}{a}\left(\frac{\partial^2 w_1}{\partial \theta \partial x} + \frac{\partial v_1}{\partial x}\right), \tag{2.7}$$

and $(k_1)^2 = (h_1)^2/12$ for inner shell. As an additional note, here we consider an inward normal for the 'elastic' part of the problem, so some of the signs differ from those within Love's work.

Equations (2.4) and (2.5), with the expressions for the kinetic energy per unit area of the shell E_2^k and E_1^k,

$$E_2^k = \frac{1}{2}\rho_2 h_2 \left\{\left(\frac{\partial u_2}{\partial t}\right)^2 + \left(\frac{\partial v_2}{\partial t}\right)^2 + \left(\frac{\partial w_2}{\partial t}\right)^2\right\}, \tag{2.8}$$

$$E_1^k = \frac{1}{2}\rho_1 h_1 \left\{\left(\frac{\partial u_1}{\partial t}\right)^2 + \left(\frac{\partial v_1}{\partial t}\right)^2 + \left(\frac{\partial w_1}{\partial t}\right)^2\right\} \tag{2.9}$$

are used to derive the equations of shell dynamics using Hamilton's principle.

The pressure loads on each of the shells, p_2 and p_1, can be expressed as a sum of the incident pressure, p_0, diffraction pressure, p_d, external radiation pressure, p_r^e and internal radiation pressures from each shell, $p_r^{i,1}$ and $p_r^{i,2}$,

$$p_1 = p_r^{i,2} - p_r^{i,1}, \tag{2.10}$$

$$p_2 = p_0 + p_d + p_r^e + p_r^{i,2} - p_r^{i,1}. \tag{2.11}$$

The total fluid potential is expressed similarly

$$\phi_e = \phi_0 + \phi_d + \phi_r^e + \phi_r^i, \tag{2.12}$$

$$\phi_i = \phi_r^i, \tag{2.13}$$

where ϕ_0 is the incident shock wave potential, ϕ_d is the diffracted wave potential, ϕ_r^e is the external radiated potential and ϕ_r^i is the internal radiated potentials. The individual surface pressure components are therefore

$$p_0 = -\frac{\partial \phi_0}{\partial t}\bigg|_{r=r_0}, \quad p_d = -\frac{\partial \phi_d}{\partial t}\bigg|_{r=r_0}, \quad p_r^e = -\frac{\partial \phi_r^e}{\partial t}\bigg|_{r=r_0}, \tag{2.14}$$

and

$$p_r^{i,2} = -\frac{\rho_i}{\rho_e}\frac{\partial \phi_r^i}{\partial t}\bigg|_{r=r_0}, \tag{2.15}$$

for the external shell and

$$p_r^{i,1} = -\frac{\rho_i}{\rho_e}\frac{\partial \phi_r^i}{\partial t}\bigg|_{r=a/r_0}, \tag{2.16}$$

for the internal shell.

The fluid velocity potential of the spherical, step-exponential shock wave acting on the external shell is expressed as [31]

$$\phi_0 = -\frac{\lambda p_\alpha S_R}{\rho_e R^*}\left\{e^{-(t-(R^*-S_R)c_e^{-1})\lambda^{-1}} - 1\right\} H\left(t - (R^* - S_R)c_e^{-1}\right) \tag{2.17}$$

where λ is the decay constant, p_α is the pressure in the front of the shock wave when it first makes contact with the shell, $S_R = R_0 - r_2$, the stand-off distance between the shockwave origin and the outer shell, $R^* = \sqrt{R_0^2 + x^2 + r^2 - 2R_0 r\cos\theta}$, the distance between the source and the point (x, r, θ) in the cylindrical coordinates, τ is dimensionless time, and finally $H(z)$ is the Heaviside unit step function

$$H(z) = \begin{cases} 1, & z \geq 0, \\ 0, & z < 0. \end{cases} \tag{2.18}$$

Here it is assumed that $\tau = (t - (R^* - S_R)c_e^{-1}) = 0$ is the moment the wave front makes contact with the outer shell. The parameters λ and p_α vary depending on R_0 and a few other factors as described by Cole in 1948 [6].

Finally, the boundary and initial conditions are stated, which completes the setup of the problem. The shell dynamics is coupled to the fluid dynamics through the boundary conditions on the shell surfaces

$$\frac{\partial \phi_r^e}{\partial r}\bigg|_{r=r_0} = -\frac{\partial w_2}{\partial t} \quad \text{and} \quad \frac{\partial \phi_r^i}{\partial r}\bigg|_{r=r_0} = -\frac{\partial w_2}{\partial t}, \tag{2.19}$$

and

$$\frac{\partial \phi_r^i}{\partial r}\bigg|_{r=a/r_0} = -\frac{\partial w_1}{\partial t}. \tag{2.20}$$

For the diffraction pressure

$$\left.\frac{\partial \phi_d}{\partial r}\right|_{r=r_0} = \left.\frac{\partial \phi_0}{\partial r}\right|_{r=r_0}, \tag{2.21}$$

and also

$$(\phi_d + \phi_r^e) \longrightarrow 0 \quad \text{when} \quad r \to \infty \tag{2.22}$$

In order to formulate the boundary conditions with respect to x, we make use of the fact that hydrodynamic waves in the fluids and elastic waves in the shell have a finite velocity of propagation. Therefore we introduce a large parameter L and state the boundary conditions at $x = \pm L$ for the displacements as

$$\left.\frac{\partial u_2}{\partial x}\right|_{x=\pm L} = 0, \quad v_2|_{x=\pm L} = 0, \quad w_2|_{x=\pm L} = 0, \quad \left.\frac{\partial^2 w_2}{\partial x^2}\right|_{x=\pm L} = 0, \tag{2.23}$$

and

$$\left.\frac{\partial u_1}{\partial x}\right|_{x=\pm L} = 0, \quad v_1|_{x=\pm L} = 0, \quad w_1|_{x=\pm L} = 0, \quad \left.\frac{\partial^2 w_1}{\partial x^2}\right|_{x=\pm L} = 0, \tag{2.24}$$

as well as zero boundary conditions for all potential components. We assume that the displacements and potentials are periodic with respect to θ, and we also assume zero initial conditions.

2.2 Fluid dynamics

In order to obtain the hydrodynamic components, we first apply the Laplace transform with respect to the time to the wave equations (2.1) and (2.2) to arrive at

$$\frac{\partial^2\Phi_e}{\partial r^2}+\frac{1}{r}\frac{\partial\Phi_e}{\partial r}+\frac{\partial^2\Phi_e}{\partial x^2}+\frac{1}{r^2}\frac{\partial^2\Phi_e}{\partial\theta^2}-s^2\Phi_e=0, \tag{2.25}$$

and

$$\frac{\partial^2\Phi_i}{\partial r^2}+\frac{1}{r}\frac{\partial\Phi_i}{\partial r}+\frac{\partial^2\Phi_i}{\partial x^2}+\frac{1}{r^2}\frac{\partial^2\Phi_i}{\partial\theta^2}-\frac{s^2c_e^2}{c_i^2}\Phi_i=0, \tag{2.26}$$

where Φ_e and Φ_i are the Laplace transforms of ϕ_e and ϕ_i where s is the transform variable.

Then, we separate the spatial variables in order to obtain the general solutions of (2.25) and (2.26) satisfying the zero condition for r at infinity as

$$\Phi^e_{mn}=D_{mn}\mathrm{K}_n(r\beta_m(s))\cos(\tilde{m}x)\cos(n\theta) \tag{2.27}$$

and

$$\Phi^i_{mn}=\left\{F_{mn}\mathrm{I}_n(r\beta_m(sc_ec_i^{-1}))+G_{mn}\mathrm{K}_n(r\beta_m(sc_ec_i^{-1}))\right\}\cos(\tilde{m}x)\cos(n\theta). \tag{2.28}$$

Within these series $m=0,1,\ldots$, $n=0,1,\ldots$, $\tilde{m}=(2m+1)\pi(2L)^{-1}$, $\beta_m(s)=\sqrt{\tilde{m}^2+s^2}$, I_n and K_n are the modified Bessel functions of the first and second kind of order n, and D_{mn}, F_{mn}, and G_{mn} are arbitrary functions of s.

We must determine the coefficients D_{mn}, F_{mn}, and G_{mn}. This is done through a process of expanding our terms into double series. First we expand our w_2, w_1, p_0, and $\left.\frac{\partial\phi_0}{\partial r}\right|_{r=r_0}$ terms into series form

$$w_2=\sum_{m=0}^{\infty}\sum_{n=0}^{\infty}w_{mn,2}(t)\cos(\tilde{m}x)\cos(n\theta), \tag{2.29}$$

$$w_1=\sum_{m=0}^{\infty}\sum_{n=0}^{\infty}w_{mn,1}(t)\cos(\tilde{m}x)\cos(n\theta), \tag{2.30}$$

$$p_0=\sum_{m=0}^{\infty}\sum_{n=0}^{\infty}p^0_{mn}(t)\cos(\tilde{m}x)\cos(n\theta), \tag{2.31}$$

$$\left.\frac{\partial\phi_0}{\partial r}\right|_{r=r_0}=\sum_{m=0}^{\infty}\sum_{n=0}^{\infty}b_{mn}(t)\cos(\tilde{m}x)\cos(n\theta), \tag{2.32}$$

respectively. By imposing the boundary conditions, we obtain the Laplace transforms of the harmonics of the unknown potential components as

$$\Phi^d_{mn} = B_{mn}(s)\Xi^e_{mn}(s)\cos(\tilde{m}x)\cos(n\theta), \tag{2.33}$$

$$\Phi^{r,e}_{mn} = sW^2_{mn}(s)\Xi^e_{mn}(s)\cos(\tilde{m}x)\cos(n\theta), \tag{2.34}$$

$$\Phi^{r,i,2}_{mn} = -sW^2_{mn}(s)\Xi^{i,2}_{mn}(sc_ec_i^{-1})\cos(\tilde{m}x)\cos(n\theta) \tag{2.35}$$

and

$$\Phi^{r,i,1}_{mn} = -sW^1_{mn}(s)\Xi^{i,1}_{mn}(sc_ec_i^{-1})\cos(\tilde{m}x)\cos(n\theta) \tag{2.36}$$

where B_{mn}, W^2_{mn}, and W^1_{mn} are the Laplace transforms of b_{mn}, $w_{mn,2}$, and $w_{mn,1}$; and Ξ^e_{mn}, $\Xi^{i,2}_{mn}$, and $\Xi^{i,1}_{mn}$ are the Laplace transforms of the response functions of the problem, the response functions defined as

$$\xi^e_{mn} = \xi^e_n(t) - \tilde{m}\int_0^t \xi^e_n(\sqrt{t^2-\tau^2})J_1(\tilde{m}\tau)\partial\tau \tag{2.37}$$

$$\xi^{i,2}_{mn} = \xi^{i,2}_n(t) - \tilde{m}\int_0^t \xi^{i,2}_n(\sqrt{t^2-\tau^2})J_1(\tilde{m}\tau)\partial\tau \tag{2.38}$$

$$\xi^{i,1}_{mn} = \xi^{i,1}_n(t) - \tilde{m}\int_0^t \xi^{i,1}_n(\sqrt{t^2-\tau^2})J_1(\tilde{m}\tau)\partial\tau \tag{2.39}$$

where ξ^e_n, $\xi^{i,2}_n$, and $\xi^{i,1}_n$ are the corresponding two-dimensional functions [38].

These response functions represent the response of the fluid to the motion of the shell surface and/or the scattering by the shell [31][34]. They are useful from a computational standpoint because after being computed to the necessary accuracy once, the calculations can be re-used for any shell of the same geometry. As these response functions represent a large portion of the computations within this problem, pre-computing them allows for a wide variety of parameters to be analyzed without adding undue computation time[34].

With the response functions and applying certain theorems related to the Laplace transforms, we can fully develop the components of the pressure on the shells. These components are

$$p_d = \sum_{m=0}^{\infty}\sum_{n=0}^{\infty} p^d_{mn}(t)\cos(\tilde{m}x)\cos(n\theta), \tag{2.40}$$

$$p^e_r = \sum_{m=0}^{\infty}\sum_{n=0}^{\infty} p^e_{mn}(t)\cos(\tilde{m}x)\cos(n\theta), \tag{2.41}$$

$$p_r^{i,2} = \sum_{m=0}^{\infty}\sum_{n=0}^{\infty} p_{mn}^{i,2}(t)\cos(\tilde{m}x)\cos(n\theta), \tag{2.42}$$

and

$$p_r^{i,1} = \sum_{m=0}^{\infty}\sum_{n=0}^{\infty} p_{mn}^{i,1}(t)\cos(\tilde{m}x)\cos(n\theta), \tag{2.43}$$

where

$$p_{mn}^{d}(t) = -b_{mn}(t) - \int_0^t b_{mn}(\tau)\dot{\xi}_{mn}^{e}(t-\tau)\partial\tau, \tag{2.44}$$

$$p_{mn}^{e}(t) = -\int_0^t \ddot{w}_{mn}^{2}(t)\xi_{mn}^{e}(t-\tau)\partial\tau, \tag{2.45}$$

$$p_{mn}^{i,2}(t) = \frac{\rho_i c_i}{\rho_e c_e}\int_0^t \ddot{w}_{mn}^{2}(\tau)\xi_{mn}^{i,2}(c_i c_e^{-1}(t-\tau))\partial\tau. \tag{2.46}$$

and

$$p_{mn}^{i,1}(t) = \frac{\rho_i c_i}{\rho_e c_e}\int_0^t \ddot{w}_{mn}^{1}(\tau)\xi_{mn}^{i,1}(c_i c_e^{-1}(t-\tau))\partial\tau. \tag{2.47}$$

The total pressure on the surface of the shells is therefore given in series form by

$$p_1 = \sum_{m=0}^{\infty}\sum_{n=0}^{\infty} p_{mn,1}(t)\cos(\tilde{m}x)\cos(n\theta), \tag{2.48}$$

$$p_2 = \sum_{m=0}^{\infty}\sum_{n=0}^{\infty} p_{mn,2}(t)\cos(\tilde{m}x)\cos(n\theta), \tag{2.49}$$

where, for the inner and outer shells

$$p_{mn,1} = (p_{mn}^{i,2} - p_{mn}^{i,1})\Big|_{r=a/r_0}, \tag{2.50}$$

and

$$p_{mn,2} = (p_{mn}^{0} + p_{mn}^{d} + p_{mn}^{e} + p_{mn}^{i,2} - p_{mn}^{i,1})\Big|_{r=r_0}. \tag{2.51}$$

2.3 Structural dynamics

With the loading on the shells known, the process for computing the stress strain states on both the inner and outer shells is very similar. The components u, v, and w are expanded into series form for each shell

$$u_1 = \sum_{m=0}^{\infty}\sum_{n=0}^{\infty} u_{mn,1}(t)\cos(\tilde{m}x)\cos(n\theta), \tag{2.52}$$

$$v_1 = \sum_{m=0}^{\infty}\sum_{n=0}^{\infty} v_{mn,1}(t)\cos(\tilde{m}x)\cos(n\theta), \tag{2.53}$$

$$w_1 = \sum_{m=0}^{\infty}\sum_{n=0}^{\infty} w_{mn,1}(t)\cos(\tilde{m}x)\cos(n\theta), \tag{2.54}$$

and

$$u_2 = \sum_{m=0}^{\infty}\sum_{n=0}^{\infty} u_{mn,2}(t)\cos(\tilde{m}x)\cos(n\theta), \tag{2.55}$$

$$v_2 = \sum_{m=0}^{\infty}\sum_{n=0}^{\infty} v_{mn,2}(t)\cos(\tilde{m}x)\cos(n\theta), \tag{2.56}$$

$$w_2 = \sum_{m=0}^{\infty}\sum_{n=0}^{\infty} w_{mn,2}(t)\cos(\tilde{m}x)\cos(n\theta), \tag{2.57}$$

We can now express the strain and kinetic energy in terms of these harmonics of the displacements. Integrating them over the shell surface and applying Hamilton's principle result in the following system of integro-differential equations for each combination of m and n. The mn subscripts have been removed from each c, u, v, w, and p term for ease of presentation:

$$\begin{aligned}
&(\gamma_1)^2\frac{\partial^2 u_1}{\partial t^2} + c_1^{11}u_1 + c_1^{12}v_1 + c_1^{13}w_1 = 0,\\
&(\gamma_1)^2\frac{\partial^2 v_1}{\partial t^2} + c_1^{21}u_1 + c_1^{22}v_1 + c_1^{23}w_1 = 0,\\
&(\gamma_1)^2\frac{\partial^2 w_1}{\partial t^2} + c_1^{31}u_1 + c_1^{32}v_1 + c_1^{33}w_1 = \chi_1 p_1,
\end{aligned} \tag{2.58}$$

and

$$\begin{aligned}
&(\gamma_2)^2\frac{\partial^2 u_2}{\partial t^2} + c_2^{11}u_2 + c_2^{12}v_2 + c_2^{13}w_2 = 0,\\
&(\gamma_2)^2\frac{\partial^2 v_2}{\partial t^2} + c_2^{21}u_2 + c_2^{22}v_2 + c_2^{23}w_2 = 0,\\
&(\gamma_2)^2\frac{\partial^2 w_2}{\partial t^2} + c_2^{31}u_2 + c_2^{32}v_2 + c_2^{33}w_2 = \chi_2 p_2,
\end{aligned} \tag{2.59}$$

where

$$
\begin{aligned}
c_1^{11} &= \frac{1-\nu_1}{2}n^2 + \tilde{m}^2, \\
c_1^{12} &= c_1^{21} = \frac{1+\nu_1}{2}\tilde{m}n, \\
c_1^{13} &= c_2^{31} = -\nu_1\tilde{m}, \\
c_1^{22} &= \frac{1-\nu_1}{2}\tilde{m}^2 + n^2 + (k_1)^2(n^2 + (1-\nu_1)\tilde{m}^2), \\
c_1^{23} &= c_1^{32} = -n - (k_1)^2(n^3 + n\tilde{m}^2), \\
c_1^{33} &= 1 + (k_1)^2(\tilde{m}^2 + n^2)^2,
\end{aligned} \tag{2.60}
$$

and

$$
\begin{aligned}
c_2^{11} &= \frac{1-\nu_2}{2}n^2 + \tilde{m}^2, \\
c_2^{12} &= c_2^{21} = \frac{1+\nu_2}{2}\tilde{m}n, \\
c_2^{13} &= c_2^{31} = -\nu_2\tilde{m}, \\
c_2^{22} &= \frac{1-\nu_2}{2}\tilde{m}^2 + n^2 + (k_2)^2(n^2 + (1-\nu_2)\tilde{m}^2), \\
c_2^{23} &= c_2^{32} = -n - (k_2)^2(n^3 + n\tilde{m}^2), \\
c_2^{33} &= 1 + (k_2)^2(\tilde{m}^2 + n^2)^2,
\end{aligned} \tag{2.61}
$$

and additionally $\gamma_1 = (c_{s,1})^{-1}$, $\gamma_2 = (c_{s,2})^{-1}$, $\chi_1 = (\rho_{s,1}(c_{s,1})^2 h_1)^{-1}$, $\chi_2 = (\rho_{s,2}(c_{s,2})^2 h_2)^{-1}$ and all initial conditions are zero.

The system (2.59) is then solved numerically using finite differences. The derivatives are approximated using the central difference theorem, and the integrals using the trapezoidal rule. Removing the mn subscripts from each term allows for the external shell finite difference scheme for the inner shell to be expressed as

$$
\begin{aligned}
u_1^{i+1} &= 2u_1^i - u_1^{i-1} - \frac{h^2}{(\gamma_1)^2}\{c_1^{11}u_1^i + c_1^{12}v_1^i + c_1^{13}w_1^i\}, \\
v_1^{i+1} &= 2v_1^i - v_1^{i-1} - \frac{h^2}{(\gamma_1)^2}\{c_1^{21}u_1^i + c_1^{22}v_1^i + c_1^{23}w_1^i\}, \\
w_1^{i+1} &= 2w_1^i - w_1^{i-1} - \frac{h^2}{(\gamma_1)^2 + \chi_1\gamma_0 h}\{(c_1^{31}u_1^i + c_1^{32}v_1^i + c_1^{33}w_1^i + \chi_1\gamma_0(J_{1a}^i - J_{2a}^i)\},
\end{aligned} \tag{2.62}
$$

where h is the time step.

With the same conventions the outer shell can is expressed as

$$
\begin{aligned}
u_2^{i+1} &= 2u_2^i - u_2^{i-1} - \frac{h^2}{(\gamma_2)^2}\{c_2^{11}u_2^i + c_2^{12}v_2^i + c_2^{13}w_2^i\},\\
v_2^{i+1} &= 2v_2^i - v_2^{i-1} - \frac{h^2}{(\gamma_2)^2}\{c_2^{21}u_2^i + c_2^{22}v_2^i + c_2^{23}w_2^i\},\\
w_2^{i+1} &= 2w_2^i - w_2^{i-1} - \Omega_h\{(c_2^{31}u_2^i + c_2^{32}v_2^i + c_2^{33}w_2^i + \chi_2(-p_0^i + J_e^i - \gamma_0(J_{11}^i - J_{21}^i))\},
\end{aligned}
\tag{2.63}
$$

where $\Omega_h = \frac{2h^2}{2(\gamma_2)^2 + h\chi_2}$. The J terms are summations, defined as

$$J_{1a}^i = \sum_{j=1}^{i-1}\{w_1^{j+1} - 2w_1^j + w_1^{j-1}\}\, h^{-1}\, \xi_{1a}^{i-j}, \tag{2.64}$$

$$J_{2a}^i = \sum_{j=1}^{i-1}\{w_2^{j+1} - 2w_2^j + w_2^{j-1}\}\, h^{-1}\, \xi_{2a}^{i-j}, \tag{2.65}$$

$$J_{11}^i = \sum_{j=1}^{i-1}\{w_1^{j+1} - 2w_1^j + w_1^{j-1}\}\, h^{-1}\, \xi_{11}^{i-j}, \tag{2.66}$$

$$J_{21}^i = \sum_{j=1}^{i-1}\{w_2^{j+1} - 2w_2^j + w_2^{j-1}\}\, h^{-1}\, \xi_{21}^{i-j}, \tag{2.67}$$

$$J_e^i = \sum_{j=1}^{i-1}\{w_2^{j+1} - 2w_2^j + w_2^{j-1}\}\, h^{-1}\, \xi_e^{i-j}, \tag{2.68}$$

where u_1^i, v_1^i, w_1^i, u_2^i, v_2^i, w_2^i, ξ_{1a}^i, ξ_{2a}^i, ξ_{11}^i, ξ_{21}^i, and ξ_e^i, are the nodal values of $u_{mn,1}(t)$, $v_{mn,1}(t)$, $w_{mn,1}(t)$, $u_{mn,2}(t)$, $v_{mn,2}(t)$, $w_{mn,2}(t)$, $\xi_n^{i,1}(c_i c_e^{-1}t)|_{r=r_0}$, $\xi_n^{i,2}(c_i c_e^{-1}t)|_{r=r_0}$, $\xi_n^{i,1}(c_i c_e^{-1}t)|_{r=a/r_0}$, $\xi_n^{i,2}(c_i c_e^{-1}t)|_{r=a/r_0}$, and $\xi_n^e(t)|_{r=r_0}$.

The convergence of the scheme was analyzed and it was established that the step size of $h = 0.001$ is sufficient to ensure convergence in all cases of interest.

Chapter 3

Results and Shell Thickness Analysis

3.1 Overview

To analyze the effects of the different variables of the system, a parametric approach was used. This approach involved two major geometries of the problem, a model with a relatively small inter-hull space, and a model with a much larger inter-hull space. For each model, three different material configurations were considered. These different cases included a baseline steel inner and outer shell setup with water as the inter-hull fluid, one with the water replaced by diesel fuel, and one where a composite material was used for the outer shell. The simulations are named according to this shell and fluid configuration: steel-water-steel, steel-diesel-steel, and steel-water-composite.

For each of these configurations, multiple simulations are carried out to test the effect of the inner and outer shell thicknesses. There are six thickness values used for the inner shell and a further six values used for the outer shell for a total of 36 thickness combinations. The values of interest are then extracted from each dataset, most notably the location, timing, and value of the stress and strain experienced during the simulations. From these, three-dimensional plots are generated that show the extreme values for each thicknesses of the inner and outer shells.

The mathematical model used requires the input of material properties of the shell and shockwave. For the purposes of this analysis the shockwave is defined as follows. Its origin is fixed at 4 radii from the shell, with variables corresponding to a 50kg charge of TNT. The properties of the external fluid will remain constant and correspond to water.

For the purposes of this parametric study two different geometries will be used, a large and small inner shell radius. This is handled with the variable, a, which expresses radius of the inner shell normalized to the radius of the outer shell, which itself is expressed dimensionlessly within the model as $r_0 = 1$. With these response functions calculated, the parametric analysis branches off into multiple cases that explore the

effects of different material and fluid configurations of the shell structure. The two geometries present within this study are the large inter-hull geometry, ($a = 0.5$), and the small inter-hull geometry, ($a = 0.09$).

With the geometries fixed, the different cases that make up the next level of the parametric analysis are all material-related. For each shell, the density ρ, speed of sound c, and Poissons ratio ν are defined. The internal fluid is similarly defined by density ρ, and speed of sound c. By modifying these variable sets we create our three major cases for study. The steel-water-steel configuration will serve as the first case and will act as the baseline for comparison. Modifying the fluid used gives us our steel-diesel-steel case to analyze the effect of the internal fluid. Finally, by modifying the values of the external shell material, we create a steel-water-composite case.

Finally, for each of these cases our shell thicknesses, h_1 and h_2 will be varied. Six values of the inner shell thickness will be used, equally spaced between $h_1 = 0.0025$ and $h_1 = 0.01$, or 0.25% to 1% of the inner radius. Similarly, six values of the outer shell radius will be used for each of these, varying between 20% and 100% of the inner shell thickness. The combination of the two gives a total of 36 datasets per case. These datasets include values of stress for both shells, from which maximum values can be extracted, including the time and location of those maxima.

Each dataset is an individual execution of the three-dimensional model, which takes approximately 8 hours to complete. To make computation easier the model was broken up into multiple steps with the datasets saved in text form after each step. Up to six datasets were run concurrently, increasing the time spent on individual simulations, but allowing for easier scheduling and greatly speeding up the overall process. The majority of the data was computed over the course of a month in June of 2014, with additional computations done later as needed. The two-dimensional model, by comparison, took under two hours to complete a simulation. Overall, due to efficient scheduling, running more instances of the model concurrently, and reducing the number of variables analyzed, the three-dimensional parametric analysis took a comparable amount of time to the two-dimensional analysis.

3.2 Individual Case Results

Each case is considered plotted separately on a three-dimensional graph against the thickness of the inner and outer shell to examine what trends are present with respect to shell thickness.

3.2.1 Steel-Water-Steel Case (a=0.5)

The steel-water-steel case was the simplest case and served as the basis for comparison for the others. For this geometry the dimensionless external radius was $r_0 = 1$ and internal radius was $a = 0.5$. Both shells of this structure were comprised of steel with densities ρ_1 and ρ_2 of $7800kg/m^3$, sound speeds c_1 and c_2 of $5000m/s$, and Poisson's ratios ν_1 and ν_2 of 0.3. The thickness of the inner shell, h_1, varied between 0.25% and 1% of r_0. The thickness of the outer shell, h_2 similarly varied between 20% and 100% of h_1. All fluids used were water, with densities ρ_e and ρ_i of $1000kg/m^3$, and sound speeds c_e and c_i of $1400m/s$. Results from this case can be found in Figures 3.1 to 3.8.

The steel-water-steel case illustrates the general trend seen within all of the stress and strain results. The maximum stress was found to decrease as the thickness of the inner shell was increased. Additionally, there was also some decrease in the maximum as the outer shell thickness as increased, but at a much lower rate. For the inner shell the maximum stress peaked at $2273.8MPa$ and the maximum normal displacement was 0.0256, both at the minimum thickness of inner and outer shells. For the outer shell, the maximum stress peaked at $1057.8MPa$ with normal displacement 0.0207. Again, these maxima occurred at the point where the thicknesses were at their minimum.

For the inner shell, the maximum stress occurred at different points along the surface of the shell depending on the thicknesses of the shell. For higher thicknesses of the inner shell the maxima were located at the point nearest the origin of the shockwave. For lower thicknesses, however, the maxima occurred at intermediate points along the surface of the shell, neither at the point closest nor furthest from the shockwave origin. For the outer shell, the maximum stresses only appeared at two distinct points. For small thicknesses, the maxima were located at the point nearest

to the origin of the shockwave, but as the thicknesses were increased, the maximum values moved to the point farthest from the shockwave origin. It is also worth noting that for the outer shell, the maxima that occur nearest to the origin were actually occuring at a later time within the simulation, as can be seen in Figures 3.6 and 3.8; they are stress wave superpositions, rather than part of the initial impact.

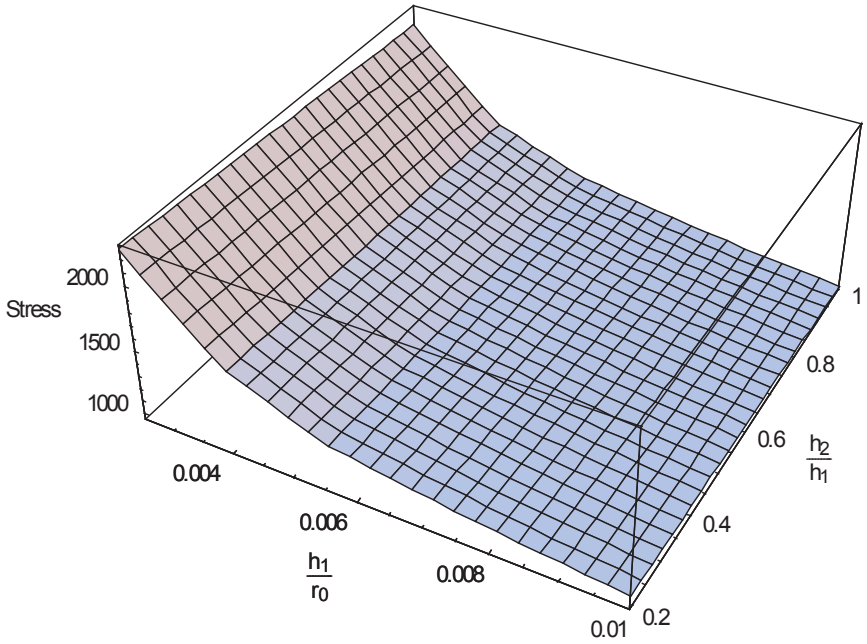

Figure 3.1: Steel-Water-Steel (a=0.5), Maximum Inner Shell Stress (MPa)

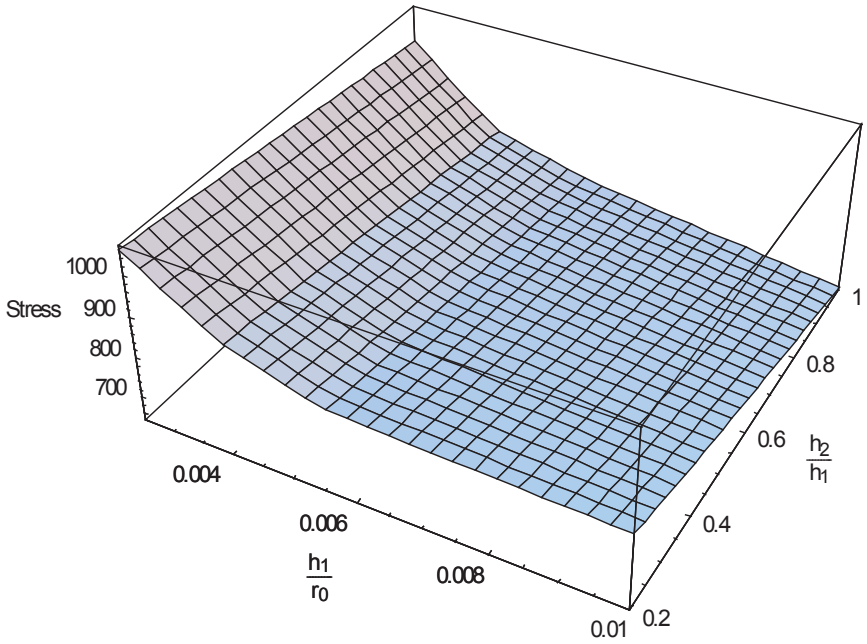

Figure 3.2: Steel-Water-Steel (a=0.5), Maximum Outer Shell Stress (MPa)

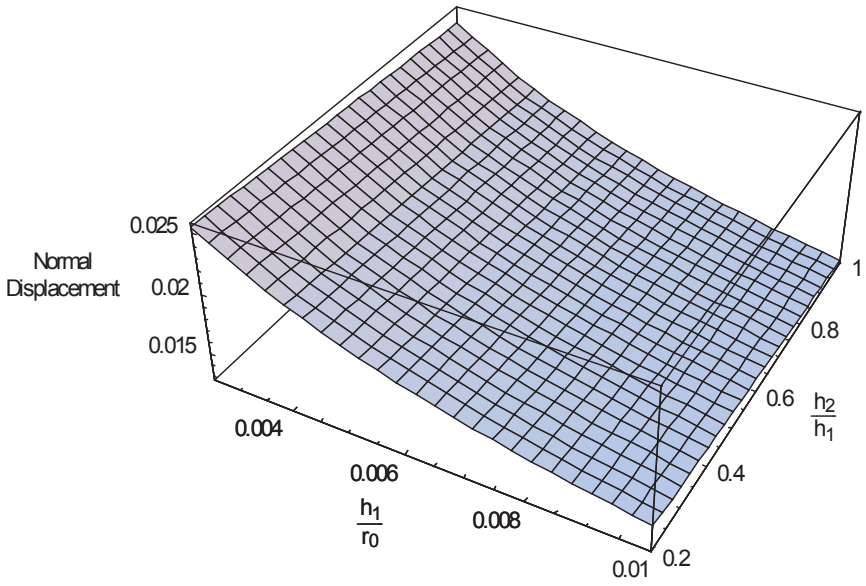

Figure 3.3: Steel-Water-Steel (a=0.5), Maximum Inner Shell Normal Displacement

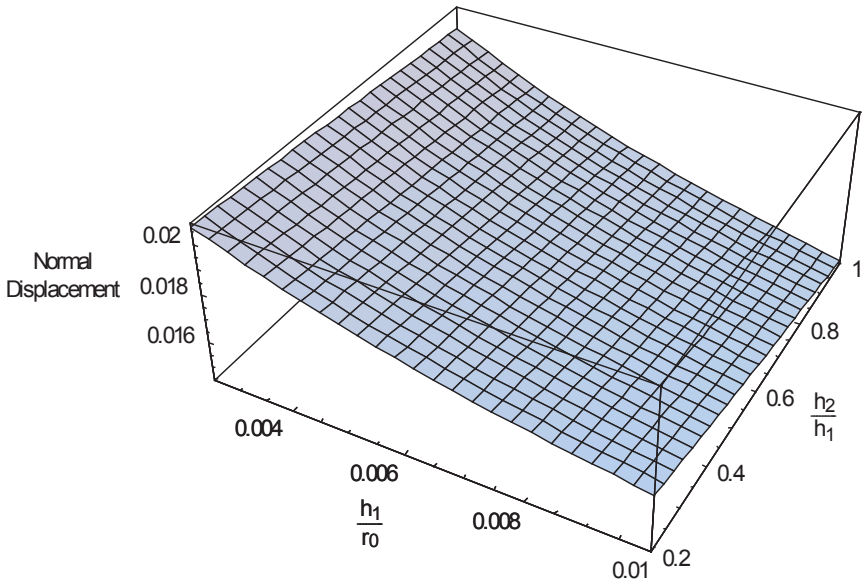

Figure 3.4: Steel-Water-Steel (a=0.5), Maximum Outer Shell Normal Displacement

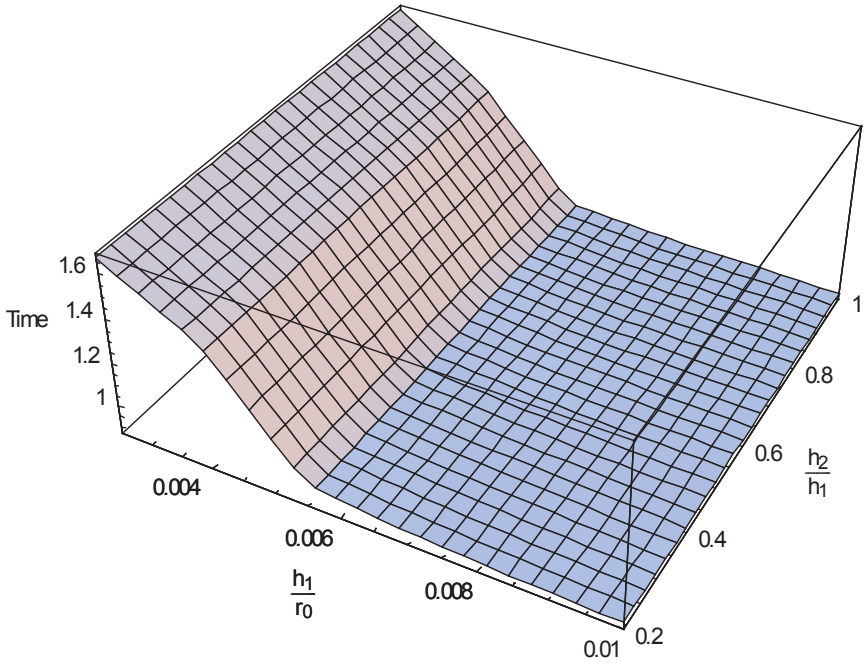

Figure 3.5: Steel-Water-Steel (a=0.5), Timing of Maximum Inner Shell Stress (Dimentionless)

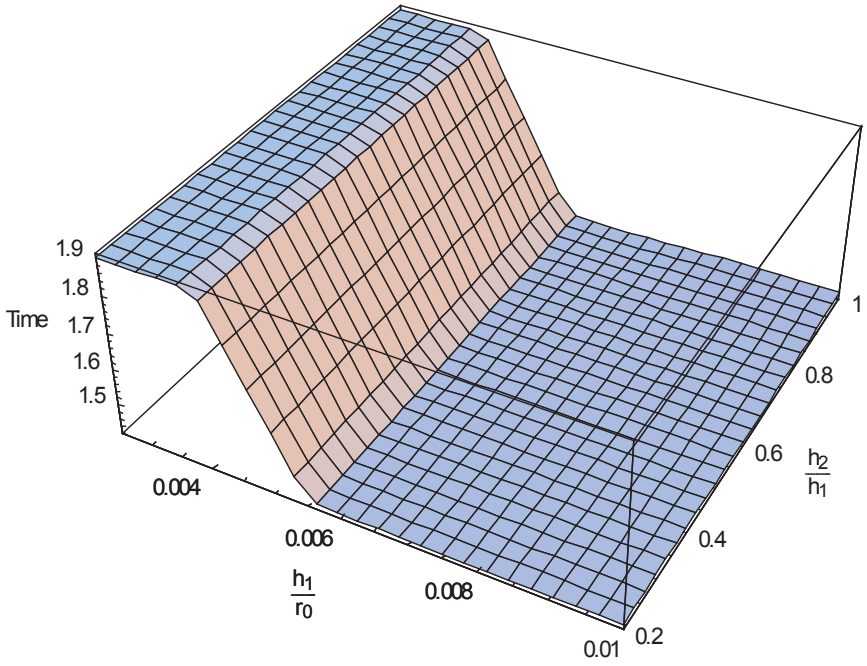

Figure 3.6: Steel-Water-Steel (a=0.5), Timing of Maximum Outer Shell Stress (Dimentionless)

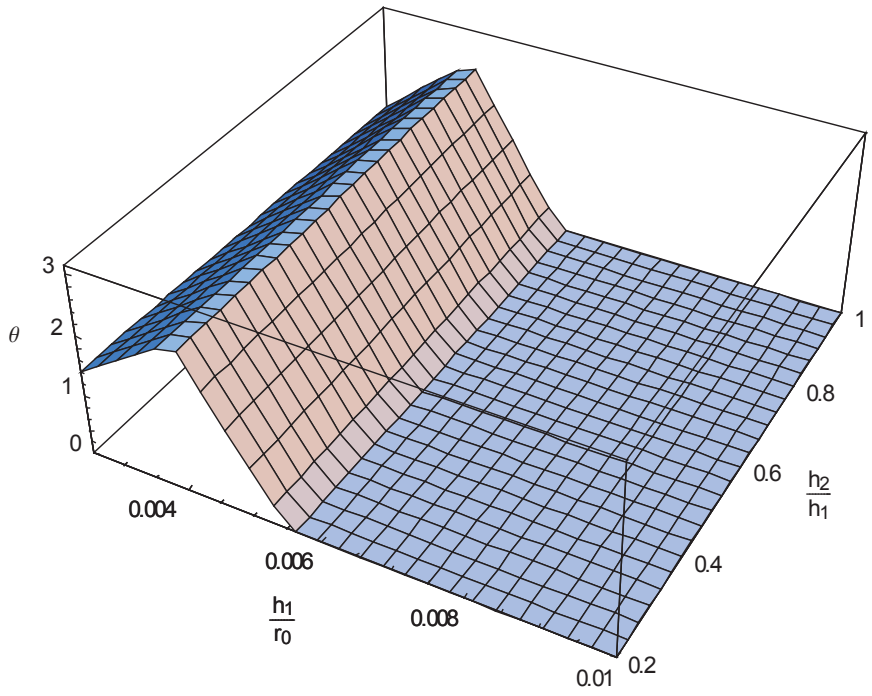

Figure 3.7: Steel-Water-Steel (a=0.5), Location of Maximum Inner Shell Stress (Radians)

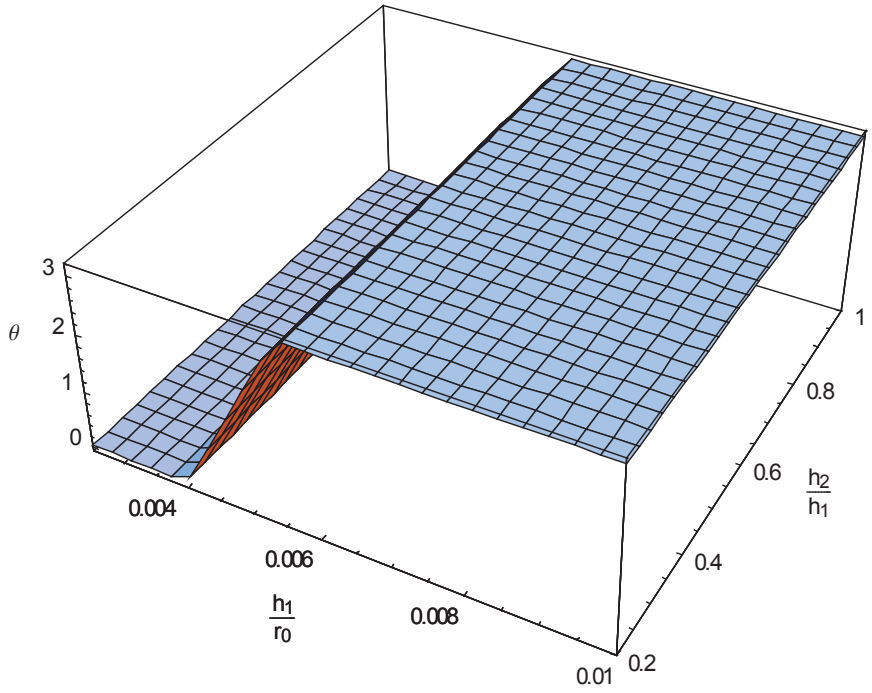

Figure 3.8: Steel-Water-Steel (a=0.5), Location of Maximum Outer Shell Stress (Radians)

3.2.2 Steel-Diesel-Steel Case (a=0.5)

The steel-diesel-steel case examined the effect of the inner fluid. Most of the variables were identical to the steel-water-steel case; the dimensionless external radius was $r_0 = 1$ and the internal radius was $a = 0.5$. Again, both shells of this structure were comprised of steel with densities ρ_1 and ρ_2 of $7800kg/m^3$, sound speeds c_1 and c_2 of $5000m/s$, and Poisson's ratios ν_1 and ν_2 of 0.3. The thickness of the inner shell, h_1, varied between 0.25% and 1% of r_0. The thickness of the outer shell, h_2 similarly varied between 20% and 100% of h_1. The difference only appeared within the fluid variables. While the external fluid variables remained the same, with a ρ_e of $1000kg/m^3$ and c_e of $1400m/s$, the internal fluid density and sound speed were reduced to a ρ_i of $880kg/m^3$ and a c_i of $1250m/s$. Results of this case can be found in Figures 3.9 to 3.16.

The results of the steel-diesel-steel case were very similar to those of the steel-water-steel case. The trends were essentially the same, with the maximum stress very clearly decreasing as the inner shell increased in thickness, and also slightly decreasing as the outer shell increased in thickness. For the inner shell the maximum stress peaked at $2262.3MPa$ and the normal displacement at 0.0266, both at the minimum thicknesses of inner and outer shells. For the outer shell, the maximum stress peaked at $1188.7MPa$ and the normal displacement at 0.0220. Once again these values all occurred at the point where the thicknesses are at their minimum. Compared to the steel-water-steel case, all of these peakss were slightly higher, with the exception of the internal stress, which was slightly lower.

Compared to the steel-water-steel case, the timings and locations of the maxima were very similar, but some additional dependance on the outer shell thickness appeared within the results. Once again, for the inner shell, the maximum stress occured at multiple points. For higher thicknesses of the inner shell the maxima was always at the point nearest the origin of the shockwave. However, for lower thicknesses of the inner shell two possibilities occurred. First, when both the inner and outer shells were thin, the maxima appeared at intermediate points along the side of the shell, neither at the point closest to the shockwave origin, nor at the point furthest from the shockwave origin. However, at some points where the outer shell was thicker, the maxima occured once again at the point nearest the shockwave origin.

For the outer shell, a similar dependance appeared. For large thicknesses of the inner shell the maxima all occurred at the point farthest to the origin of the shockwave. For small thicknesses of the inner shell there was some variation depending on the thickness of the outer shell. When both inner and outer shell were thin, the maxima was located at the point nearest the shockwave origin, but as the outer shell thickness was increased the maxima shifted to the point point farthest from the shockwave origin. Like in the steel-water-steel case the maxima that were located nearest to the origin were actually happening at a later time within the simulations; a superposition of the different shockwave components, rather than part of the initial impact.

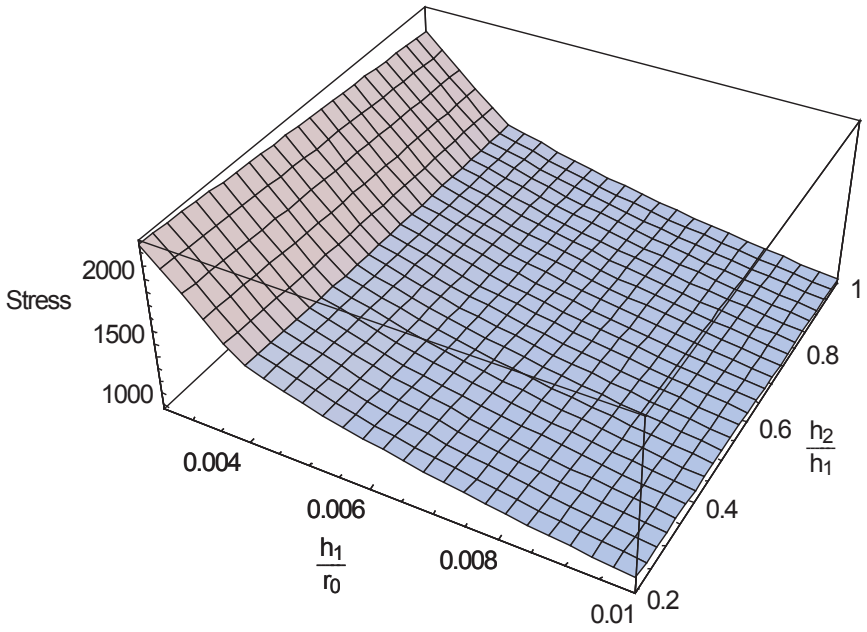

Figure 3.9: Steel-Diesel-Steel (a=0.5), Maximum Inner Shell Stress (MPa)

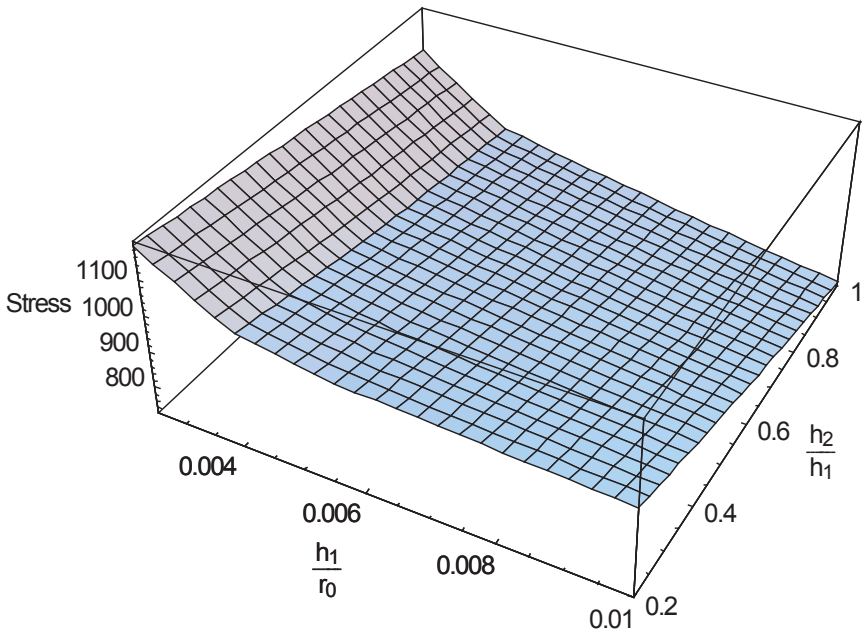

Figure 3.10: Steel-Diesel-Steel (a=0.5), Maximum Outer Shell Stress (MPa)

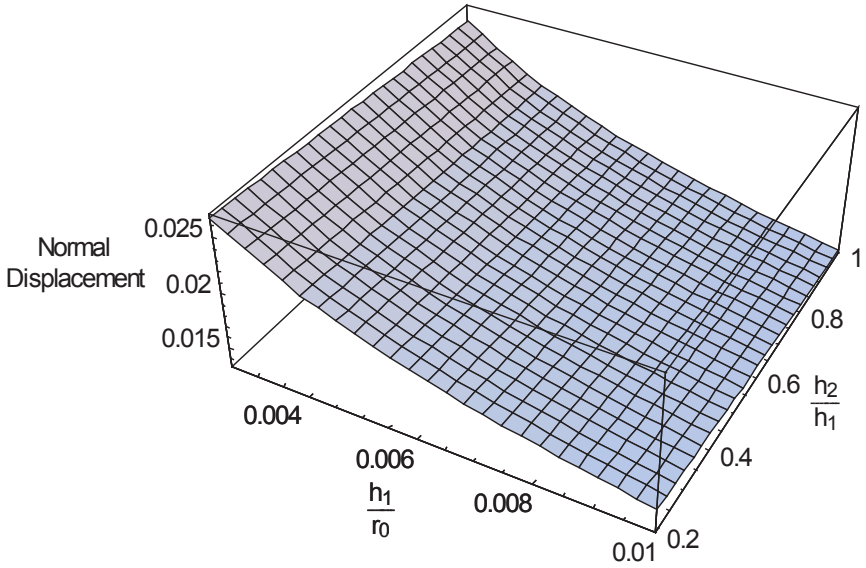

Figure 3.11: Steel-Diesel-Steel (a=0.5), Maximum Inner Shell Normal Displacement

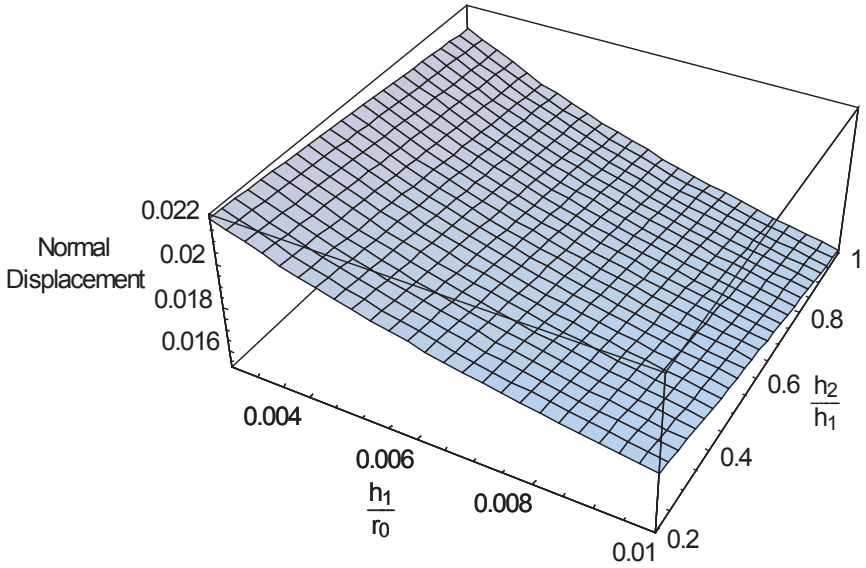

Figure 3.12: Steel-Diesel-Steel (a=0.5), Maximum Outer Shell Normal Displacement

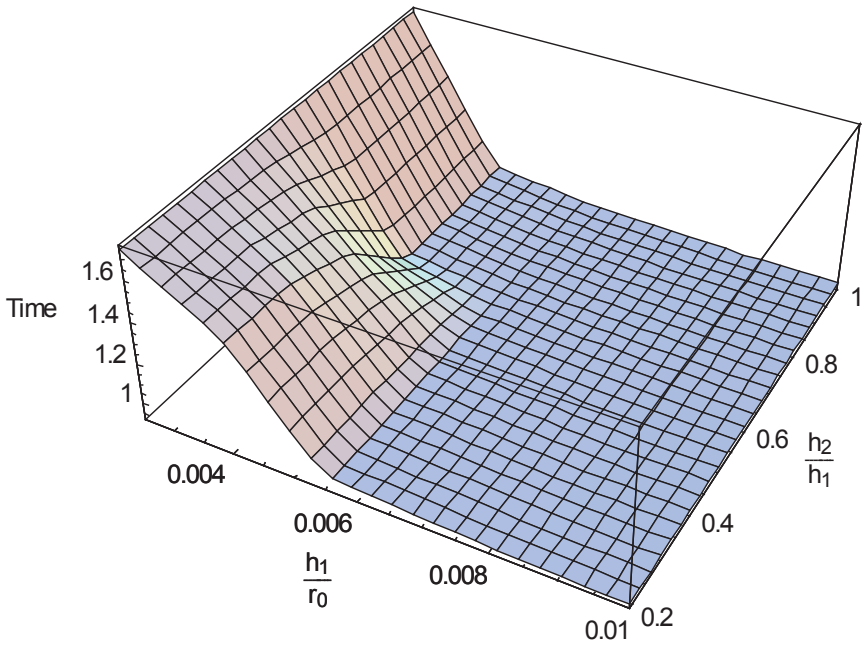

Figure 3.13: Steel-Diesel-Steel (a=0.5), Timing of Maximum Inner Shell Stress (Dimentionless)

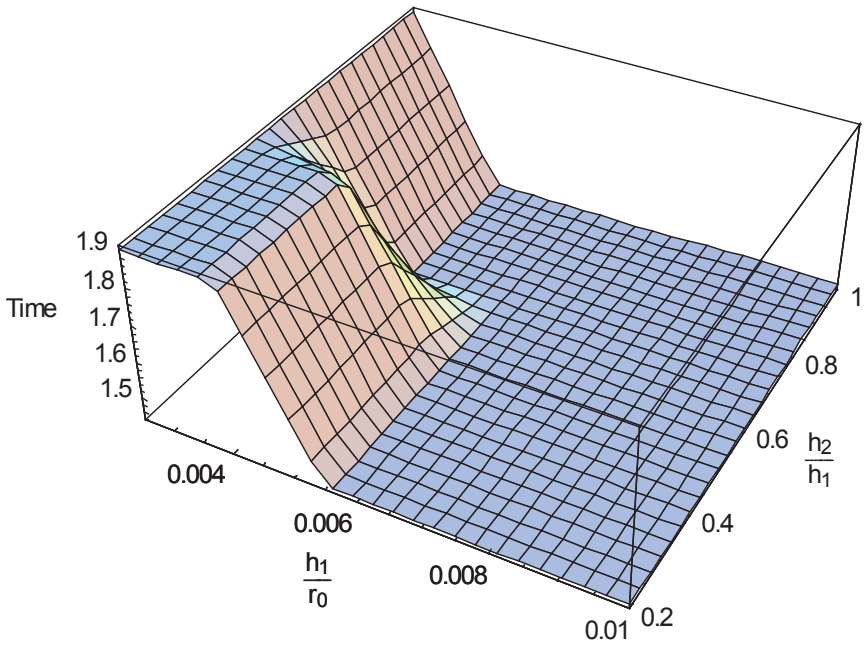

Figure 3.14: Steel-Diesel-Steel (a=0.5), Timing of Maximum Outer Shell Stress (Dimentionless)

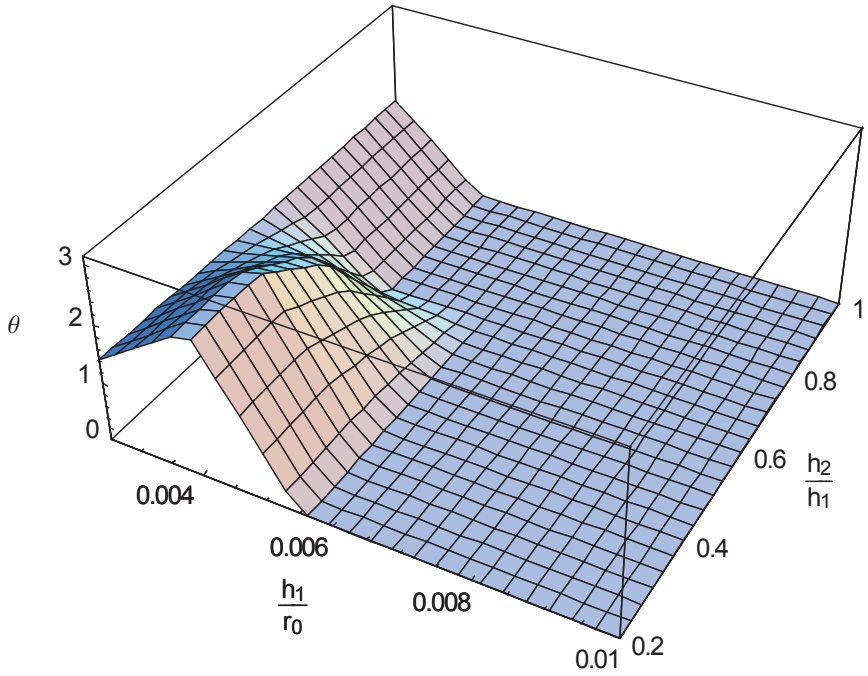

Figure 3.15: Steel-Diesel-Steel (a=0.5), Location of Maximum Inner Shell Stress (Radians)

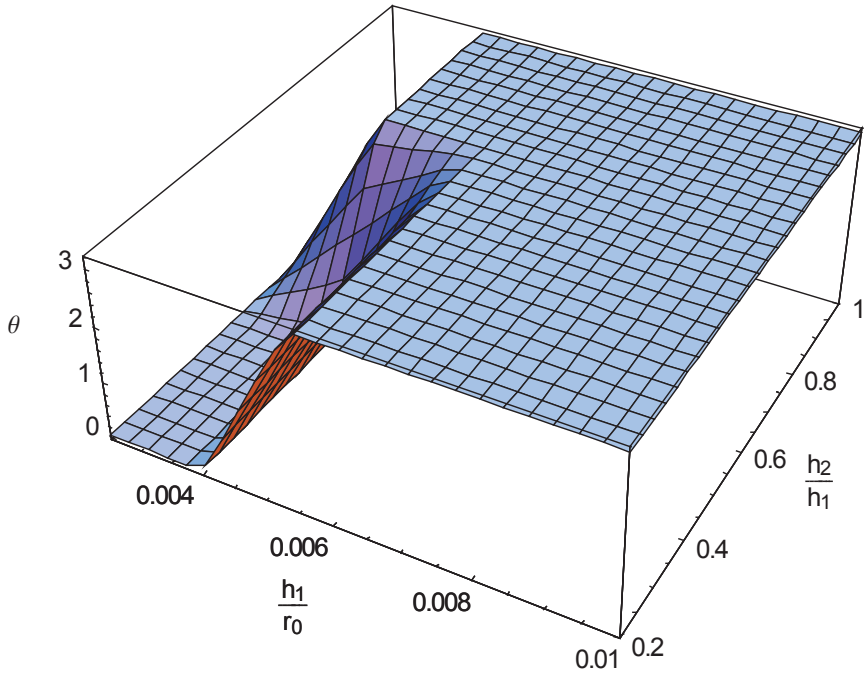

Figure 3.16: Steel-Diesel-Steel (a=0.5), Location of Maximum Outer Shell Stress (Radians)

3.2.3 Steel-Water-Composite Case (a=0.5)

The steel-water-composite case examined the effect of modifying the material composition of the outer shell. Like the previous cases, the dimensionless external radius was $r_0 = 1$ and the internal radius was $a = 0.5$. The difference in this case that rather than both shells of this structure being comprised of steel, only the internal shell was, with density ρ_1 of $7800kg/m^3$, sound speed c_1 of $5000m/s$, and Poisson's ratio ν_1 of 0.3. The external shell was comprised of a composite material, with density ρ_2 of $1800kg/m^3$, sound speed c_2 of $3430m/s$, and Poisson's ratio ν_2 of 0.15. Besides these changes, the simulation was identical to the steel-water-steel case, with the thickness of the inner shell, h_1, varied between 0.25% and 1% of r_0 and the thickness of the outer shell, h_2, varied between 20% and 100% of h_1. The fluid variables used were those of water, density ρ_e and ρ_i of $1000kg/m^3$, and sound speed c_e and c_i of $1400m/s$. Results of this case can be found in Figures 3.17 to 3.24.

The results of the steel-water-composite case varied greatly from the steel-water-steel case, mostly when it came to the results of the external shell. For the inner shell, the results were similar as the maximum stress decreased as the inner shell thickness increased. However, unlike previous cases, the stress did not seem affected by the thickness of the outer shell. For the outer shell, the numbers are an order of magnitude lower than what was seen previously. The outer shell stress decreased as the inner shell thickness was increased, but minimally so, only seeing a drop of around 10% after the initial increase, and remaining mostly constant after that. For the inner shell the peak stress experienced was $2309.1MPa$ and the normal displacement was 0.0266. For the outer shell, the absolute maximum stress was $134.8MPa$ and the normal displacement was 0.0208. As seen in the previous cases, all of these values occur when the thicknesses of the shells were at their lowest. With the exception of the outer shell stress, all of these peaks are slightly higher than the values seen in the steel-water-steel case. The outer shell stress, however is a full order of magnitude lower than what was seen in the steel-water-steel case.

As for the timings and locations, the results of the steel-water-composite case were very similar to the steel-water-steel case for the inner shell, but not for the outer outer shell. The inner shell maximum stress occured at multiple locations as before, depending on the particular shell thicknesses. For higher thicknesses of the

inner shell the maxima was at the point nearest the origin of the shockwave and for lower thicknesses the maxima ocurred at intermediate points along the side of the shell. For the outer shell, the maximum stress occurred at the point furthest from the shockwave at all points except for when the inner shell was at it's thinnest. In those cases, the maximum values happened slightly later, and were located along the side of the shell, at points neither furthest nor nearest the shockwave origin.

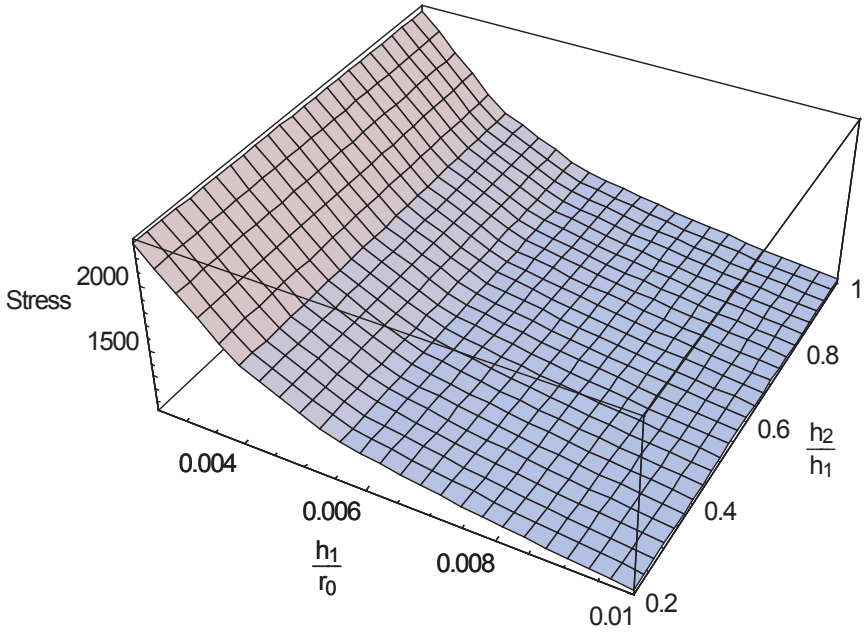

Figure 3.17: Steel-Water-Composite (a=0.5), Maximum Inner Shell Stress (MPa)

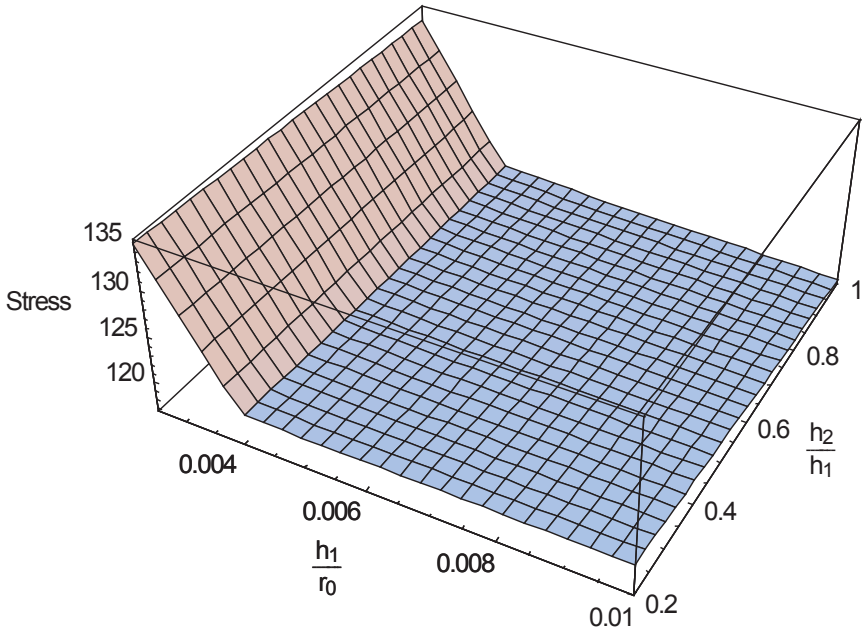

Figure 3.18: Steel-Water-Composite (a=0.5), Maximum Outer Shell Stress (MPa)

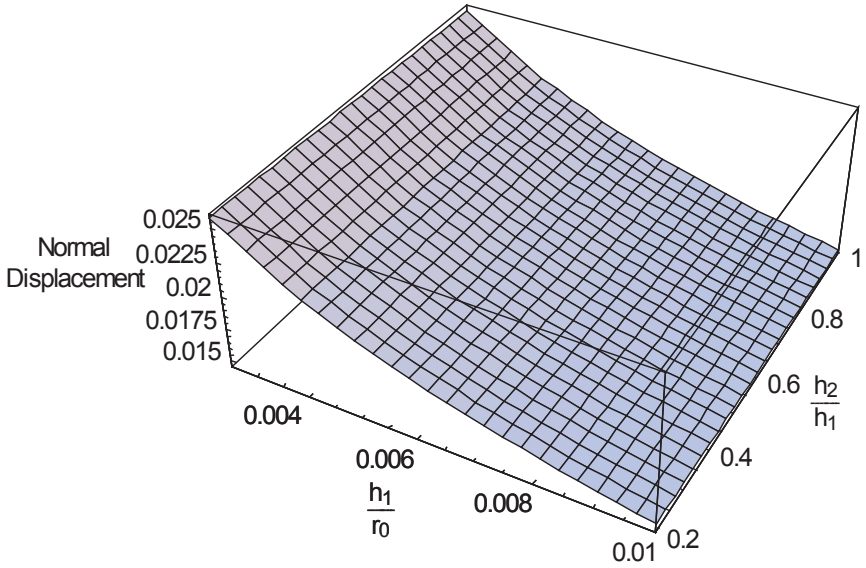

Figure 3.19: Steel-Water-Composite (a=0.5), Maximum Inner Shell Normal Distribution

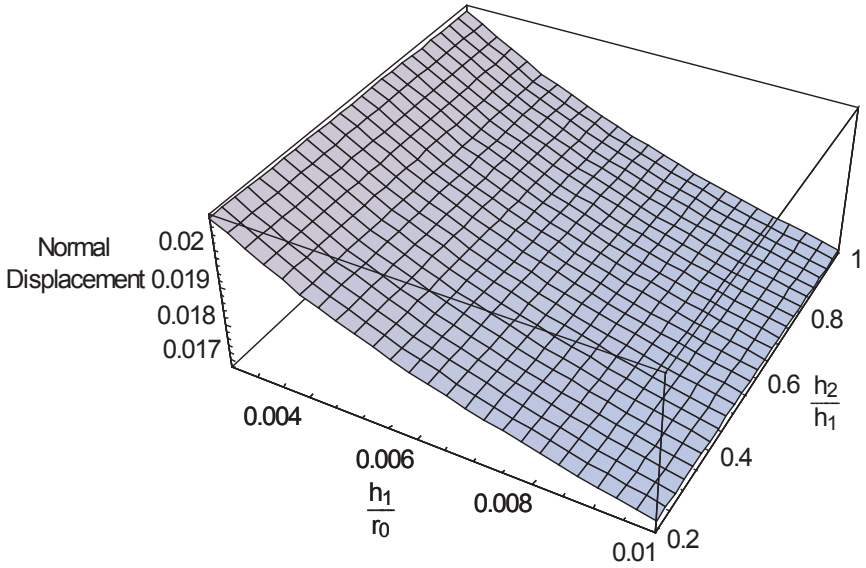

Figure 3.20: Steel-Water-Composite (a=0.5), Maximum Outer Shell Normal Distribution

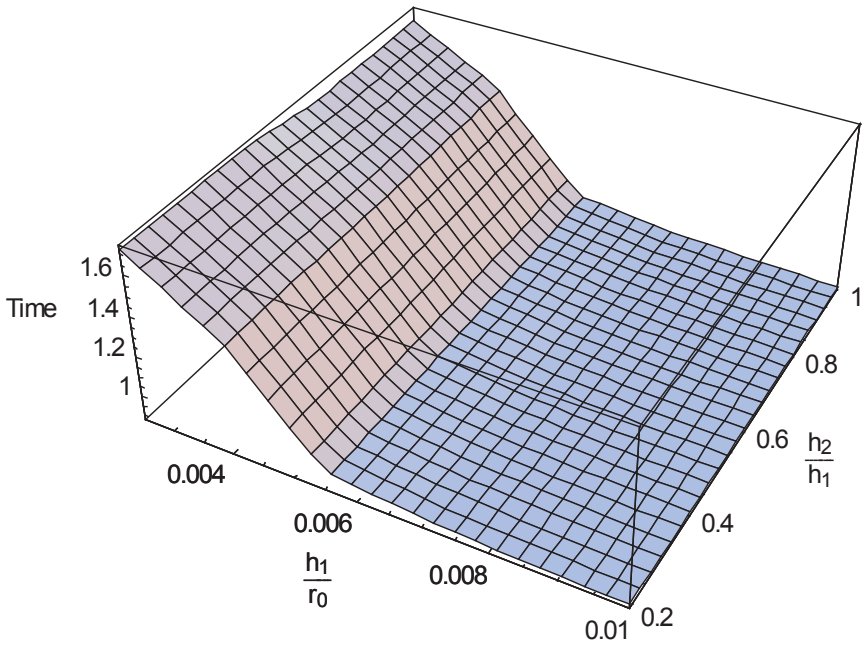

Figure 3.21: Steel-Water-Composite (a=0.5), Timing of Maximum Inner Shell Stress (Dimentionless)

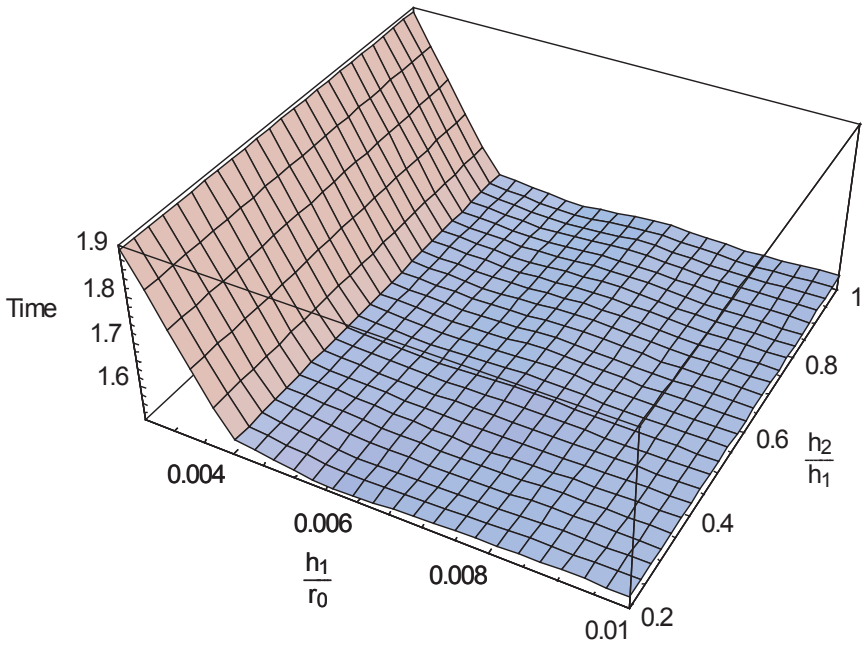

Figure 3.22: Steel-Water-Composite (a=0.5), Timing of Maximum Outer Shell Stress (Dimentionless)

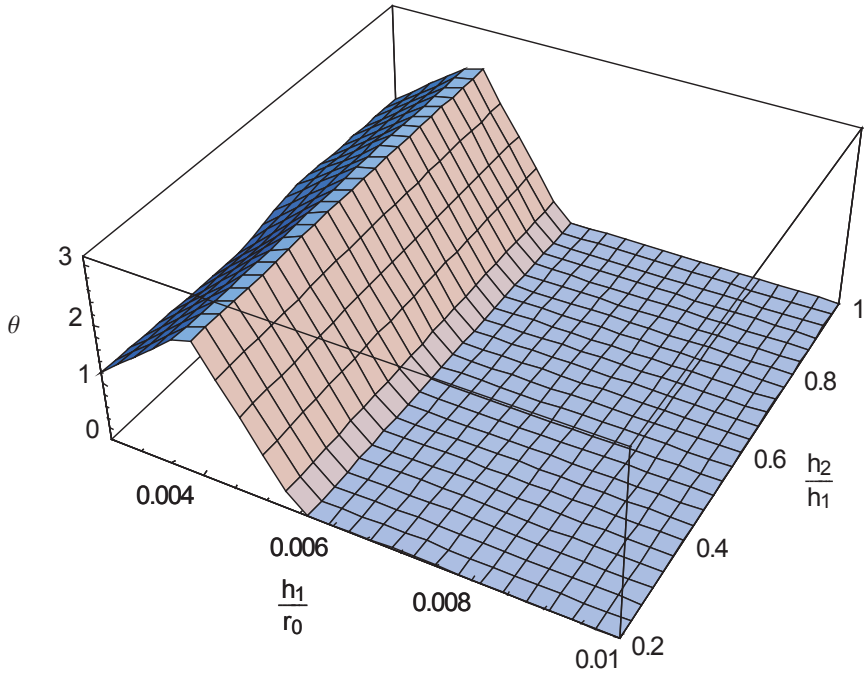

Figure 3.23: Steel-Water-Composite (a=0.5), Location of Maximum Inner Shell Stress (Radians)

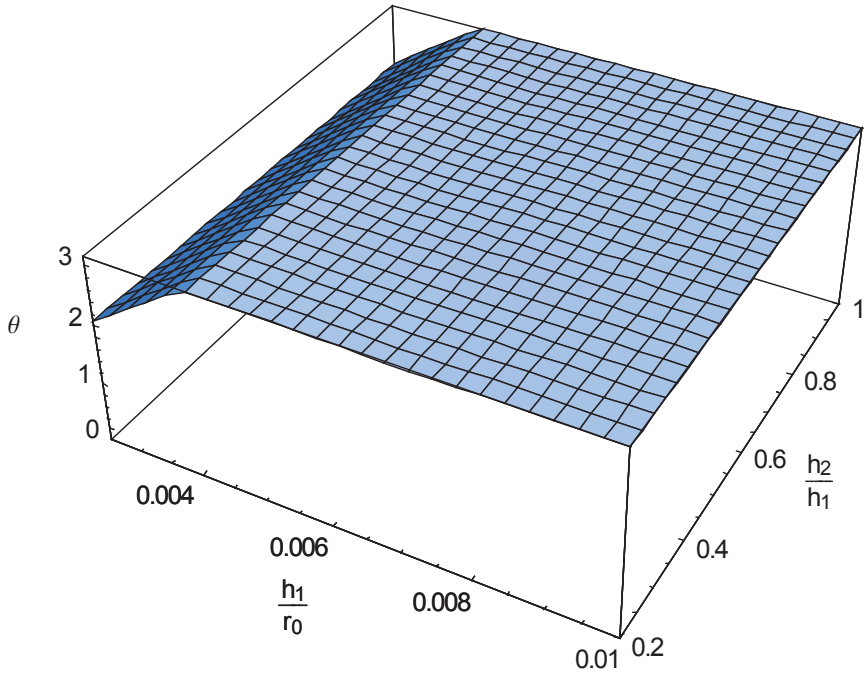

Figure 3.24: Steel-Water-Composite (a=0.5), Location of Maximum Outer Shell Stress (Radians)

3.2.4 Steel-Water-Steel Case (a=0.9)

This second iteration of the steel-water-steel case was the basis for comparison for the other small inter-hull clearance models, as well as providing the first point of comparison for the previous $a = 0.5$ cases. The only changes in this model were those of the shell geometry. While the dimensionless external radius remained $r_0 = 1$, the internal radius was increased to $a = 0.9$. Otherwise, both shells were steel with densities ρ_1 and ρ_2 of $7800kg/m^3$, sound speeds c_1 and c_2 of $5000m/s$, and Poisson's ratios ν_1 and ν_2 of 0.3. As before, inner shell thickness, h_1, varied between 0.25% and 1% of r_0 and outer shell thickness, h_2 varied between 20% and 100% of h_1. All fluids were water with densities ρ_e and ρ_i of $1000kg/m^3$, and sound speeds c_e and c_i of $1400m/s$. Results of this case can be found in Figures 3.25 to 3.32.

One of the differences seen in the stress and normal displacement, Figures 3.25 to 3.28 is the larger effect of the outer shell thickness compared to the results from the previous geometry, seen in Figures 3.1 to 3.4. Other than this the general trends within the stress and displacement were similar. The peak of the inner shell maximum stress was $2382.2MPa$ with a normal displacement of 0.0376. For the outer shell, the peak of the maximum stress was $1720.7MPa$ with a normal displacement of 0.0303. As before, these peaks occur at the point where the thicknesses were at their minimum.

The timing and location results for these maximum values, Figures 3.29 to 3.29, show very different patterns than those seen in the previous geometry, Figures 3.5 to 3.8. This case had three distinct times and locations where the maximum stress occurred on the inner shell. The first was when the inner and outer shells were near their thinnest, and the maximum stress was at the point closest to the shockwave origin. As the inner and outer shells were increased in thicknesses the second location was seen, where the maximum value appared at the point furthest from the shockwave origin. Finally, when both thicknesses approached their highest a third location was witnessed where the maximum value returned to a point close to the shockwave origin. The timing data for these three locations indicated that they occurred separately, as the shockwave reflects within the structure. For the outer shell, two distict times were seen. Similar to the inner shell, as the thicknesses were brought to their highest the maximum stresses occurred at a point near the shockwave origin at the front of the shell. At low thicknesses, the maximum stress was far from the shockwave origin.

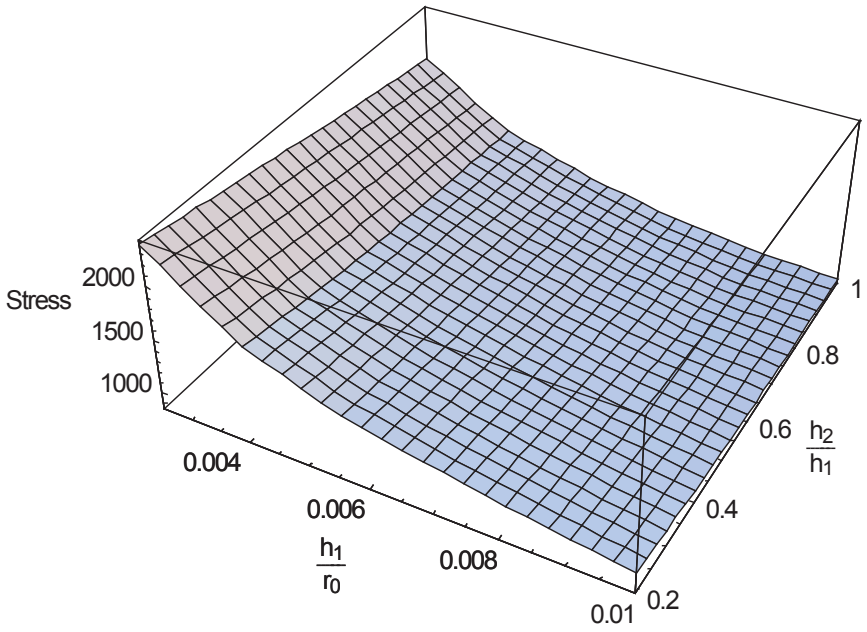

Figure 3.25: Steel-Water-Steel (a=0.9), Maximum Inner Shell Stress (MPa)

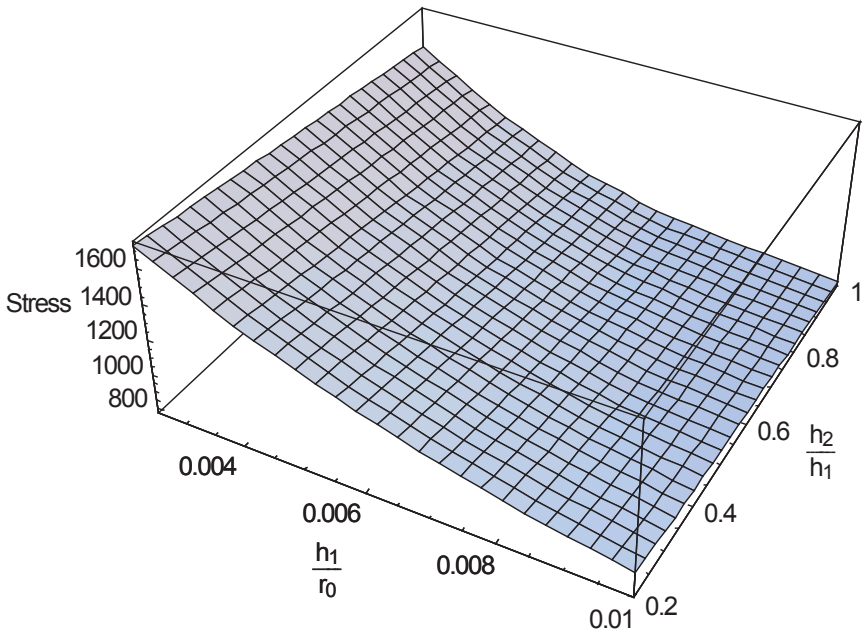

Figure 3.26: Steel-Water-Steel (a=0.9), Maximum Outer Shell Stress (MPa)

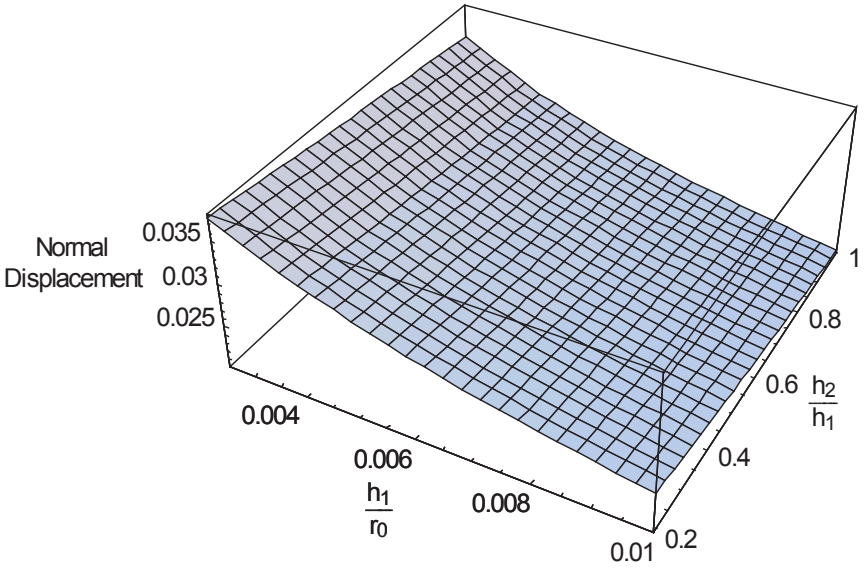

Figure 3.27: Steel-Water-Steel (a=0.9), Maximum Inner Shell Normal Displacement

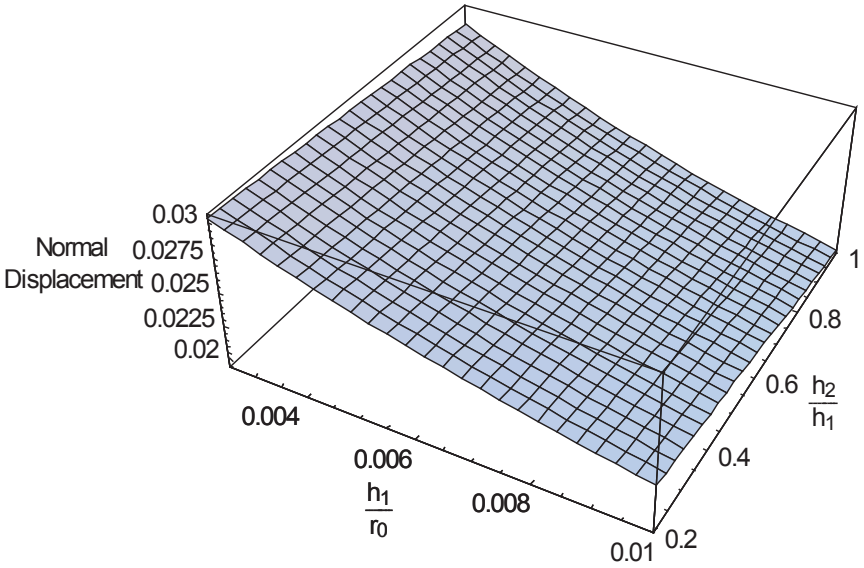

Figure 3.28: Steel-Water-Steel (a=0.9), Maximum Outer Shell Normal Displacement

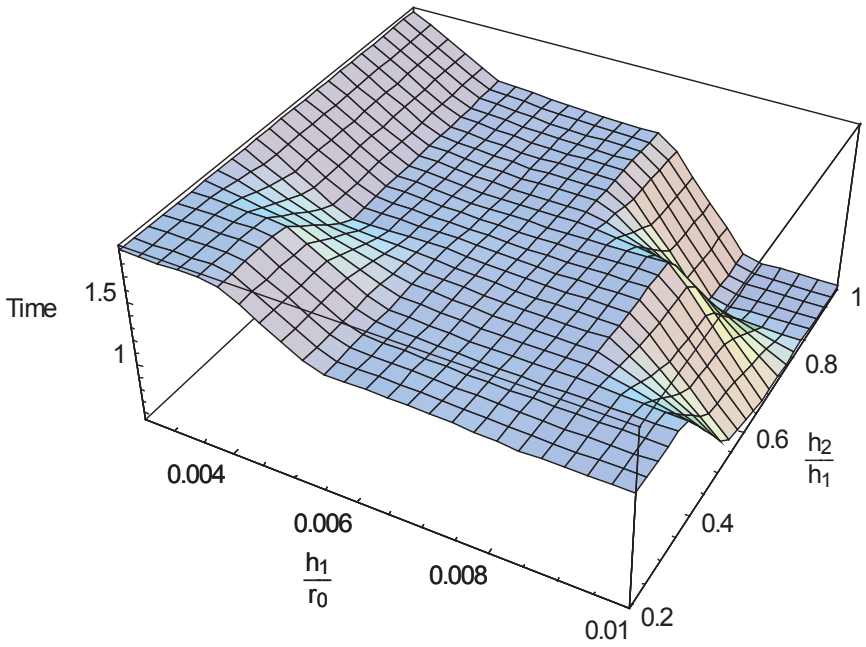

Figure 3.29: Steel-Water-Steel (a=0.9), Timing of Maximum Inner Shell Stress (Dimentionless)

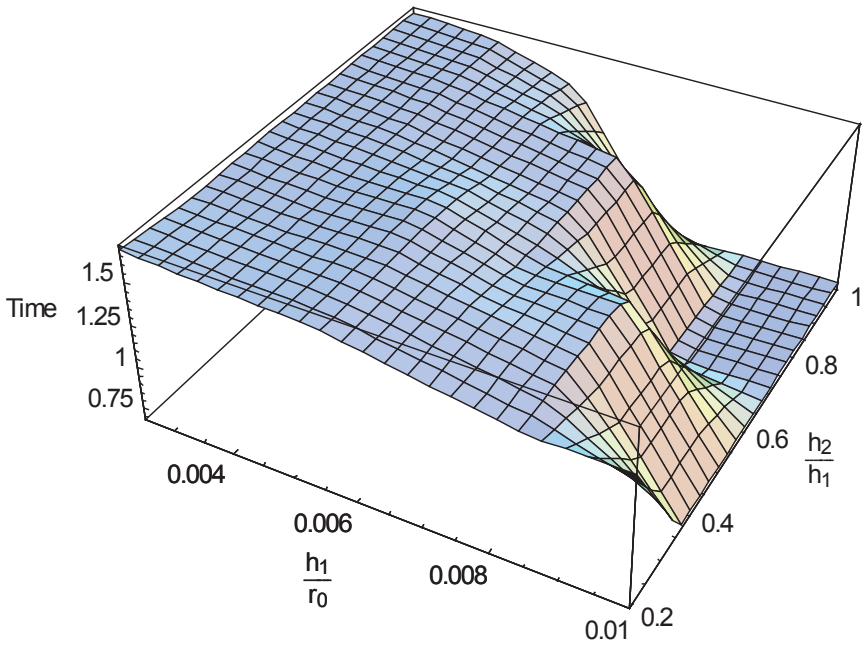

Figure 3.30: Steel-Water-Steel (a=0.9), Timing of Maximum Outer Shell Stress (Dimentionless)

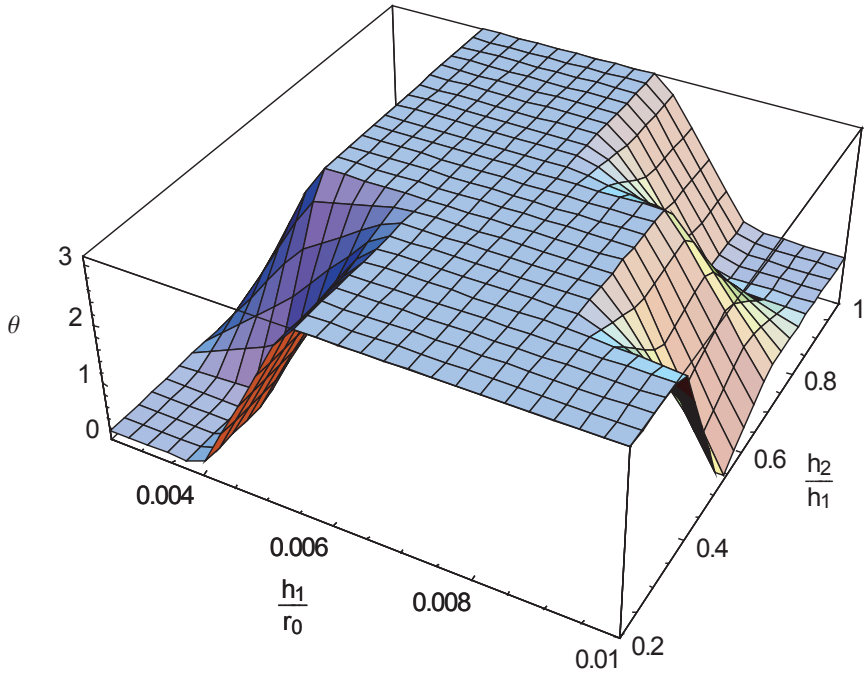

Figure 3.31: Steel-Water-Steel (a=0.9), Location of Maximum Inner Shell Stress (Radians)

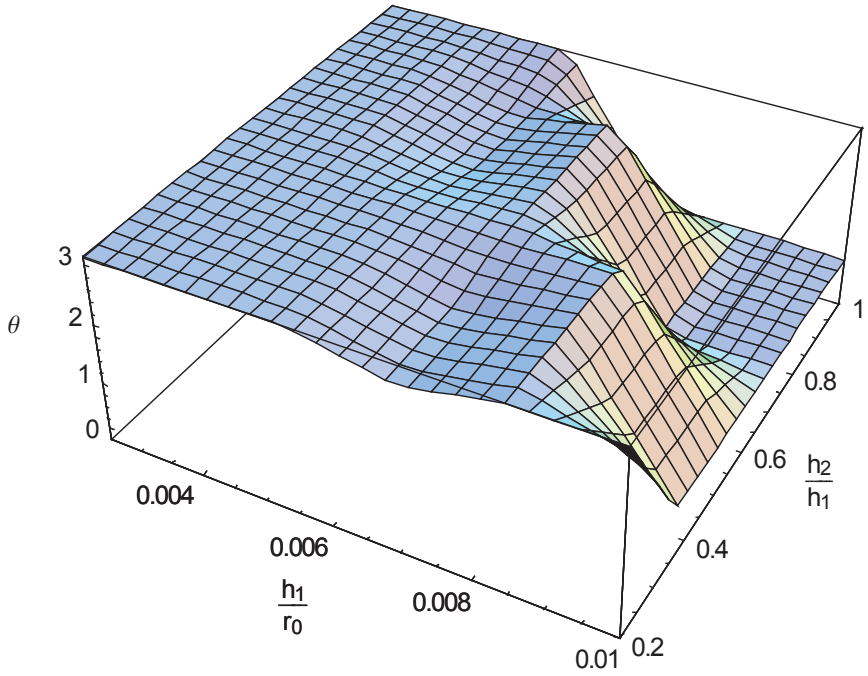

Figure 3.32: Steel-Water-Steel (a=0.9), Location of Maximum Outer Shell Stress (Radians)

3.2.5 Steel-Diesel-Steel Case (a=0.9)

The second steel-diesel-steel case continued to examine the effects of the internal fluid, as well as to provide more data on the effect of the small inter-hull geometry. As such, only this geometry was changed compared to the steel-diesel-steel large inter-hull model. The dimensionless external radius was $r_0 = 1$ and the internal radius was increased to $a = 0.9$. Once again,the shells of this structure were steel with densities ρ_1 and ρ_2 of $7800kg/m^3$, sound speeds c_1 and c_2 of $5000m/s$, and Poisson's ratios ν_1 and ν_2 of 0.3. Inner shell thickness, h_1, varied between 0.25% and 1% of r_0 and outer shell thickness, $h_2$varied between 20% and 100% of h_1. The external fluid density ρ_e was $1000kg/m^3$ and sound speed c_e was $1400m/s$, the internal fluid density ρ_i was $880kg/m^3$ and sound speed c_i was $1250m/s$. Results of this case can be found in Figures 3.33 to 3.40.

The results of this steel-diesel-steel analysis was very simular to those from the steel-water-steel analysis. For the stress and displacement results, seen in Figures 3.33 to 3.36, only a small amount of variation can be seen compared to the previous steel-water-steel results from Figures 3.25 to 3.28. The highest inner shell stress was $2133.18MPa$ and the highest normal displacement was 0.0366. The highest outer shell stress was $1743.09MPa$ and the highest normal displacement was 0.0320. All of these values continue to occur at the points where the shells are at their thinnest. Compared to the steel-water-steel case, all of the inner shell values are slightly lower, while the outer shell values are slightly higher.

The timing and location results for this case, Figures 3.37 to 3.40, are once again similar to the steel-water-steel case seen in Figures 3.29 to 3.32. The three distinct times and locations for the inner shell stress were again present, though slightly shifted. The first when the inner shell was at it's minimum the maximum stress was at the point closest to the shockwave origin. Increasing the thickness shifted the maximum to the second location where the maximum value appared at the point furthest from the shockwave origin. Finally, when the thicknesses approached their highest the maximum stress returned to a point close to the shockwave origin. The timing data continued to indicate that these three locations were separate occurances, as the shockwave reflected within the structure. For the outer shell, two distict times were again seen. When the thicknesses were brought to their highest the maximum stresses

occurred at a point near the shockwave origin at the front of the shell, otherwise the maximum stress was located at a point far from the shockwave origin.

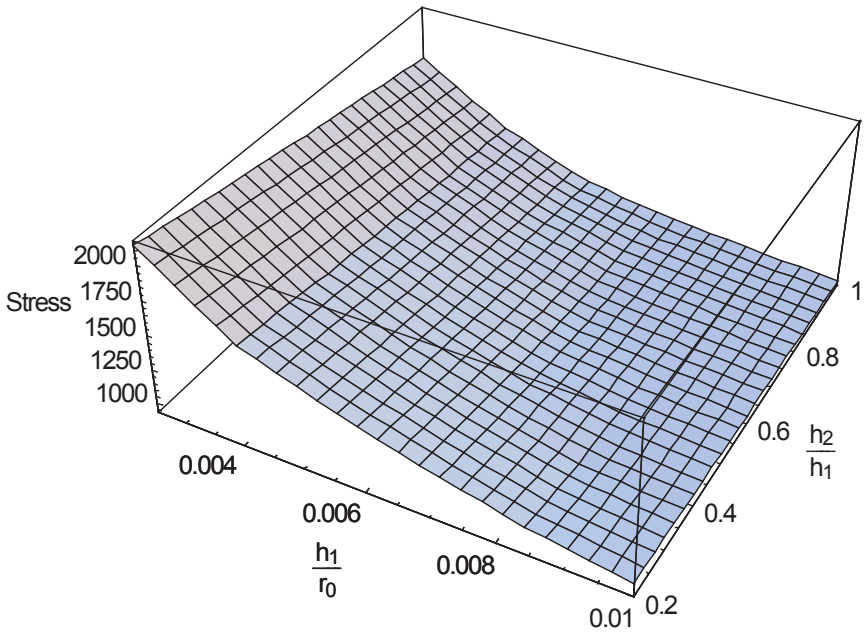

Figure 3.33: Steel-Diesel-Steel (a=0.9), Maximum Inner Shell Stress (MPa)

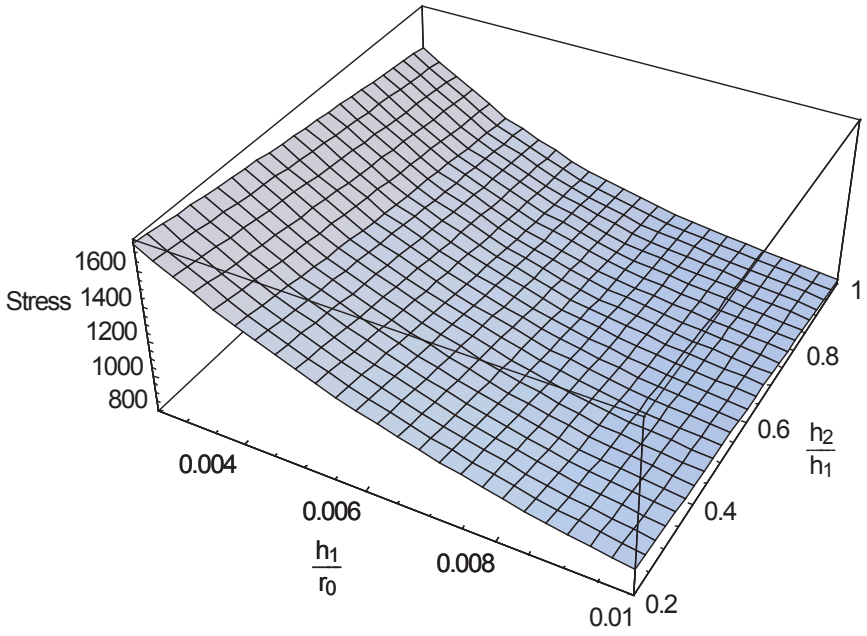

Figure 3.34: Steel-Diesel-Steel (a=0.9), Maximum Outer Shell Stress (MPa)

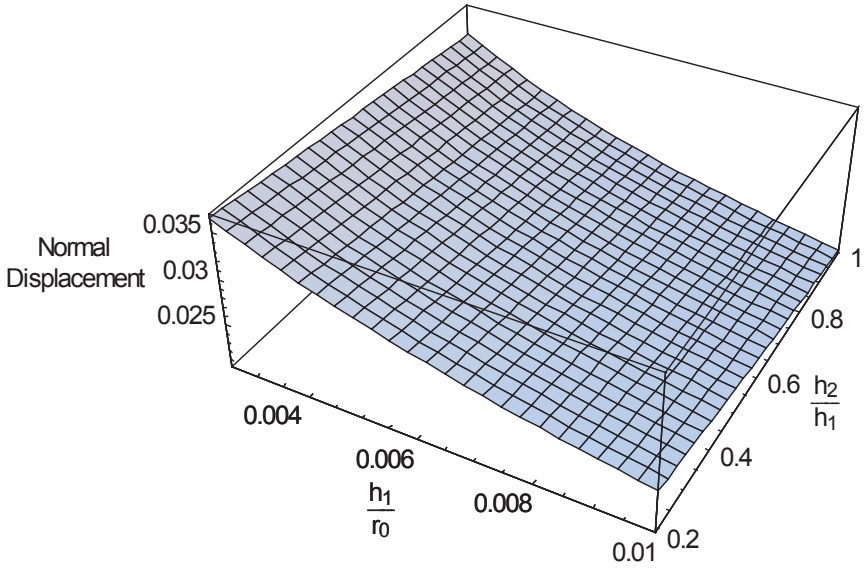

Figure 3.35: Steel-Diesel-Steel (a=0.9), Maximum Inner Shell Normal Displacement

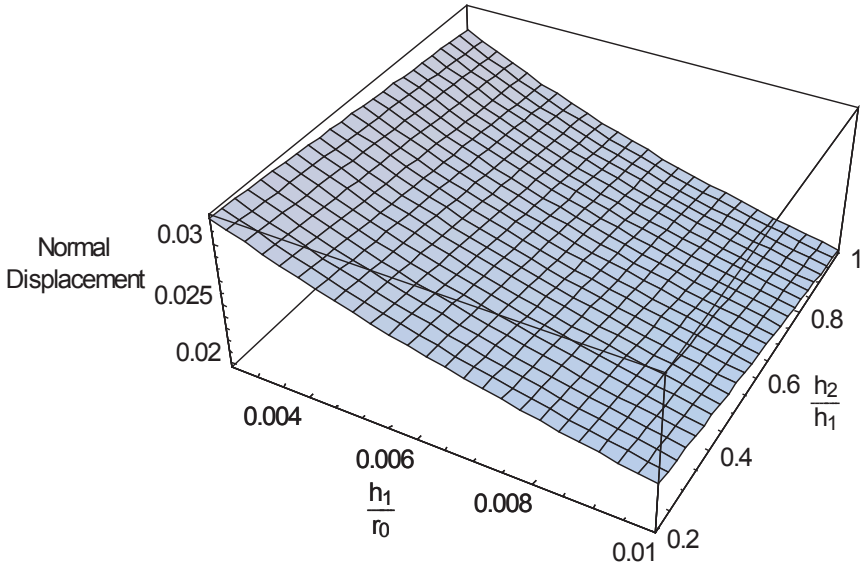

Figure 3.36: Steel-Diesel-Steel (a=0.9), Maximum Outer Shell Normal Displacement

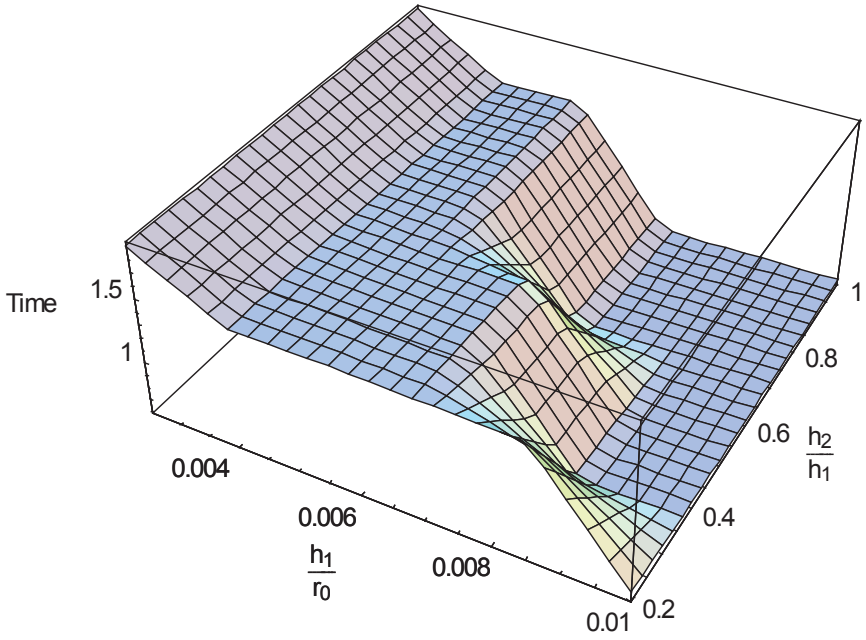

Figure 3.37: Steel-Diesel-Steel (a=0.9), Timing of Maximum Inner Shell Stress (Dimentionless)

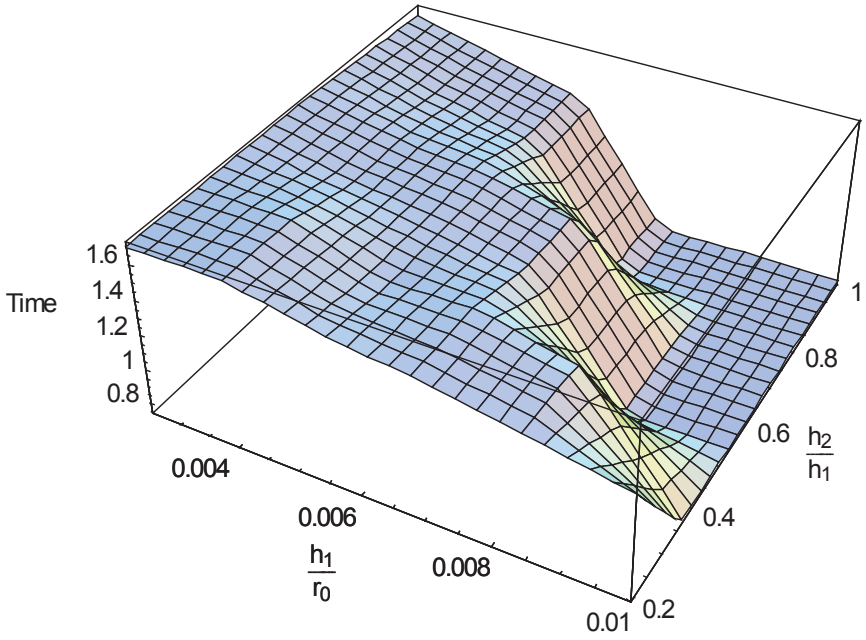

Figure 3.38: Steel-Diesel-Steel (a=0.9), Timing of Maximum Outer Shell Stress (Dimentionless)

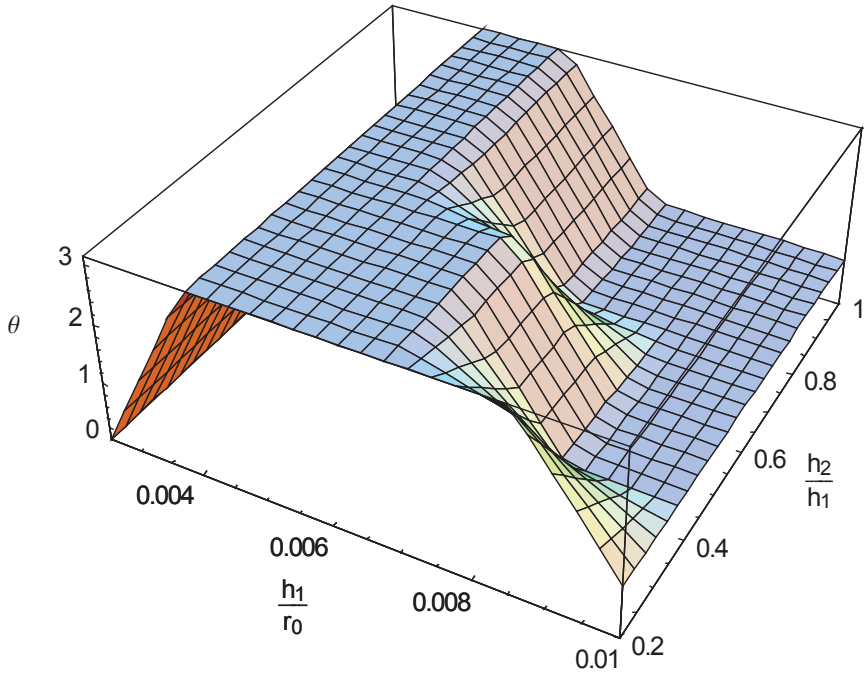

Figure 3.39: Steel-Diesel-Steel (a=0.9), Location of Maximum Inner Shell Stress (Radians)

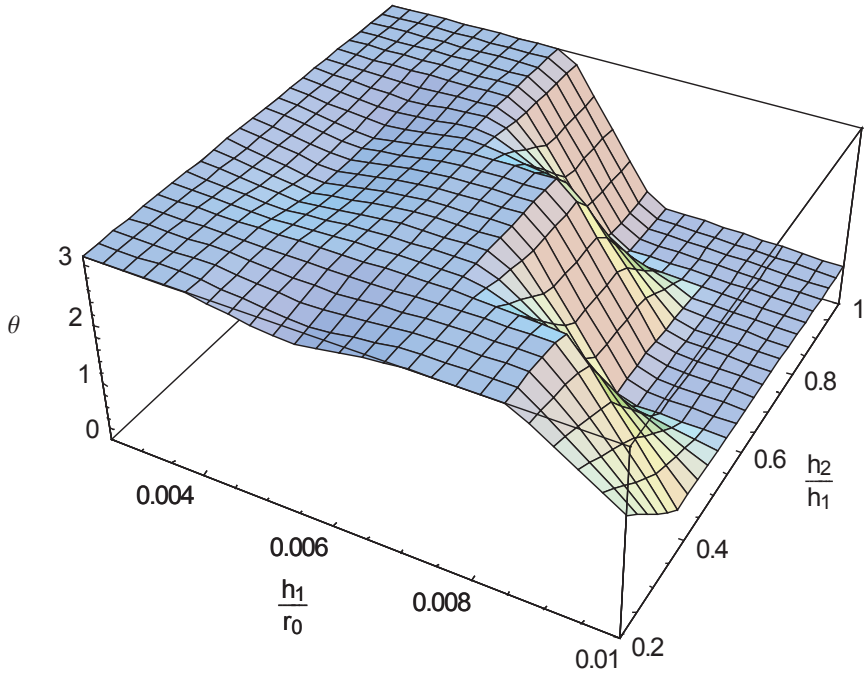

Figure 3.40: Steel-Diesel-Steel (a=0.9), Location of Maximum Outer Shell Stress (Radians)

3.2.6 Steel-Water-Composite Case (a=0.9)

The second steel-water-compsite case continued to test effects of the outer shell material, as well as provide further data for the study of the small inter-hull geometry. As such, again the only change from the steel-water-composite large inter-hull model was that of the geometry, with the dimensionless external radius kept as $r_0 = 1$ and increasing the internal radius to $a = 0.9$. The internal shell was steel with density ρ_1 of $7800kg/m^3$, sound speed c_1 of $5000m/s$, and Poisson's ratio ν_1 of 0.3 and the external shell was composite with density ρ_2 of $1800lg/m^3$, sound speed c_2 of $3430m/s$ and Poisson's ratio ν_2 of 0.15. Inner shell thickness, h_1, varied between 0.25% and 1% of r_0 and outer shell thickness, h_2, varied between 20% and 100% of h_1. All fluids were water with densities ρ_e and ρ_i of $1000kg/m^3$, and sound speeds c_e and c_i of $1400m/s$. Results of this case can be found in Figures 3.41 to 3.48.

The results of the steel-water-composite case, Figures 3.41 to 3.44, are notably different than those of the steel-water-steel case seen previously in Figures 3.25 to 3.28. While the inner shell stress results follow a similar trend to the steel-water-steel case, they do not show any apparent dependance on the outer shell thickness. Unlike the steel-water-composite $a = 0.5$ case from Figure 3.18, the outer shell here does show decreasing stress with increased inner shell thickness, much like the other cases. Peak inner shell stress was $2510.2MPa$ and normal displacement was 0.0385. Peak outer shell stress was $257.43MPa$ and normal displacement was 0.0306. All of the values were taken at the points where both shells were at their thinnest. Compared to the steel-water-steel case, the internal shel stress and displacement peaks are slightly higher. The outer shell peak stress is much lowe, and the normal displacement was slightly higher.

The timing and location results for these values, seen in Figures 3.45 to 3.48, are very different than those of other $a = 0.9$ cases. The inner shell maximum values were located at two distinct points. When the inner shell thickness was lower, the maximum values occurred at the point nearest the shockwave origin. As the inner shell thickness was increased the maximum values shifted to the point furthest from the shockwave origin. For the outer shell, the maximum value did not undergo any sort of transition, and remained at the point furthest from the shockwave origin regardless of the thickness of the inner and outer shells, unlike previous results.

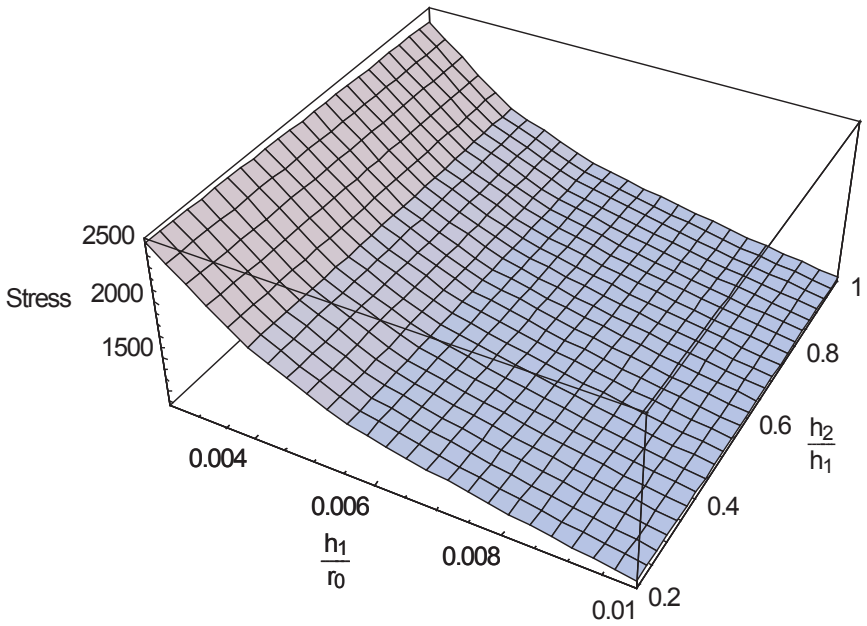

Figure 3.41: Steel-Water-Composite (a=0.9), Maximum Inner Shell Stress (MPa)

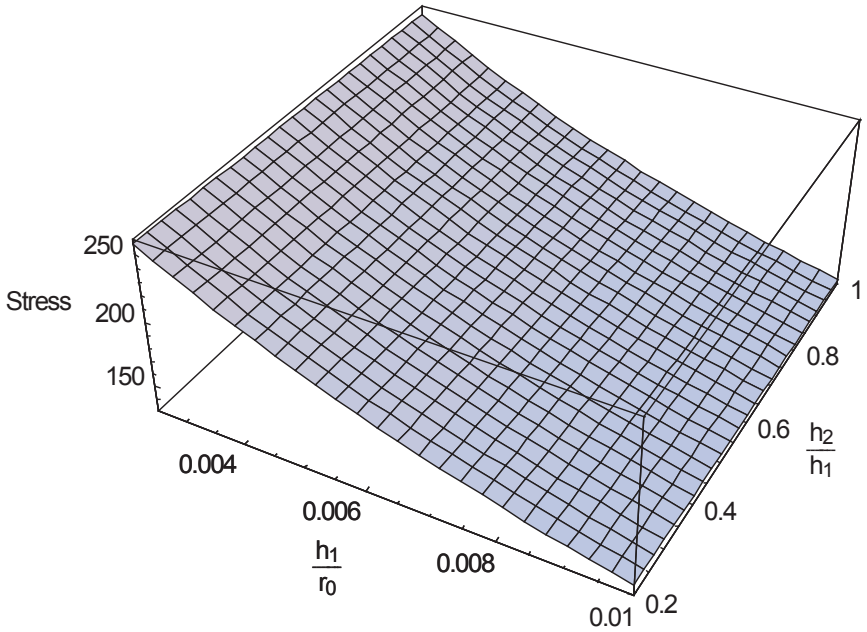

Figure 3.42: Steel-Water-Composite (a=0.9), Maximum Outer Shell Stress (MPa)

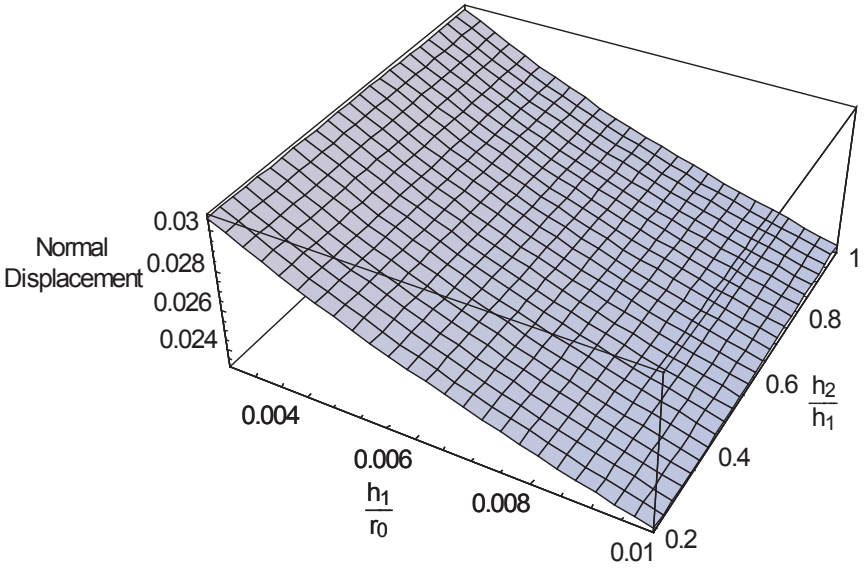

Figure 3.43: Steel-Water-Composite (a=0.9), Maximum Inner Shell Normal Displacement

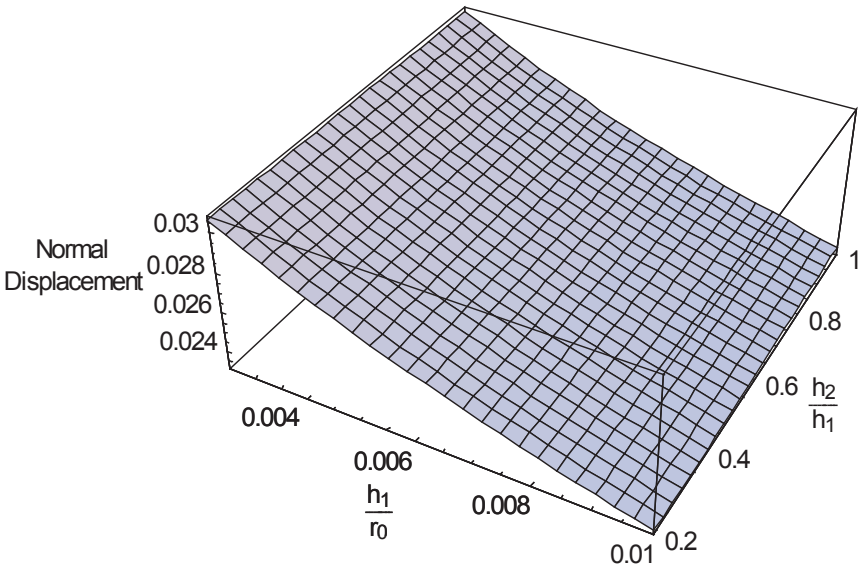

Figure 3.44: Steel-Water-Composite (a=0.9), Maximum Outer Shell Normal Displacement

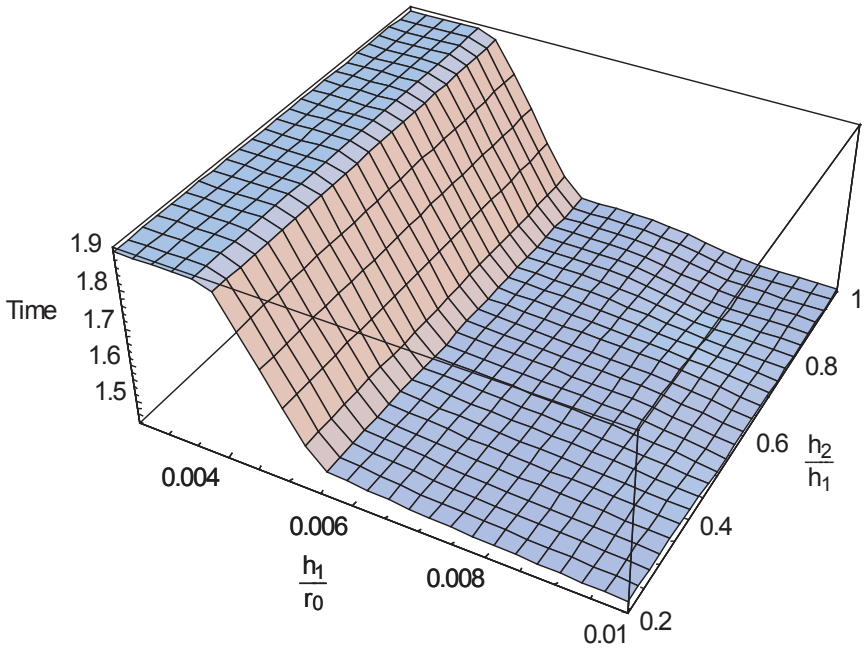

Figure 3.45: Steel-Water-Composite (a=0.9), Timing of Maximum Inner Shell Stress (Dimentionless)

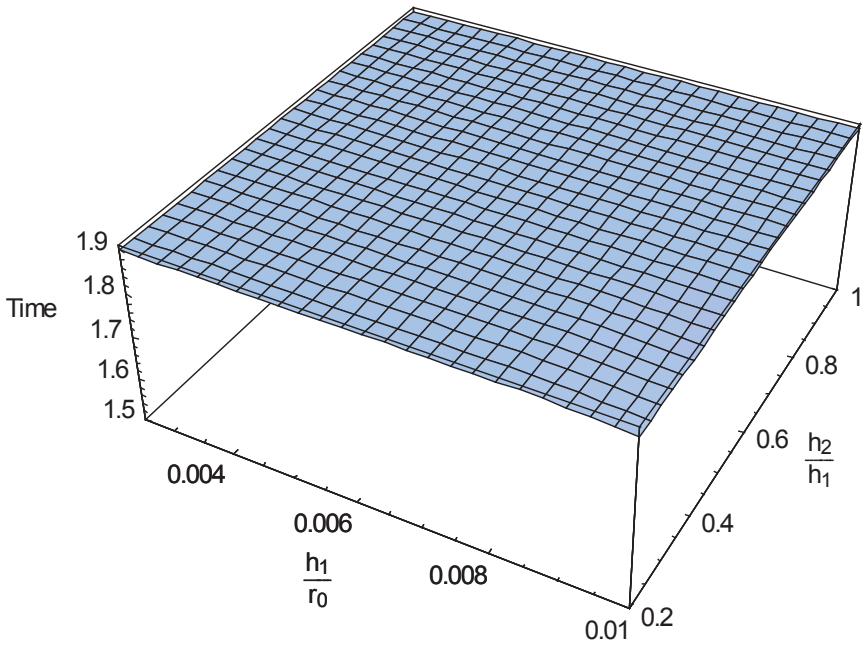

Figure 3.46: Steel-Water-Composite (a=0.9), Timing of Maximum Outer Shell Stress (Dimentionless)

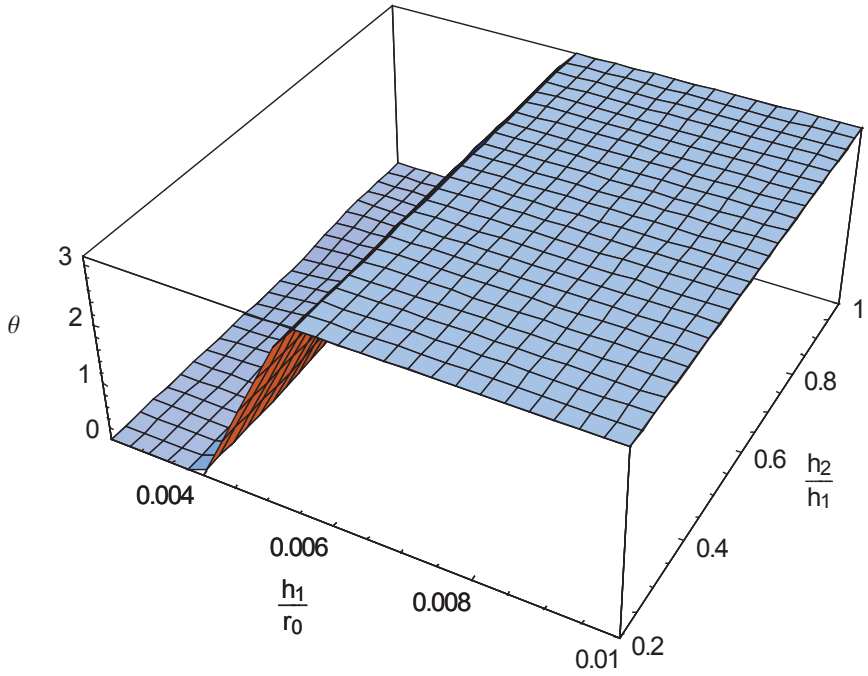

Figure 3.47: Steel-Water-Composite (a=0.9), Location of Maximum Inner Shell Stress (Radians)

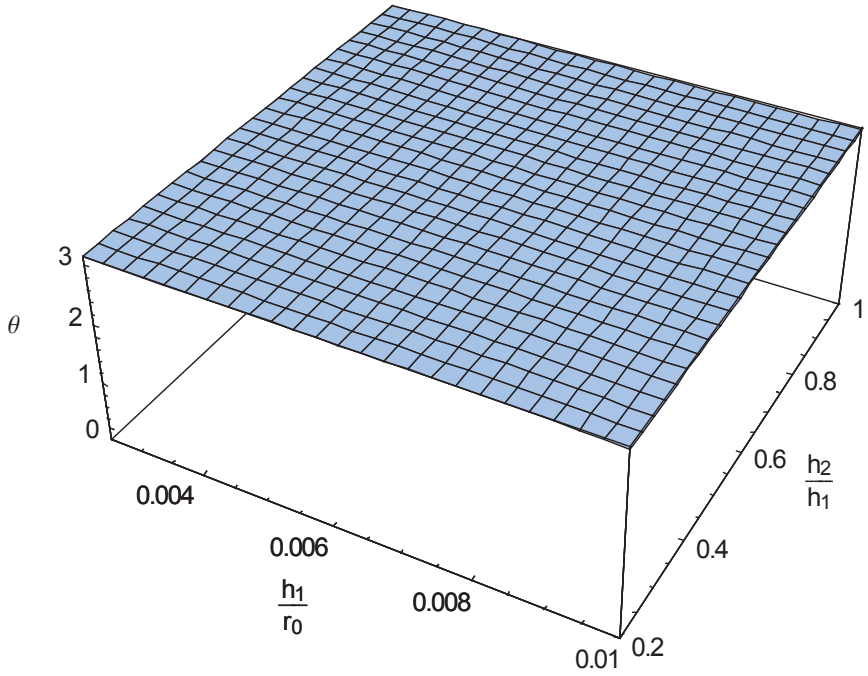

Figure 3.48: Steel-Water-Composite (a=0.9), Location of Maximum Outer Shell Stress (Radians)

Chapter 4

Individual Variable Analysis

4.1 Overview

To understand the effects of each variable, direct comparisons were made between the cases to highlight the differences within the results. For the steel-water-composite and steel-diesel-steel cases, the sets were compared with the baseline steel-water-steel case. For the differences caused by the geometry, the small inter-hull space models were compared against their large inter-hull space counterparts. For all of the cases, these comparisons were done by taking the maximum stress and maximum normal displacement results and dividing them by their baseline counterparts to create a ratio of change. These ratios allowed for visualization of the changes, indicating when the variables had a large impact and when their effects were small. The resulting graphics give a sense of the overall difference between the cases, while also containing information of smaller, localized fluctuations.

4.2 Internal Fluid Analyis

To study the effect of the internal fluid on the model, diesel and water were both used as the liquid medium between the inner and outer shells. The models were identical except for the changes to the internal fluid variables. The baseline model had density $\rho_i = 1000kg/m^3$ and sound speed $c_i = 1400m/s$ to simulate water, whereas the alternative model had density $\rho_i = 880kg/m^3$ and sound speed $c_i = 1250m/s$ to simulate diesel. The comparison was done by taking the maximum stress and normal displacement values of the diesel results and dividing them by those of the steel results to create a ratio between the two. These comparisons can be seen in Figures 4.1 to 4.8.

4.2.1 Inner Shell Stress Comparison: Diesel

The first two graphics, Figure 4.1 and Figure 4.2, show the steel-diesel-steel to steel-water-steel stress ratios for the inner shell of the $a = 0.5$ and $a = 0.9$ cases. These two images show how the stress on the inner shell changes after the shockwave has passed through the new fluid medium. In both cases, the ratio starts out low when the shells are thinnest, and increases as the shell thickness increases, but the particulars of that increase, as well as the scale, sets the two apart. When the inter-hull space is large, the internal fluid appeared to have had a lesser effect on the inner shell stress. The difference between the two models was limited to a range of approximately -2% when the shells are thin, to $+5\%$ as the shells initially become thicker, leveling out to about $+3\%$. Here there is not a definite trend in the ratio with respect to the thickness of the shells; the ratio starts near unity, sees a sharp increase, then declines slightly as the thickness is increased. Overall the inner shell appeared to experience slightly more stress as a result of the internal fluid changing to diesel, but the effect is fairly minor. When the inter-hull space is small, however, the internal fluid appeared to have a larger effect on the inner shell stress. The relative difference between these models show a range of about -10% when the shells are thinnest, to $+11\%$ when the shells are thickest. A possible explanation for this behavior relates back to the location and timing of where the peaks happen. The decrease corresponds to a situation where the maximum stress was a superposition of internal waves between the shells, so the diesel isn't able to propogate the waves as well as water, while the increase occurs when the maximum is a result of the oncoming impact, where the diesel doesn't absorb as much of the impact.

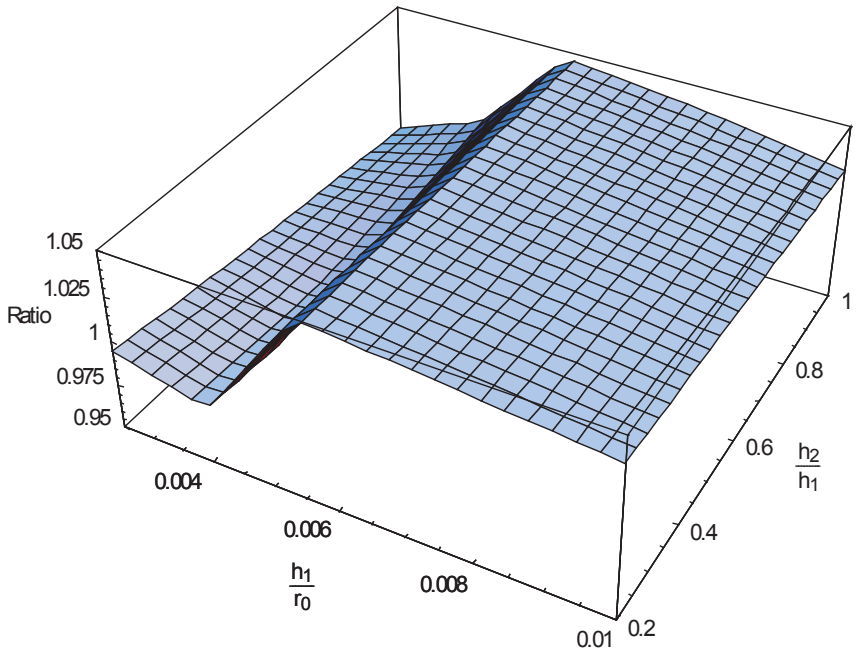

Figure 4.1: Inner Shell Stress Ratio of Steel-Diesel-Steel (a=0.5), to Steel-Water-Steel (a=0.5)

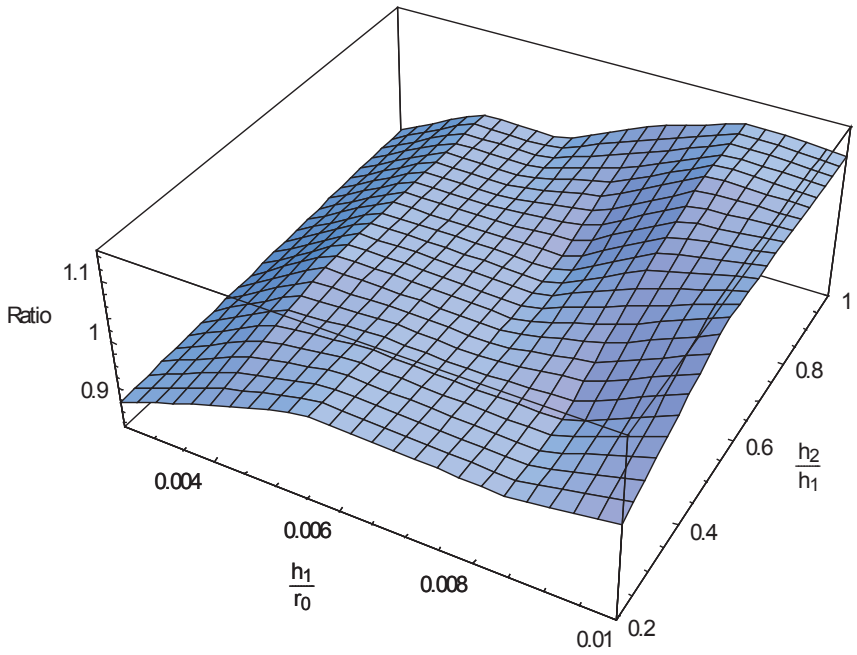

Figure 4.2: Inner Shell Stress Ratio of Steel-Diesel-Steel (a=0.9), to Steel-Water-Steel (a=0.9)

4.2.2 Outer Shell Stress Comparison: Diesel

Figure 4.3 and Figure 4.4 show the steel-diesel-steel to steel-water-steel stress ratios for the outer shells of the $a = 0.5$ and $a = 0.9$ cases respectively. The ratios here show a similar trend as their inner shell counterparts, but the values themselves are quite different. When the inter-hull space is large, the internal fluid seemed to have a larger effect on the outer shell stress. The difference between the diesel and the water models ranges from about +10% to approximately +18%. This varied a bit, tending toward the lower end when the inner shell was thinner, but overall the change in the internal fluid caused an increase in the outer shell stress for this model. This is likely a result of the internal fluid acting as a backing medium for the outer shell when the shockwave makes contact with it, and in this regard is not a suprising result. When the inter-hull space is small, the internal fluid did not have as much of an effect on the outer shell stress. Here the difference between the models ranges from 0% to +4%. There does appear to be some correllation with the shell thickness here, but it is not as promenant as seen with the inner shell. Like the large inter-hull space model, the general increase in stress may be a result of the internal fluid's role as a backing medium when the outer shell interacts with the external shockwave, and the lesser effect may be a result of less fluid present when the inter-hull space is small.

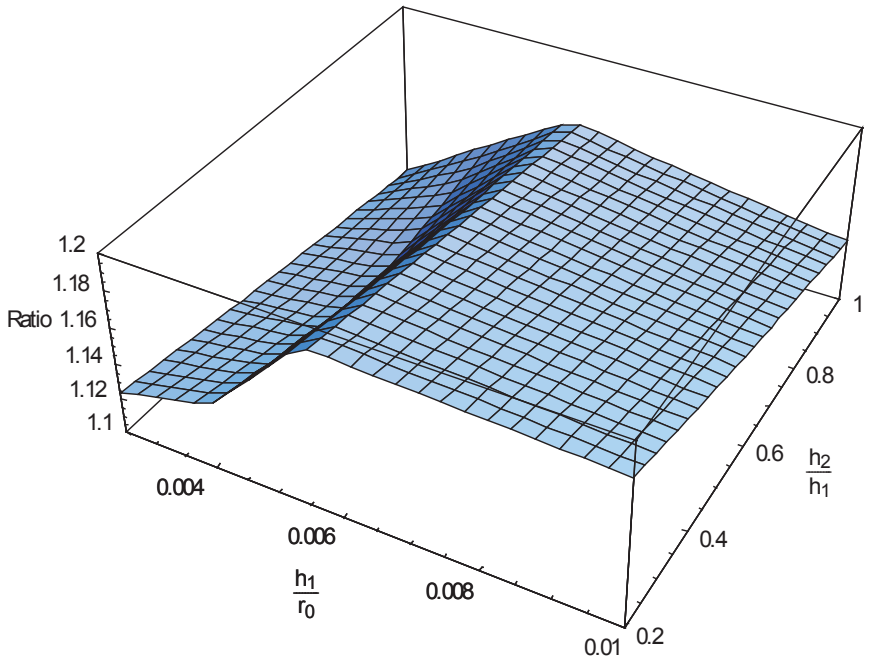

Figure 4.3: Outer Shell Stress Ratio of Steel-Diesel-Steel (a=0.5), to Steel-Water-Steel (a=0.5)

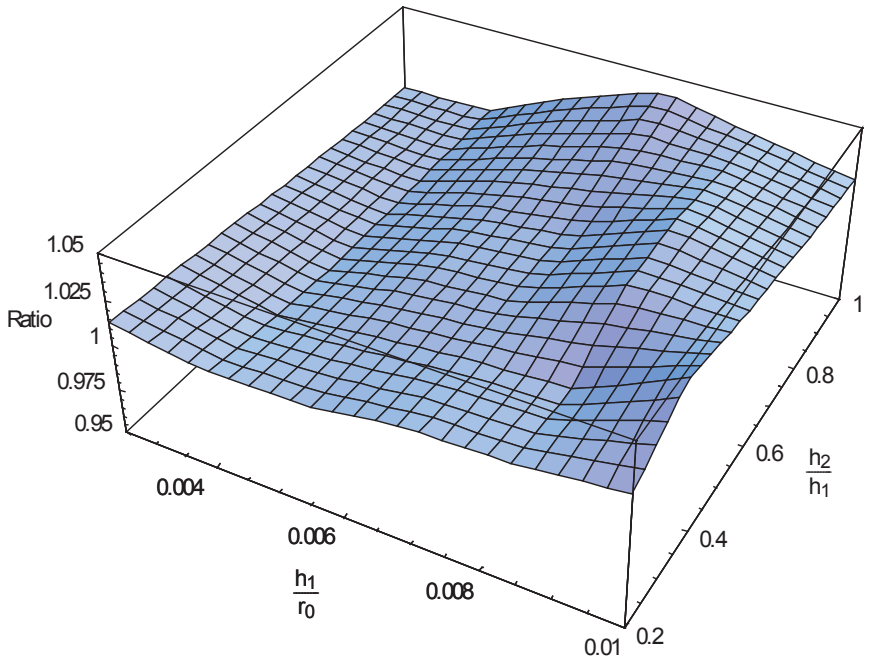

Figure 4.4: Outer Shell Stress Ratio of Steel-Diesel-Steel (a=0.9), to Steel-Water-Steel (a=0.9)

4.2.3 Inner Shell Normal Displacement Comparison: Diesel

Figure 4.5 and Figure 4.6 show the steel-diesel-steel to steel-water-steel normal displacement ratios for the inner shells of the $a = 0.5$ and $a = 0.9$ cases. The behaviour of the two shells here is quite different, with one case showing a trend with respect to shell thickness, and the other showing a largely constant result. When the inter-hull space is large the effect of the changing internal fluid seems to have had a mostly constant effect. The difference between the steel-diesel-steel and steel-water-steel cases here is limited to a small range of about +3.5% to +4.5%. While there is some variation in the figure, the results do not suggest an overall trend. The normal displacement results for when the space is small look very different, with a trend correllating with inner shell thickness. The diesel model had a lower normal displacement when the inner shell is thin, but as the thickness increased the results become essentially the same. The overall scale of the difference is, however, quite small, ranging from -3% when the inner shell is at it's thinnest to 0% when the shell is at it's thickest, suggesting a relatively minor effect overall.

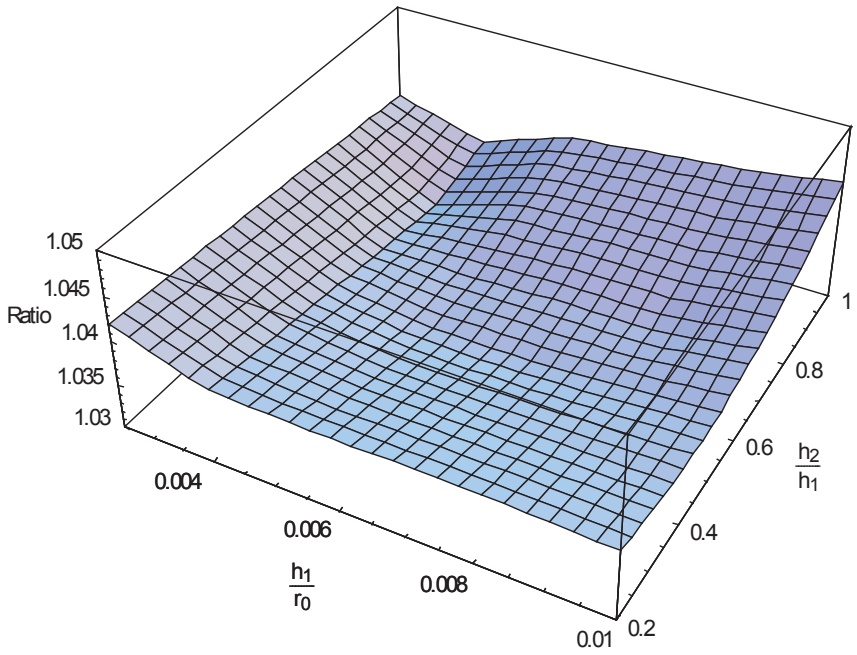

Figure 4.5: Inner Shell Normal Displacement Ratio of Steel-Diesel-Steel (a=0.5), to Steel-Water-Steel (a=0.5)

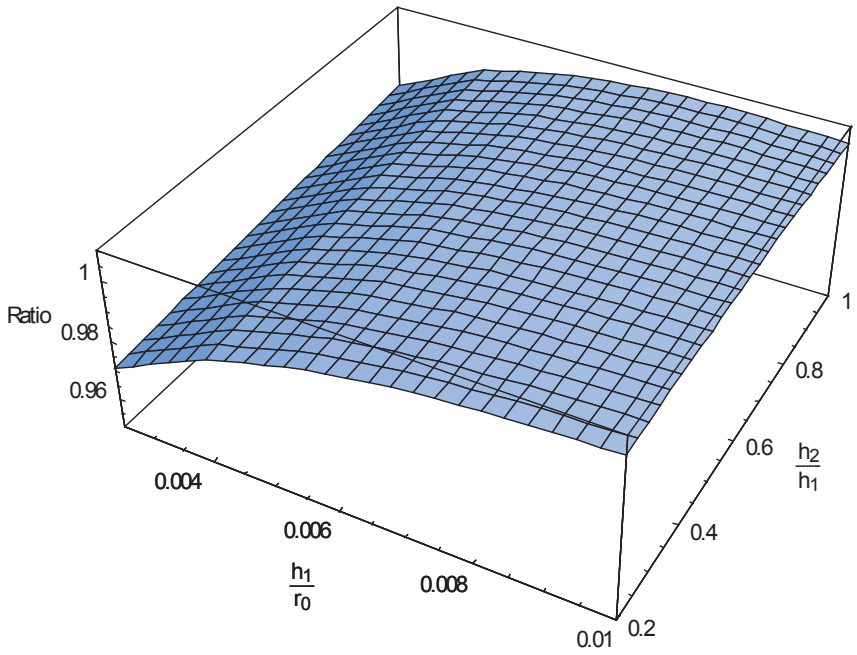

Figure 4.6: Inner Shell Normal Displacement Ratio of Steel-Diesel-Steel (a=0.9), to Steel-Water-Steel (a=0.9)

4.2.4 Outer Shell Normal Displacement Comparison: Diesel

Figure 4.7 and Figure 4.8 show the steel-diesel-steel to steel-water-steel normal displacement ratios for the outer shells of the $a = 0.5$ and $a = 0.9$ cases. The two figures are very similar, both indicating that the displacement in the outer shell increases for all shell thicknesses when the internal fluid is changed to diesel. When the inter-hull space is large the displacement of the steel-diesel-steel model sees an increase ranging from +7% to +5.5% relative to the steel-water-steel case, a tight range of differences much like the inner shell experienced. However, when the inter-hull space is small the effect of the internal fluid does appear to vary with thickness. Here the difference between the two models ranges from +5.5% when the shells are thinnest, to +1% when the shells are thickest. There is an overall trend that with increasing thickness the results of the two models become more similar, though the steel-diesel-steel results are at all points higher than the steel-water-steel results. A possible explanation for this is that as the shells get thicker and thus more rigid, the effect of the backing fluid has less of an impact on strain.

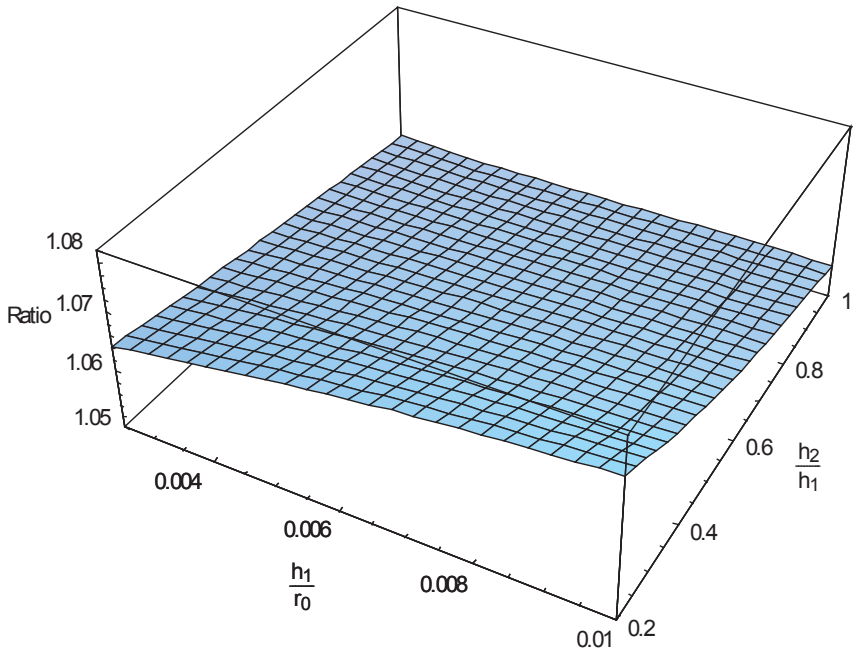

Figure 4.7: Outer Shell Normal Displacement Ratio of Steel-Diesel-Steel (a=0.5), to Steel-Water-Steel (a=0.5)

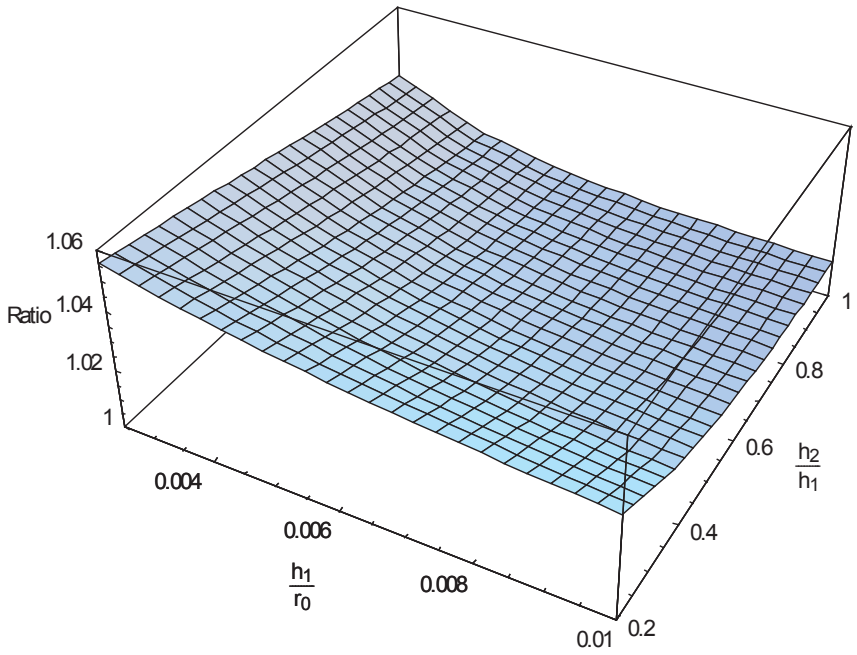

Figure 4.8: Outer Shell Normal Displacement Ratio of Steel-Diesel-Steel (a=0.9), to Steel-Water-Steel (a=0.9)

4.3 Composite External Shell Analysis

To study the effect of the external shell in greater detail, two different materials were used to model the external shells. The baseline model used an external shell made of steel to match the internal shell, while the alternative model used a composite material for the external shell. The models were identical except for the change of shell material. The baseline model had density $\rho_2 = 7800kg/m^3$, sound speed $c_2 = 5000m/s$, and Poisson's ratio $\nu_2 = 0.3$ to simulate steel, whereas the alternative model had density $\rho_2 = 1800kg/m^3$, sound speed $c_2 = 3430m/s$, and Poisson's ratio $\nu_2 = 0.15$ to simulate the composite material. The comparison was done by taking the maximum stress and normal displacement values of the composite results and dividing them by those of the steel results to create a ratio between the two. These comparisons can be seen in Figures 4.9 to 4.16.

4.3.1 Inner Shell Stress Comparison: Composite

Figure 4.9 and 4.10 show the steel-water-composite to steel-water-steel stress ratios for the inner shell of the $a = 0.5$ and $a = 0.9$ cases. These graphics show how the stress on the inner shell changes as a result of the shockwaves passing through a much lighter external shell. The results of both cases are very similar, and both make sense given the changes that were made to the model. When the inter-hull space is large the relative difference between the composite model and the steel model increases gradually as the external shell thickness is increased. This difference ranges from +1% when the external shell is thinnest, to around +10% when the external shell is thickest; the internal shell stress for the composite case being higher at all points. Presumably the steel external shell is providing a greater barrier to the shockwave than the composite shell, which is why the difference between cases increases with thickness. The trend is the same for both small and large amounts of inter-hull space, however, the magnitude of the difference increases when the inter-hull space is small, ranging from around +3% when the external shell is thinnest to a maximum of +30% when the external shell is thickest. Once again at all points the internal shell of the composite case is under more stress than the steel case, but the difference between cases is about three times larger. This also makes sense; as before, a steel external shell absorbs more than a composite one, but here, without a large fluid medium between the two shells, this external shell effect is a larger part of the interaction.

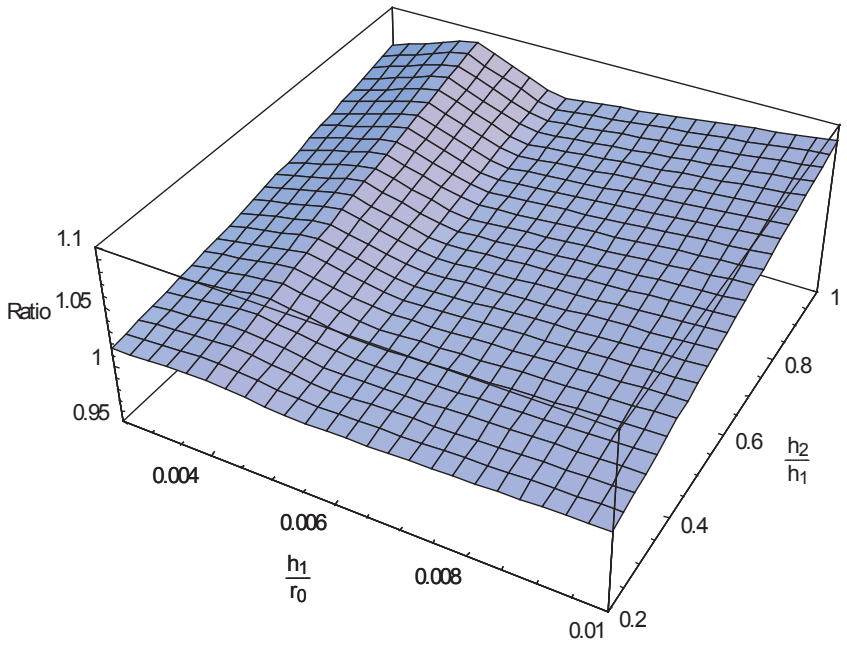

Figure 4.9: Inner Shell Stress Ratio of Steel-Water-Composite (a=0.5), to Steel-Water-Steel (a=0.5)

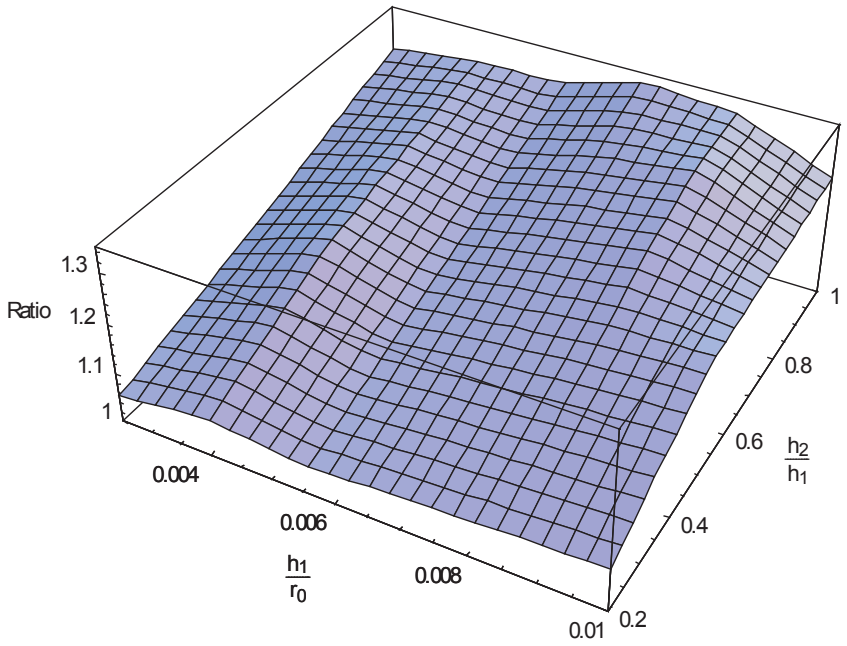

Figure 4.10: Inner Shell Stress Ratio of Steel-Water-Composite (a=0.9), to Steel-Water-Steel (a=0.9)

4.3.2 Outer Shell Stress Comparison: Composite

Figure 4.11 and 4.12 show the steel-water-composite to steel-water-steel stress ratios for the outer shell of the $a = 0.5$ and $a = 0.9$ cases. These graphics show the differences in stress carried by the two outer shell materials. The cases here differ by almost an order of magnitude, clearly setting these results apart from the others. The results are not suprising considering how different the two materials actually are. For the case where the inter-hull space is large the difference ranges from -87% to -82%. When the inter-hull space is small the difference ranges from -85% to -82%.

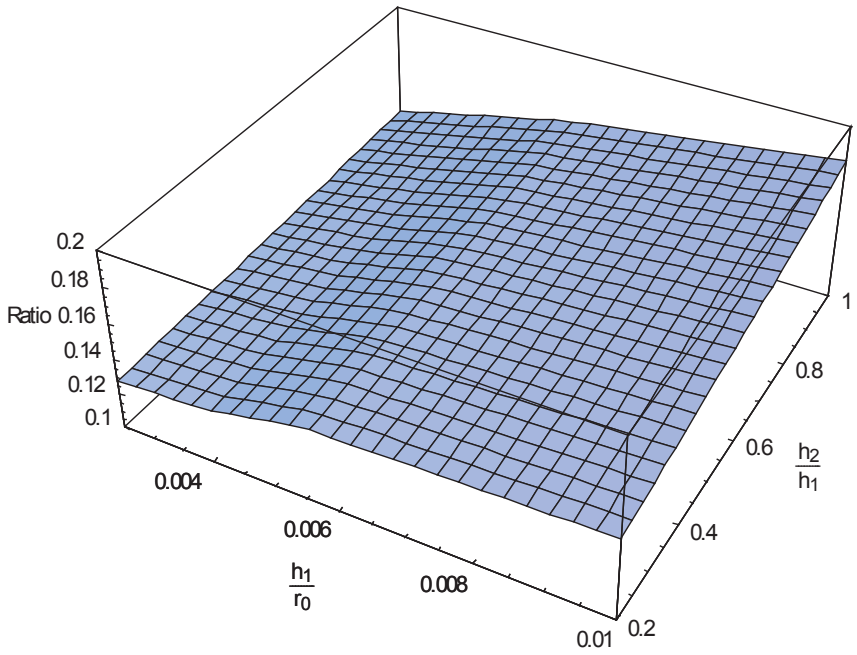

Figure 4.11: Outer Shell Stress Ratio of Steel-Water-Composite (a=0.5), to Steel-Water-Steel (a=0.5)

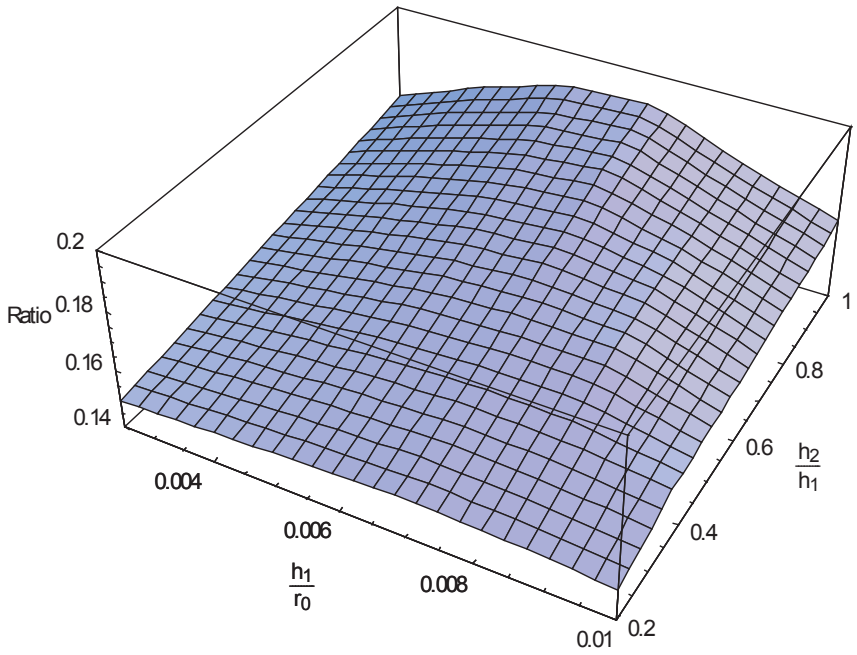

Figure 4.12: Outer Shell Stress Ratio of Steel-Water-Composite (a=0.9), to Steel-Water-Steel (a=0.9)

4.3.3 Inner Shell Normal Displacement Comparison: Composite

Figures 4.13 and 4.14 show the steel-water-composite to steel-water-steel normal displacements for the inner shells of the $a = 0.5$ and $a = 0.9$ geometries. The two figures show a similar trend as the shell thicknesses change, which suggests a straightforward relationship. In the first figure when the inter-hull space is large the difference between the cases ranges from +0% when the shells are at their thinnest, to +14% when the shells are thickest. Basically, the internal shell of the steel-water-composite case is displaced more relative to the steel-water-steel case the thicker the external shell is. This fits with what would be expected from using a lighter material for the external shell, as it absorbs less energy than a heavier shell would. In the second figure, when the inter-hull space is small, the difference between the paired cases is larger, ranging from +1% when the shells are thinnest to +21% when the shells are thickest. The difference is larger likely because when the shells are closer, and there isn't as much internal fluid present, the external shell plays a greater role in absorbing energy from the incoming shockwave.

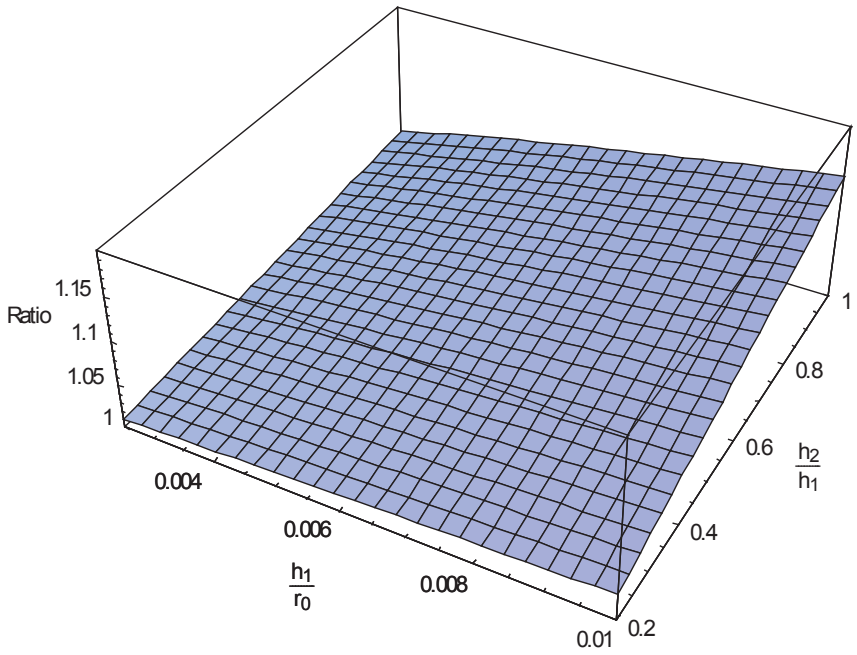

Figure 4.13: Inner Shell Normal Displacement Ratio of Steel-Water-Composite (a=0.5), to Steel-Water-Steel (a=0.5)

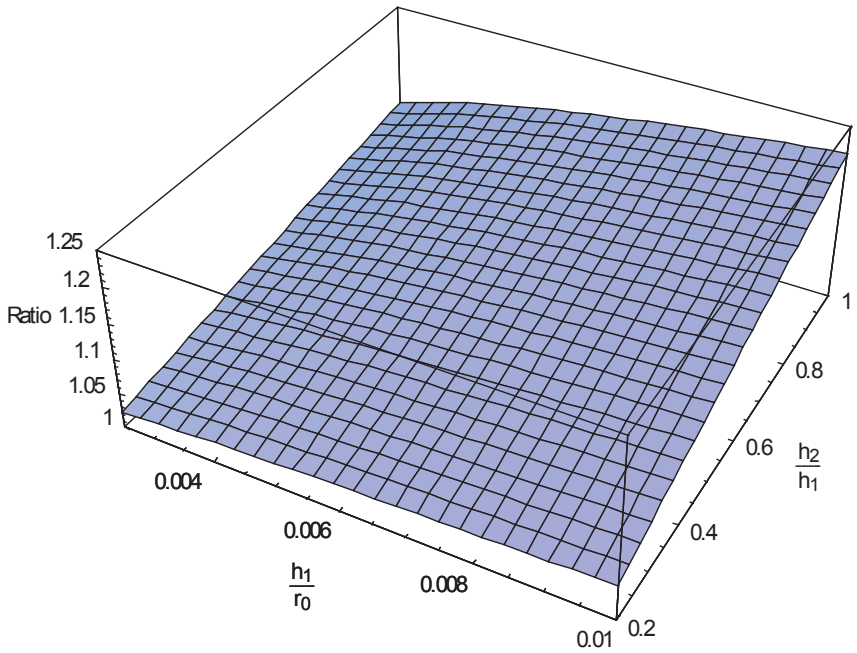

Figure 4.14: Inner Shell Normal Displacement Ratio of Steel-Water-Composite (a=0.9), to Steel-Water-Steel (a=0.9)

4.3.4 Outer Shell Normal Displacement Comparison: Composite

Figure 4.15 and 4.16 show the steel-water-composite to steel-water-steel normal displacements for the outer shells of the $a = 0.5$ and $a = 0.9$ geometries. The two figures are similar and show a trend much like the inner shells. When the shells are thinnest, the difference between the steel-water-composite and steel-water-steel cases is small, when the shells are thickest the difference is large.The difference between the cases ranges from +0% to +15% for the large inter-hull space and from +0% to +17% for the small inter-hull space. The reason the two results are so similar is likely because the displacements here are largely the result of the incoming wave and are affected minimally by the proximity of the two shells.

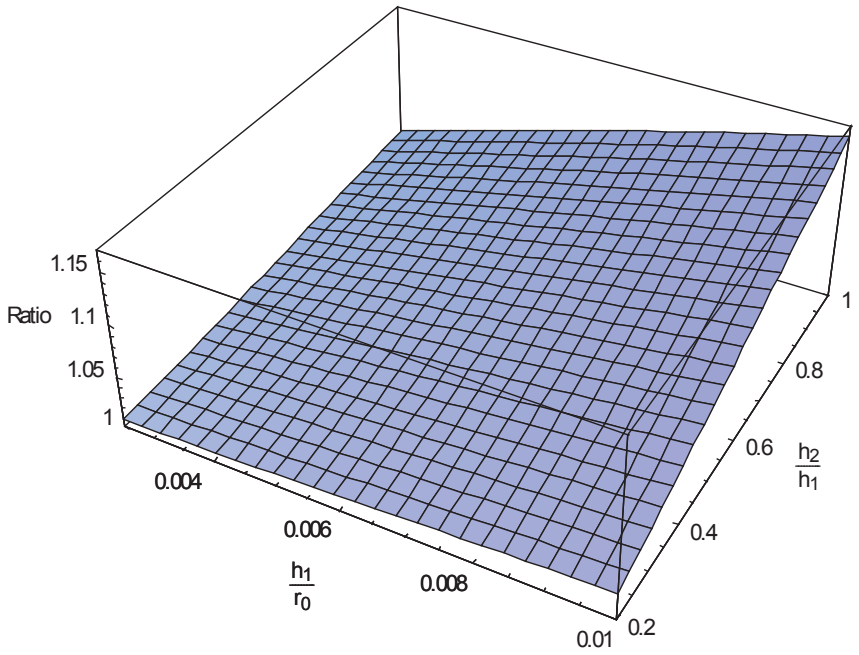

Figure 4.15: Outer Shell Normal Displacement Ratio of Steel-Water-Composite (a=0.5), to Steel-Water-Steel (a=0.5)

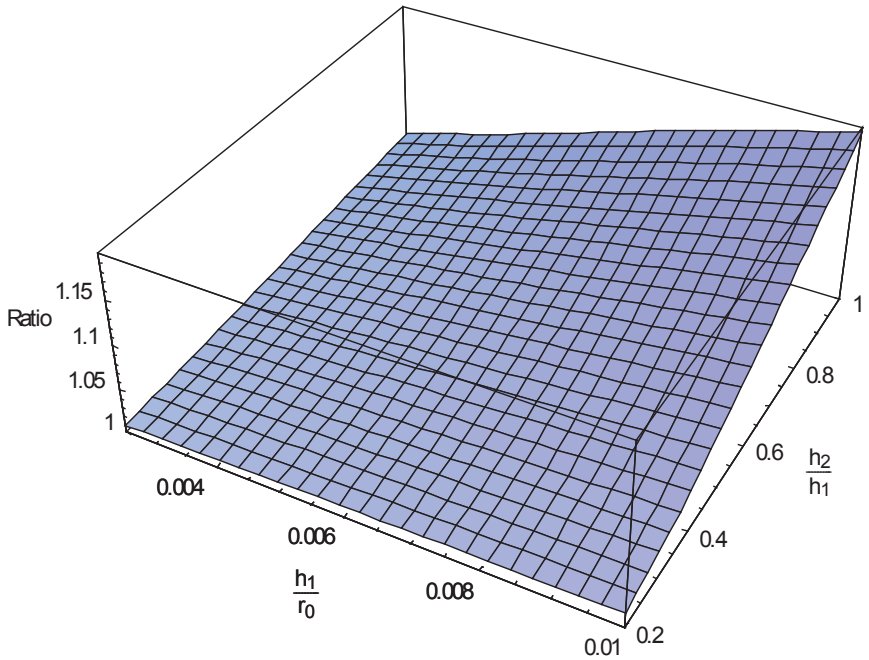

Figure 4.16: Outer Shell Normal Displacement Ratio of Steel-Water-Composite (a=0.9), to Steel-Water-Steel (a=0.9)

4.4 Geometry Analysis

To study the effect of the the shell geometry, every case was done using two distinct shell configurations. Only two configurations were used because each requires its own response function to be pre-calculated, and simulations to be run separately for each geometry. The first model used was one where the distance separating the two shells was large. Here the inner shell radius was set at $a = 0.5$, 50% of the dimentionless outer shell radius of $r_0 = 1$. The second model was one where the distance between the shells was small, the inner shell radius was set at $a = 0.9$, 90% of the outer shell radius. Each of the different material and fluid configurations were first run using the $a = 0.5$ geometry, then repeated for $a = 0.9$. Here, those results will be paired and compared to each other to better understand how the change in geometry effects the model in the presense of other variables. The results of these comparisons can be seen in Figures 4.17 to 4.28. Results were obtained by normalizing the $a = 0.9$ results to the $a = 0.5$ results to obtain a ratio of change between the two. These ratios were then plotted with respect to shell thicknesses on three-dimensional figures.

4.4.1 Inner Shell Stress Comparison: Geometry

Figures 4.17, 4.18, and 4.19 show the differences between the inner shell stress of the $a = 0.9$ and $a = 0.5$ models for the steel-water-steel, steel-diesel-steel, and steel-water-composite cases. Figure 4.17, representing the steel-water-steel cases, does not show any obvious trend with shell thickness. The relative differences range from -10% to $+8\%$, fluctuating up and down as the thicknesses change. Figure 4.18, representing the steel-diesel-steel cases, is similar. The relative differences here range from $-**\%$ to $+5\%$, and follow a similar pattern as the steel-water-steel cases. Once again there is no obvious trend correllating with shell thickness. Figure 4.19, representing the steel-water-composite cases, breaks the previous pattern. Rather than the results ranging from positive to negative, the relative difference ranges from $+2\%$ to $+13\%$. This means that for all thicknesses the $a = 0.9$ case experienced a greater stress than the $a = 0.5$ case. The composite results do however mimic the steel and diesel results in that the peak is at a similar location. All three cases experience peaks when the outer shell is at it's thinnest and $\frac{h_1}{r_0} = 0.004$. Other than this similarity there does not appear to be any clear correllation between shell thickness and the effect of changing the distance between shells.

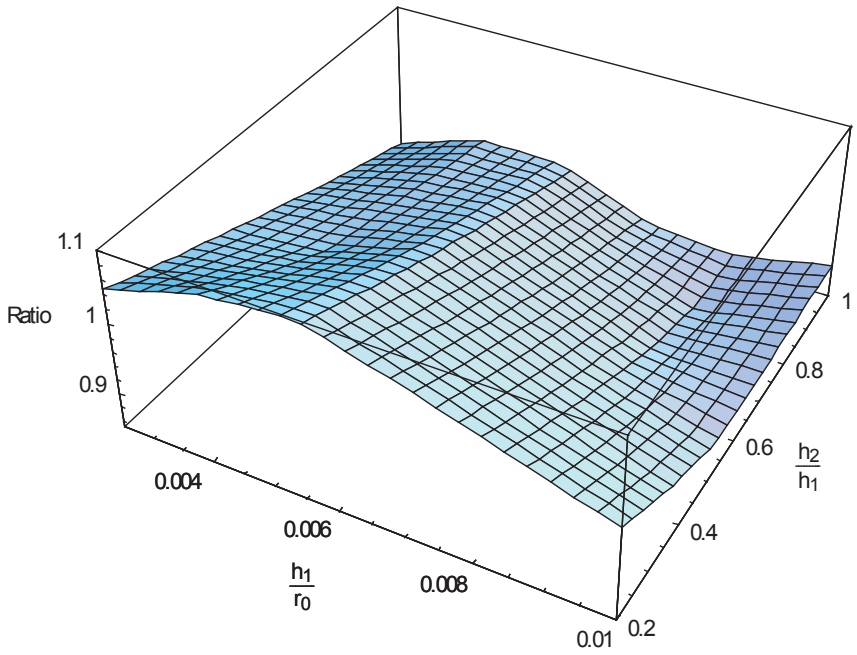

Figure 4.17: Inner Shell Stress Ratio of Steel-Water-Steel (a=0.9), to Steel-Water-Steel (a=0.5)

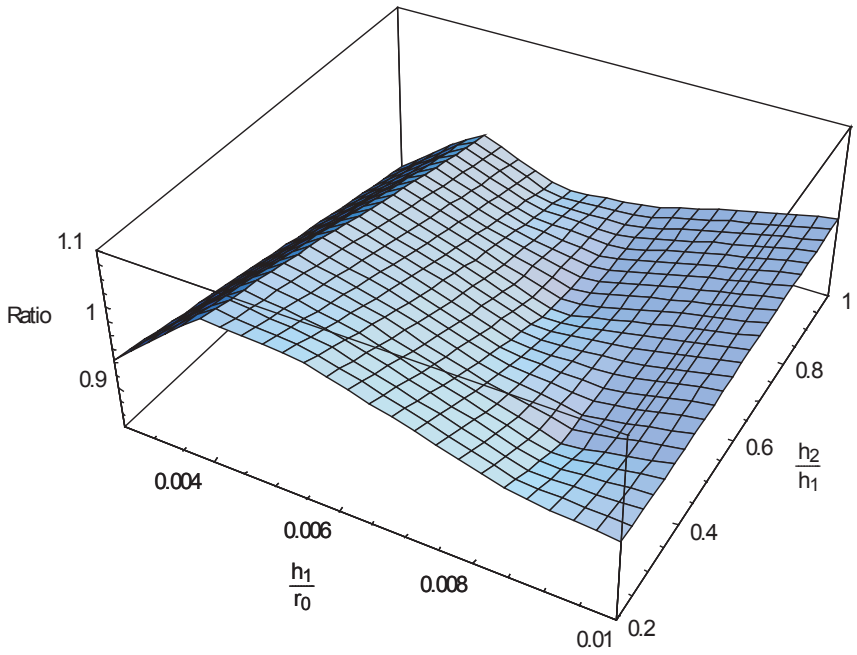

Figure 4.18: Inner Shell Stress Ratio of Steel-Diesel-Steel (a=0.9), to Steel-Diesel-Steel (a=0.5)

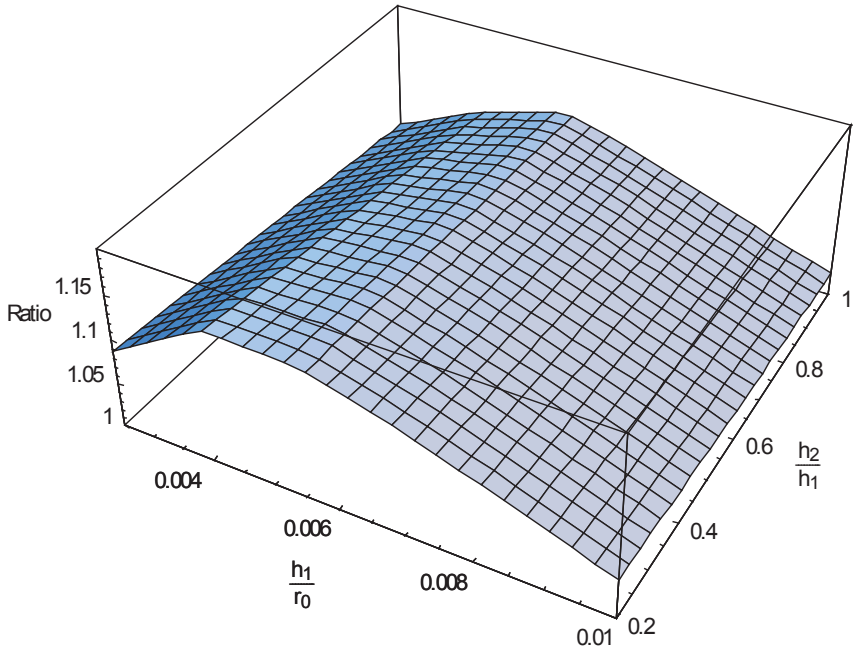

Figure 4.19: Inner Shell Stress Ratio of Steel-Water-Composite (a=0.9), to Steel-Water-Composite (a=0.5)

4.4.2 Outer Shell Stress Comparison: Geometry

Figures 4.20, 4.21, and 4.22 show the differences between the outer shell stress of the $a = 0.9$ and $a = 0.5$ models for the steel-water-steel, steel-diesel-steel, and steel-water-composite cases. All three figures for this shell show a similar pattern, with the ratio starting high and decreasing as the inner shell thickness increases. Figure 4.20, representing the steel-water-steel cases, shows a very clear relation between the inner shell thickness and the effect of the change in geometry on the outer shell. The relative difference here ranges from +60% when the inner shell is thinnest and decreases steadily as the shell becomes thicker to around +10% when the shell is thickest. A similar result can be seen in Figure 4.21, representing the steel-diesel-steel cases. Here the trend is the same though the values are slightly reduced, having a relative difference ranging from +42% to +0%. The third case shown in Figure 4.22 also has the same trend, though the values are higher, with the relative difference ranging from +90% to +9%. All three cases indicate that changing the geometry increases the stress on the outer shell. This effect is greatest when the inner shell is thin, and decreases as the inner shell is made thicker. The effect is reduced slightly when diesel is used as the internal fluid, but increases when the steel outer shell is replaced with a composite material. Additionally, the outer shell thickness seems to have only a minor effect on the relative stress in the steel-water-steel and steel-diesel-steel cases. For these models, increasing the outer shell thickness decreases the relative stress when the inner shell is thin, and increases the relative stress when the inner shell is thick. This effect does not appear in the steel-water-composite case, where the effect of the outer shell thickness is minimal at all thicknesses.

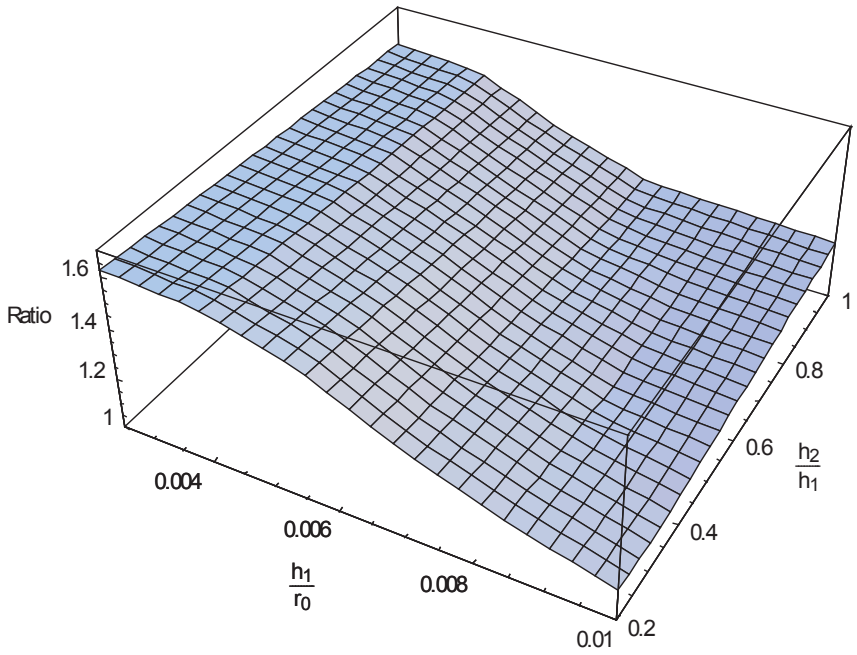

Figure 4.20: Outer Shell Stress Ratio of Steel-Water-Steel (a=0.9), to Steel-Water-Steel (a=0.5)

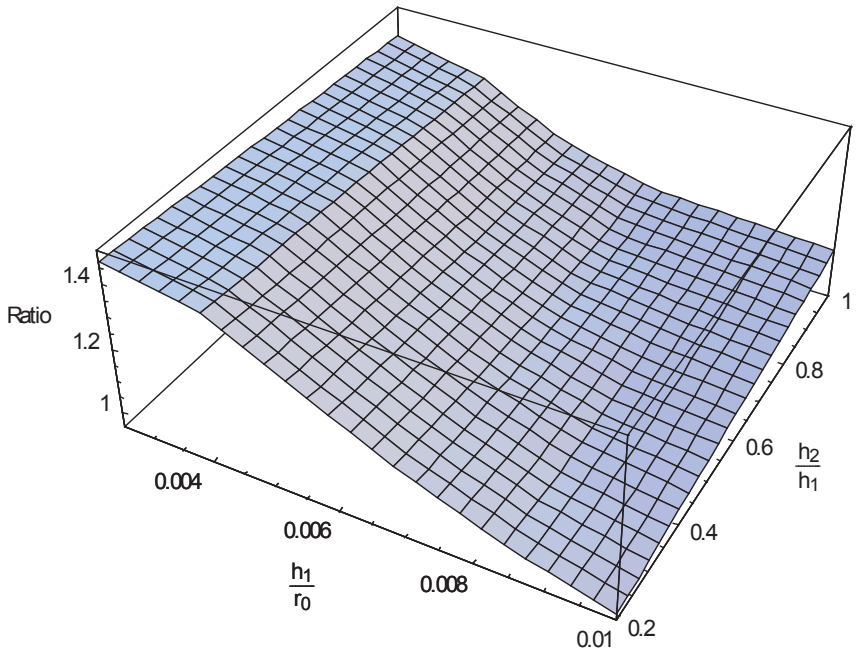

Figure 4.21: Outer Shell Stress Ratio of Steel-Diesel-Steel (a=0.9), to Steel-Diesel-Steel (a=0.5)

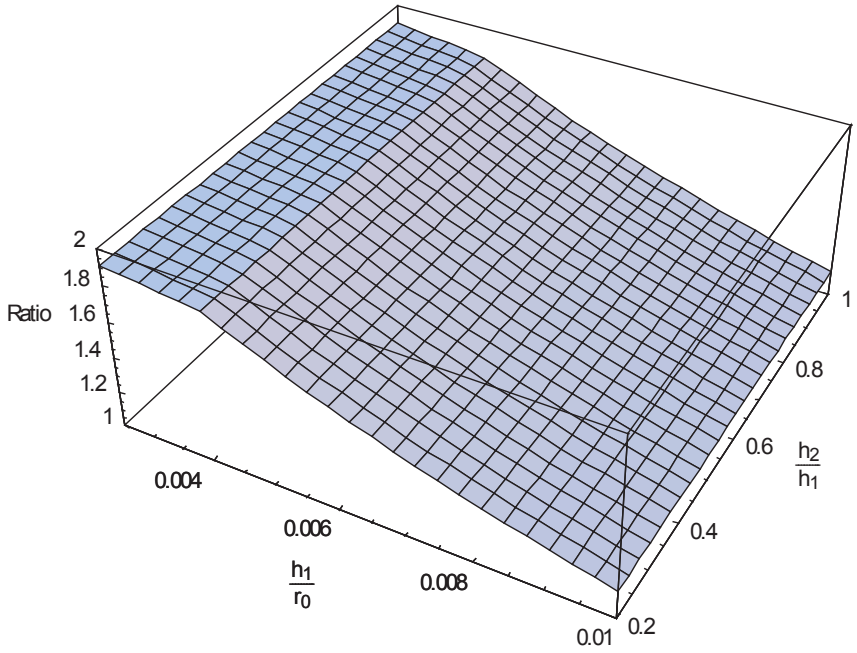

Figure 4.22: Outer Shell Stress Ratio of Steel-Water-Composite (a=0.9), to Steel-Water-Composite (a=0.5)

4.4.3 Inner Shell Normal Displacement Comparison: Geometry

Figures 4.23, 4.24, and 4.25 show the differences between the inner shell normal displacement of the $a = 0.9$ and $a = 0.5$ models for the steel-water-steel, steel-diesel-steel, and steel-water-composite cases. For the two different geometries, all three sets of cases show a similar pattern of increasing displacement as the inner shell thickness is increased. Figure 4.23 shows the steel-water-steel case, with displacement increases ranging from +46% when the inner shell is thinnest to +65% when it's thickest. Also present is a slight trend of decreasing displacement as the outer shell is made thicker. These trends also appear in the steel-diesel-steel case, seen in Figure 4.24. The diesel case does have a slightly lower range, however, with the displacement varying from +37% to +60%. The trend continued in the steel-water-composite case, seen in Figure 4.25. Here the displacements are slightly larger, ranging from +50% when the inner shell is thin to +65% when the shell is thick. No trend with respect to outer shell thickness is present in this case.

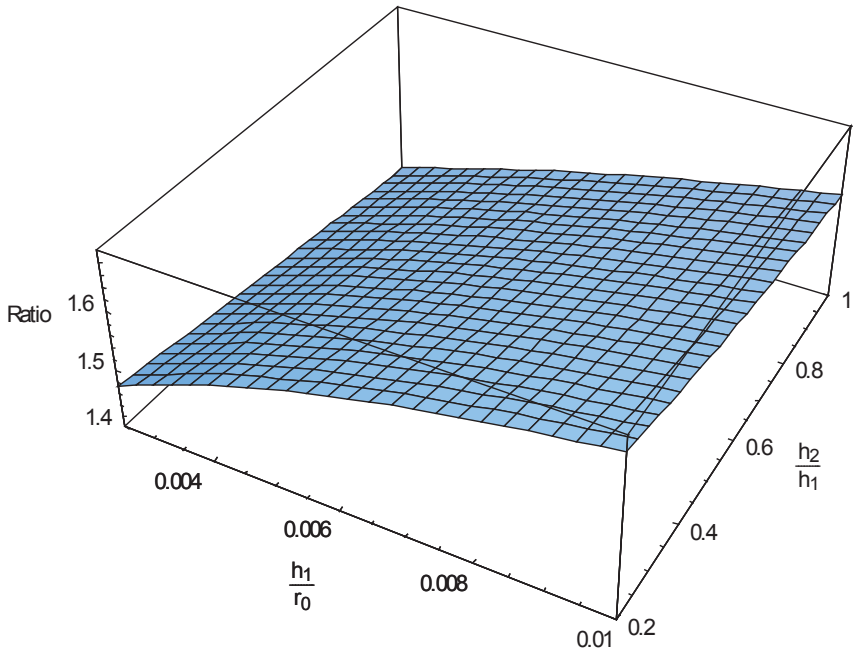

Figure 4.23: Inner Shell Normal Displacement Ratio of Steel-Water-Steel (a=0.9), to Steel-Water-Steel (a=0.5)

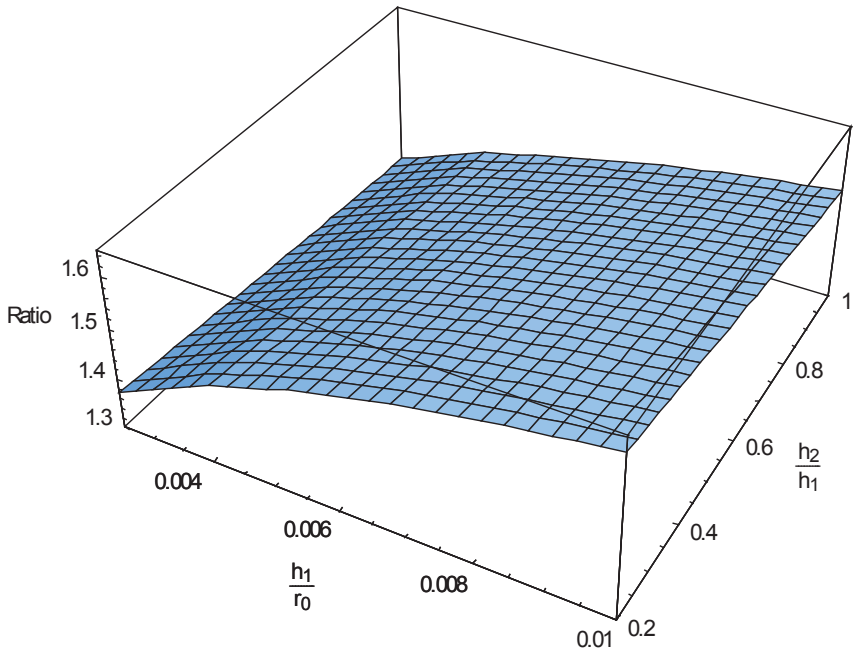

Figure 4.24: Inner Shell Normal Displacement Ratio of Steel-Diesel-Steel (a=0.9), to Steel-Diesel-Steel (a=0.5)

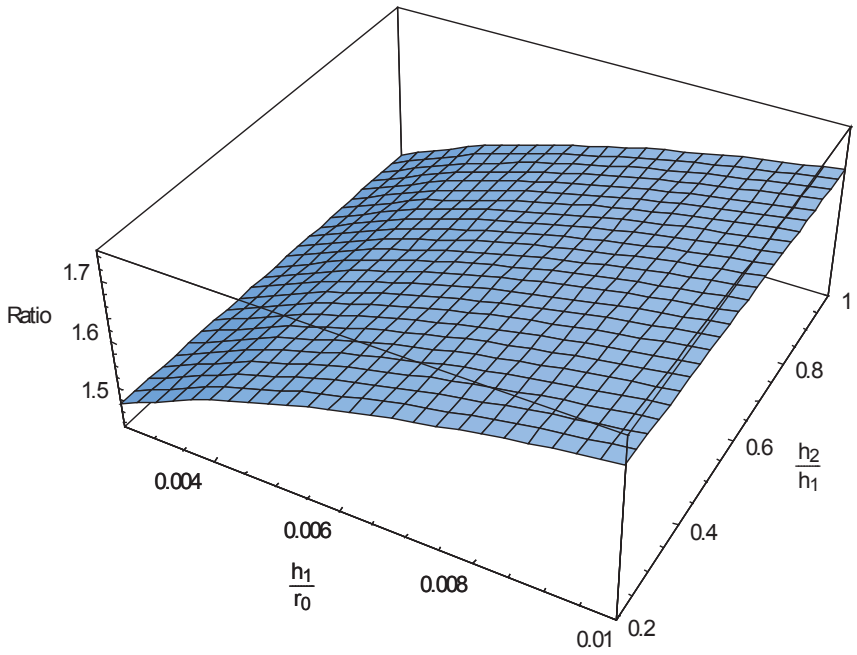

Figure 4.25: Inner Shell Normal Displacement Ratio of Steel-Water-Composite (a=0.9), to Steel-Water-Composite (a=0.5)

4.4.4 Outer Shell Normal Displacement Comparison: Geometry

Figures 4.26, 4.27, and 4.28 show the differences between the outer shell normal displacement of the $a = 0.9$ and $a = 0.5$ models for the steel-water-steel, steel-diesel-steel, and steel-water-composite cases. The results here are almost identical for all three cases, with only minor differences between each. Figure 4.26 shows the steel-water-steel case results, and indicates the general pattern. Here, reducing the distance between shells is resulting in an increase to the outer shell displacement. The difference is greatest when the inner shell is thin, at +46%, and smallest when the inner shell is thick, at +35%. In the diesel case, seen in Figure 4.27, the range is just slightly reduced, starting at +44% with a thin shell and decreasing to +30% with a thick shell. In the composite case, seen in Figure 4.28, the range is slightly increased, starting at +46% and decreasing to +35% with increasing shell thickness. In the steel-water-steel and steel-diesel-steel cases, the displacement decreases slightly as the outer shell is increased in thickness. In the composite case the displacement increased slightly as the outer shell increased in thickness.

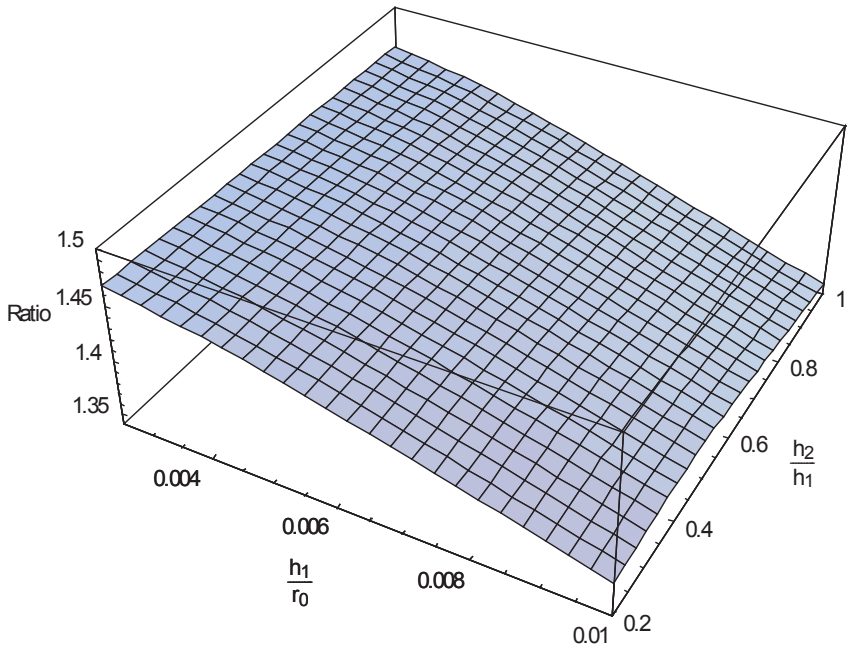

Figure 4.26: Outer Shell Normal Displacement Ratio of Steel-Water-Steel (a=0.9), to Steel-Water-Steel (a=0.5)

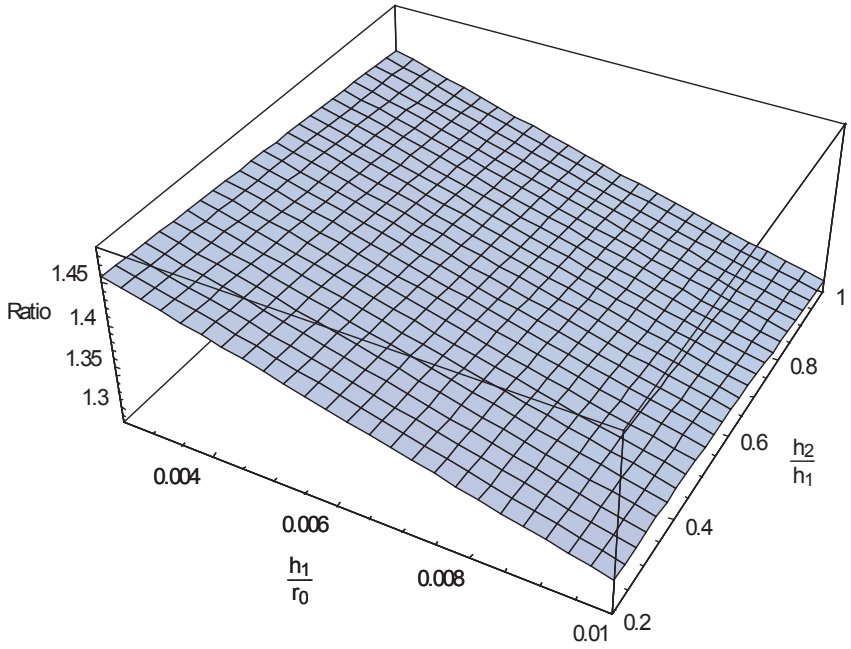

Figure 4.27: Outer Shell Normal Displacement Ratio of Steel-Diesel-Steel (a=0.9), to Steel-Diesel-Steel (a=0.5)

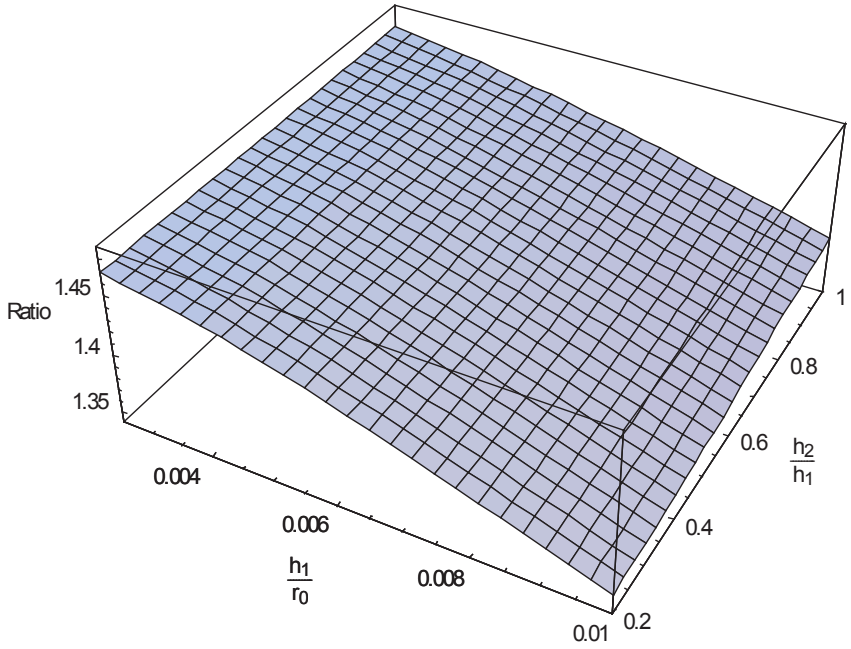

Figure 4.28: Outer Shell Normal Displacement Ratio of Steel-Water-Composite (a=0.9), to Steel-Water-Composite (a=0.5)

Chapter 5

Three-Dimensional vs. Two-Dimensional Models

In this section the stress differences between the three-dimensional results and previous, two-dimensional results are presented. This is done much the same way as the previous comparisons, with the three-dimensional results presented as a fraction of the corresponding two-dimensional results, which provides a measure of how well the two simulations match. As before, these comparisons were done for each variable set: steel-water-steel, steel-diesel-steel, and steel-water-composite, and also done for both large ($a = 0.5$) and small ($a = 0.9$) inter-hull spaces.

The visualization of the results gives an overall sense of where the simplifications cause the two models to diverge, which helps to justify the extra effort of doing a three-dimensional analysis. In all cases the two-dimensional values were higher than the three-dimensional values. If only rough approximations are needed, a two-dimensional study will get the results one needs. However, the differences between the these results and those of a three-dimensional simulations are quite varied, and often unpredictable. For some variable combinations the differences were small, within 10%, but for others they were notably larger, as much as 30%.

5.1 Steel Results

The first graph, Figure 5.1, shows the steel-water-steel results for the inner shell with $a = 0.5$, compared to the equivalent two-dimensional simulation. Here the three-dimensional results range between just under 74% and 83% of the two-dimensional results, averaging around 80%. The match is closest when the inner shell thickness is low and also when the inner shell thickness is high, the match worsens slightly when the inner shell thickness is at a moderate value. The differences between the two and three-dimensional simulations do not appear to be affected by the outer shell thickness in this case. As for the inner shell thickness, because of the up and down variation within the results it makes it difficult to say whether this affects the how close the two simulations match positively or negatively.

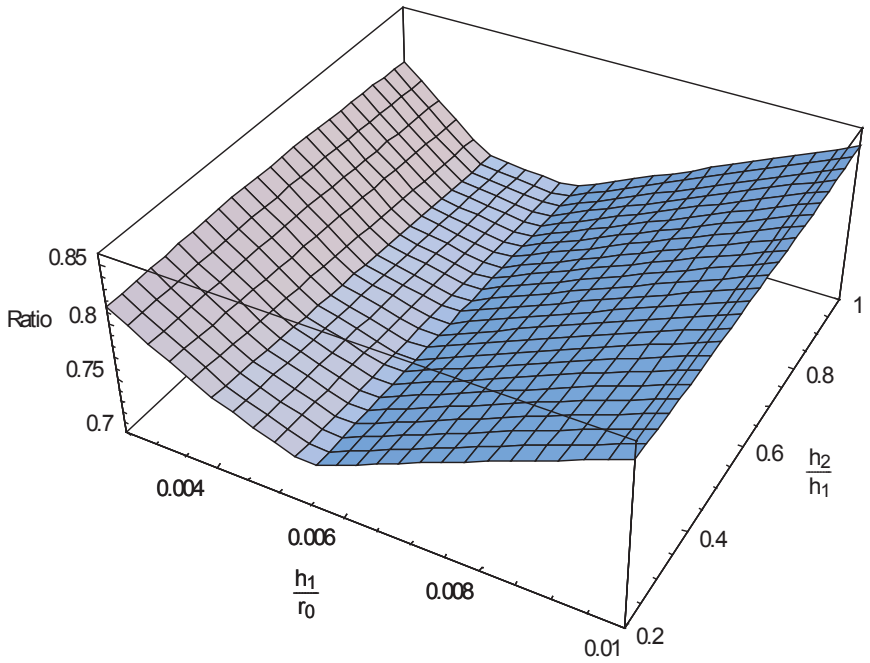

Figure 5.1: 3-D vs 2-D, Inner Shell, Steel-Water-Steel (a=0.5)

The second graph, Figure 5.2, shows the steel-water-steel results for the outer shell with $a = 0.5$, compared to the equivalent two-dimensional simulation. The three-dimensional values range between a low of 70% and a high of 77% relative to the two-dimensional results, averaging around 75%. The variations here show a somewhat different pattern for the inner shell during the same simulations. Like in the previous figure, as the inner shell thickness is increased the match between the simulations is initially high, worsens slightly, and then improves as the thickness approaches its maximum value. Again it is difficult to say whether the inner shell thickness directly affects the match between the two simulations. Unlike in the previous figure, however, the match does appear to be affected by the outer shell thickness, as it can be seen to both increase and decrease with it, depending on the particular inner shell thickness.

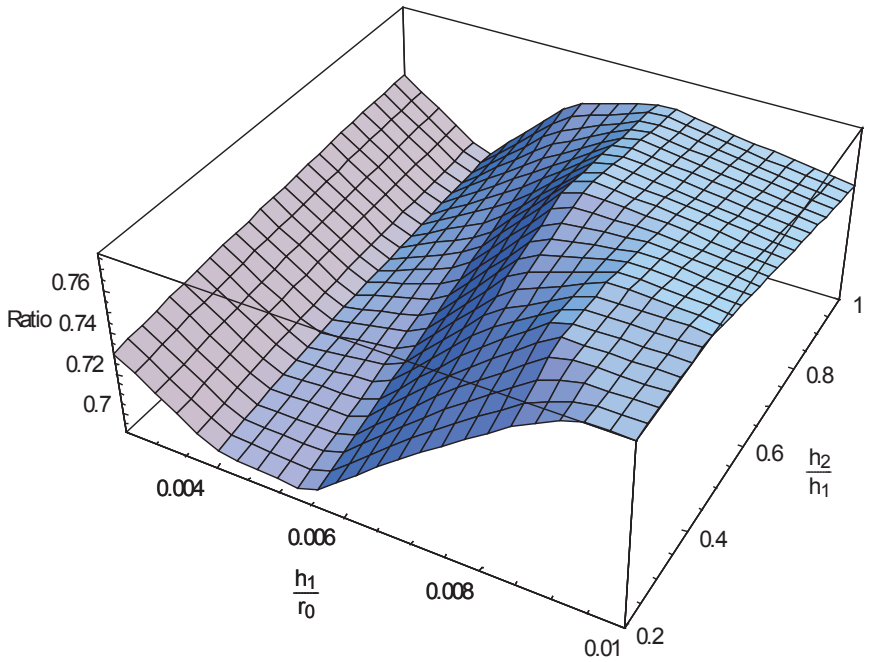

Figure 5.2: 3-D vs 2-D, Outer Shell, Steel-Water-Steel (a=0.5)

The third graph, Figure 5.3, shows the steel-water-steel results for the inner shell with $a = 0.9$, compared to the equivalent two-dimensional simulation. In this figure the match between the two simulations varies between 68% and 92%, with an average of about 80% and a clear downward trend as the shell thicknesses are increasing. The match seems primarily affected by the inner shell thickness, where there is a straightforward decline as the shell thickness is increased. Additionally, there is a slight decrease in the match as the outer shell thickness is increased, but the effect is not as notable for higher inner shell thicknesses.

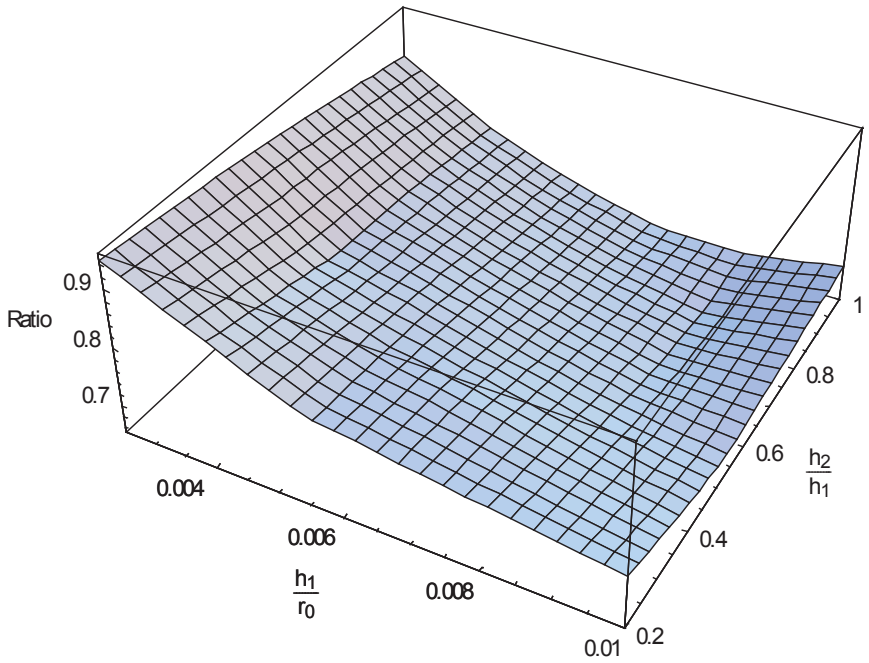

Figure 5.3: 3-D vs 2-D, Inner Shell, Steel-Water-Steel (a=0.9)

The fourth graph, Figure 5.4, shows the steel-water-steel results for the outer shell with $a = 0.9$, compared to the equivalent two-dimensional simulation. In this figure the values of the three-dimensional simulation relative to the two-dimensional can be seen to vary between a low of 72% and a high of 85%, with an average of about 80%. Where the inner shell shown in the previous figure had a clear pattern with respect to the shell thickness, for this one it is much less notable. As the inner shell is increased in thickness the results do not appear to thrend trend one way or the other, increasing at some points and decreasing at others. Additionally as the outer shell thickness is increased the match improves at most points, especially when the inner shell thickness is highest, but when the inner shell thicknesses is at a moderate value increasing the outer shell thickness has the opposite effect.

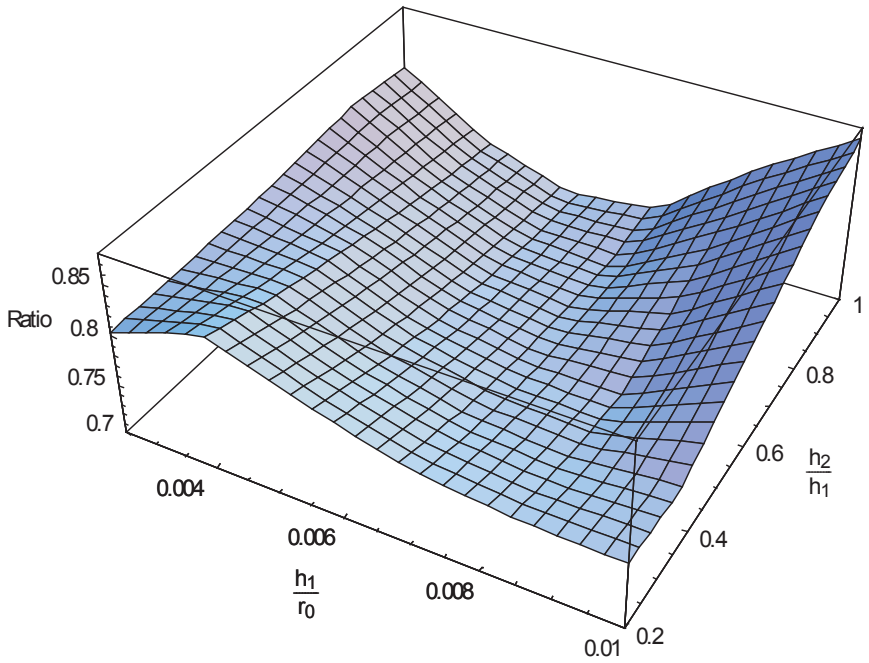

Figure 5.4: 3-D vs 2-D, Outer Shell, Steel-Water-Steel (a=0.9)

5.2 Diesel Results

The first graph, Figure 5.5, shows the steel-diesel-steel results for the inner shell with $a = 0.5$, compared to the equivalent two-dimensional simulation. Here the match between the two simulations ranges from a low of 75% to a high of 92%, with an average of about 82%. The trend is similar to the corresponding steel-water-steel case, seen in Figure 5.1, but here the match is slightly higher with a more definite upward trend. Like the steel case, as the inner shell thickness is increased there is an initial drop in the match, before it steadily begins to rise. However, because the drop is much smaller here and the upward trend more notable, it is possible to say that wit as the thickness of the inner shell is increased, the difference between the two-dimensional and three-dimensional results tends to decrease. Like the steel results, however, the outer shell thickness does not appear to play any significant role in how well the simulation values match.

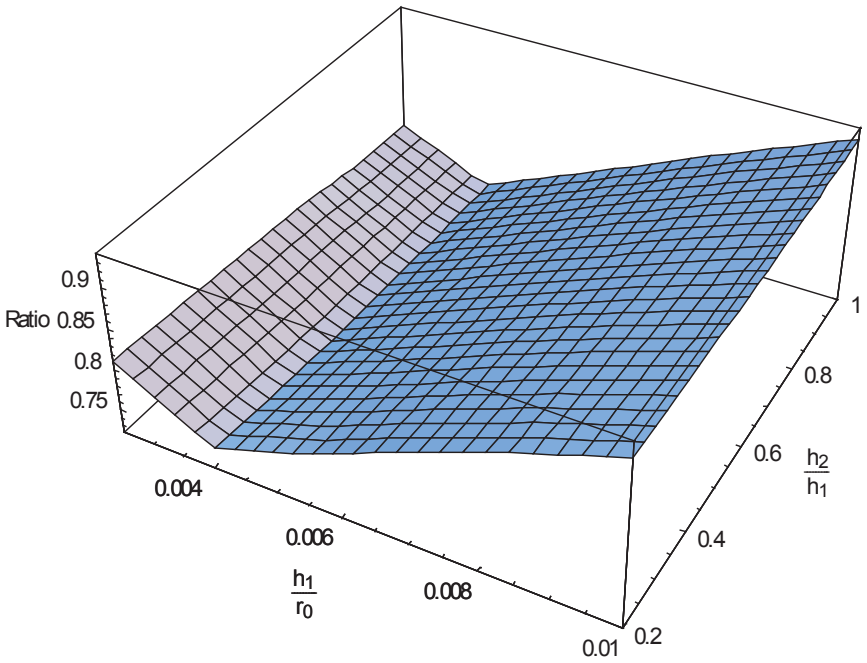

Figure 5.5: 3-D vs 2-D, Inner Shell, Steel-Diesel-Steel (a=0.5)

The second graph, Figure 5.6, shows the steel-diesel-steel results for the outer shell with $a = 0.5$, compared to the equivalent two-dimensional simulation. The match between the simulations here ranges from just under 70% to 80%, averaging around 75%. Like the previous figure, this one also bears strong similarities to the equivalent steel-water-steel case seen in Figure 5.2. At low inner shell thicknesses the match is low and even drops slightly as the thickness increases. As the inner shell thickness continues to increase, however, the match between simulations begins to improve, until it plateaus as both the inner and outer shell thicknesses approach their maximum values. Like the inner shell for this diesel case, aside from the initial fluctuations at low thicknesses, the match generally improves as the inner shell becomes thicker. Additionally, there are some variations with respect to the outer shell: at moderate inner shell thickness values, the match improves with outer shell thickness, but at the thickest values of the inner shell the match actually decreases as the outer shell thickness increases.

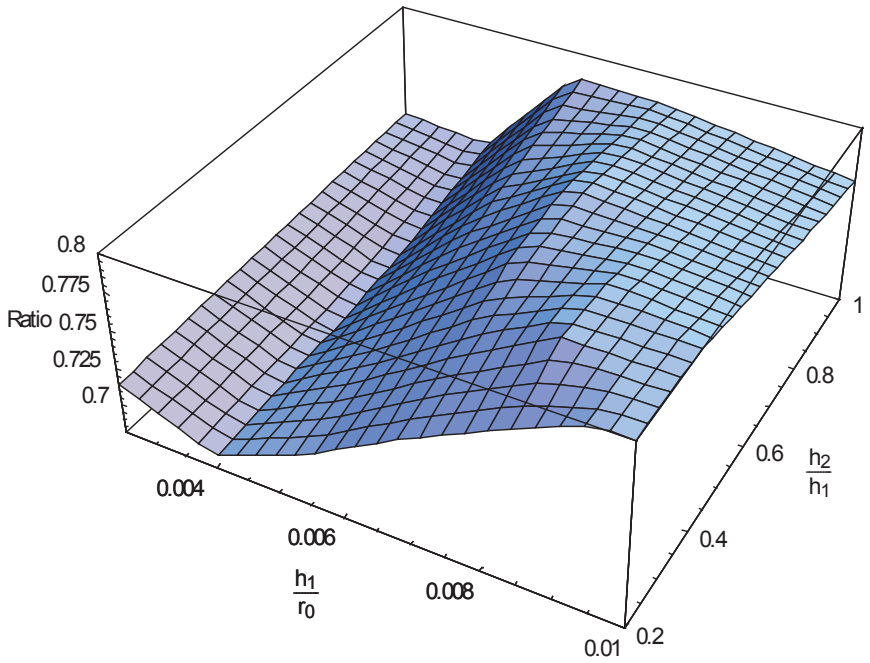

Figure 5.6: 3-D vs 2-D, Outer Shell, Steel-Diesel-Steel (a=0.5)

The third graph, Figure 5.7, shows the steel-diesel-steel results for the inner shell with $a = 0.9$, compared to the equivalent two-dimensional simulation. The three-dimensional values relative to the two-dimensional values range from 68% to 82%, with an average of about 75%. These values are at their highest point when both shells are thinnest, then reach a secondary peak when the shells are at their thickest, making it hard to isolate the effect of increasing the individual thicknesses. Increasing the thickness of the outer shell results in opposite effects depending on inner shell thickness, worsening the match when the inner shell is thin and improving it when it is thick. Like the other figures from the steel-diesel-steel case, this figure shows similarities to its steel-water-steel counterpart, shown in Figure 5.3. The steel-water-steel figure does not show significant improvement in the match at higher thicknesses, but it does follow much the same trend otherwise, so it is possible that the overall trend would be similar if the simulations were ran with higher thickness values.

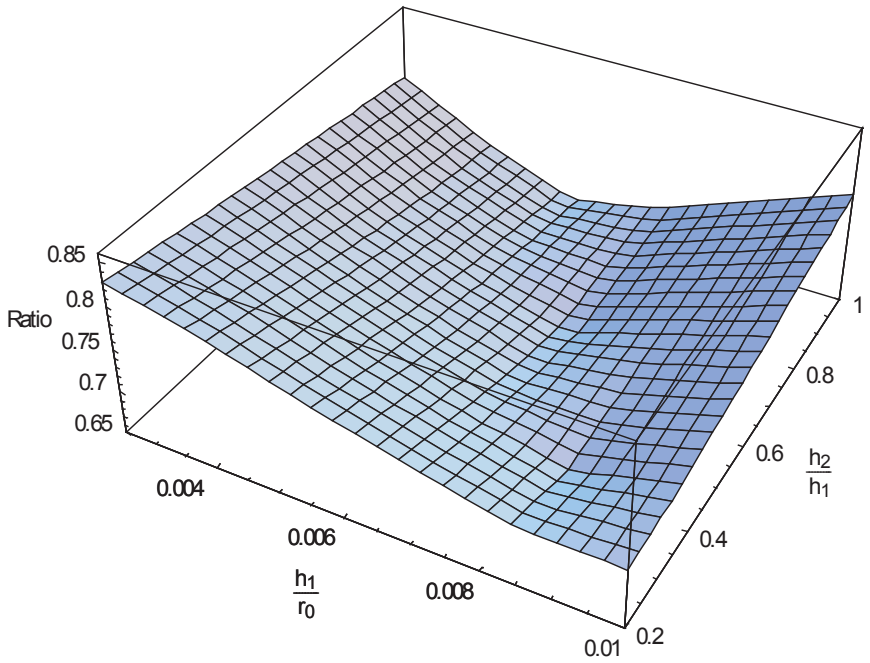

Figure 5.7: 3-D vs 2-D, Inner Shell, Steel-Diesel-Steel (a=0.9)

The fourth graph, Figure 5.8, shows the steel-diesel-steel results for the outer shell with $a = 0.9$, compared to the equivalent two-dimensional simulation. In this case the match between simulations ranges from a low of 77% to a high of 86%, averaging roughly 81%. Like its steel-water-steel counterpart seen in Figure 5.4, the graph shows the simulation match fluctuating without a definite pattern across the different thickness values. As with that case, increasing inner shell thickness does not appear to affect the match definitively. Increasing the other shell thickness, however, does tend to improve the match, most notably at higher inner shell thickness values, but the effect is less pronounced and even negative at lower thickness values.

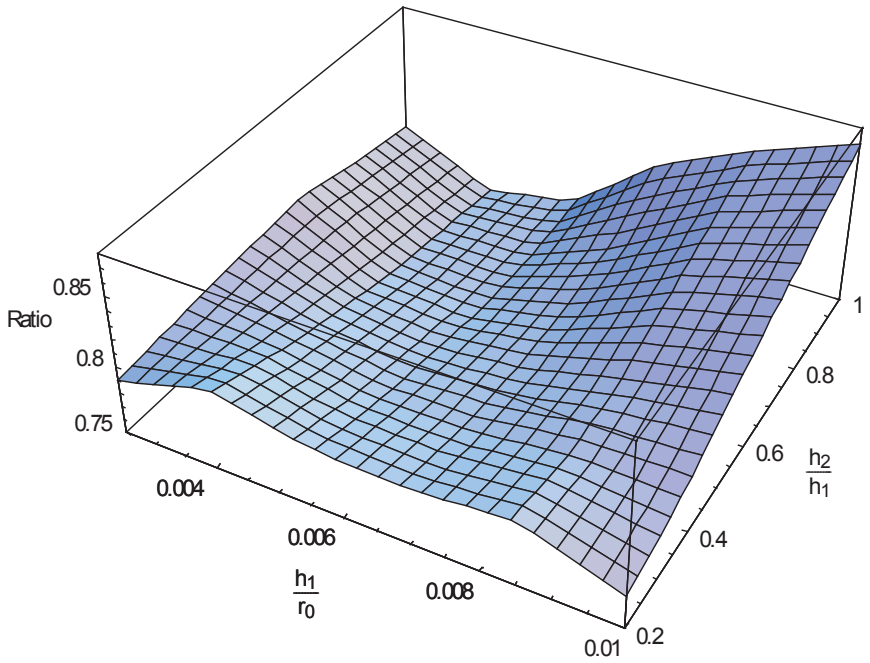

Figure 5.8: 3-D vs 2-D, Outer Shell, Steel-Diesel-Steel (a=0.9)

5.3 Composite Results

The first graph, Figure 5.9, shows the steel-water-composite results for the inner shell with $a = 0.5$, compared to the equivalent two-dimensional simulation. The graph here shows that the match between the two simulations ranges from a low of 74% to a high of 84%, with an average of about 79%. As with the corresponding steel-water-steel and steel-diesel-steel cases from Figures 5.1 and 5.5 respectively, the match here trends almost wholly with the inner shell thickness. As in those cases, the simulation match is high when the inner shell is thin and initially worsens as the shell increases in thickness. Like the other cases, the match eventually reaches a low point and the trend reverses itself, the match improving as the inner shell thickness approaches its maximum value.

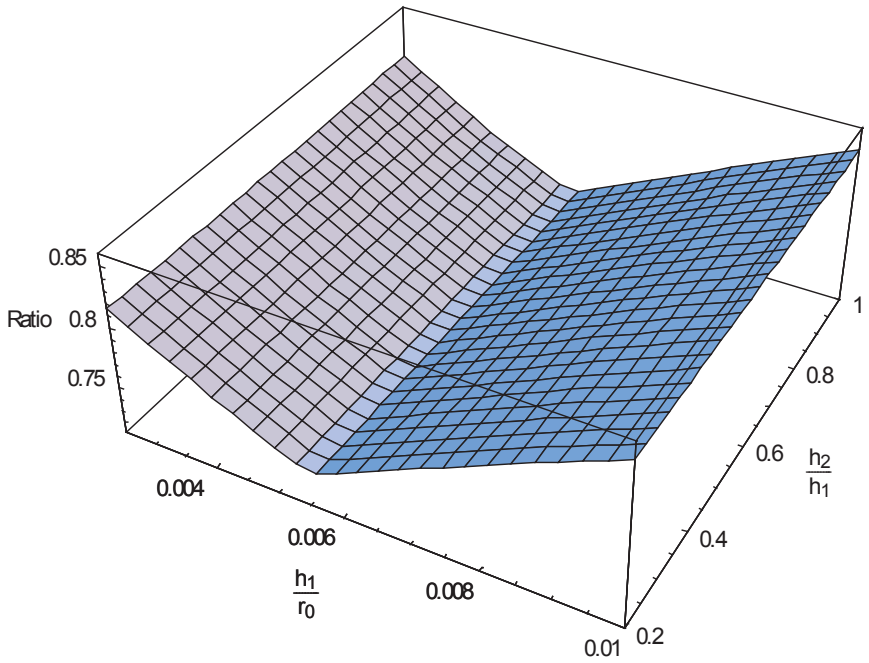

Figure 5.9: 3-D vs 2-D, Inner Shell, Steel-Water-Composite (a=0.5)

The second graph, Figure 5.10, shows the steel-water-composite results for the outer shell with $a = 0.5$, compared to the equivalent two-dimensional simulation. Here the three-dimensional results relative to the two-dimensional results have a low of 73% and a high of 81%. The results for this shell were essentially constant regardless of the shell thicknesses for both two-dimensional and three-dimensional simulations. The only notably different value was at the lowest inner shell thickness, which is shown here as the high match point. For all other thickness values of the inner shell, the match does not appear to appreciably change as the thicknesses increases. Additionally, increasing the outer shell thickness also appears to have a minimal effect on the match between the two simulations.

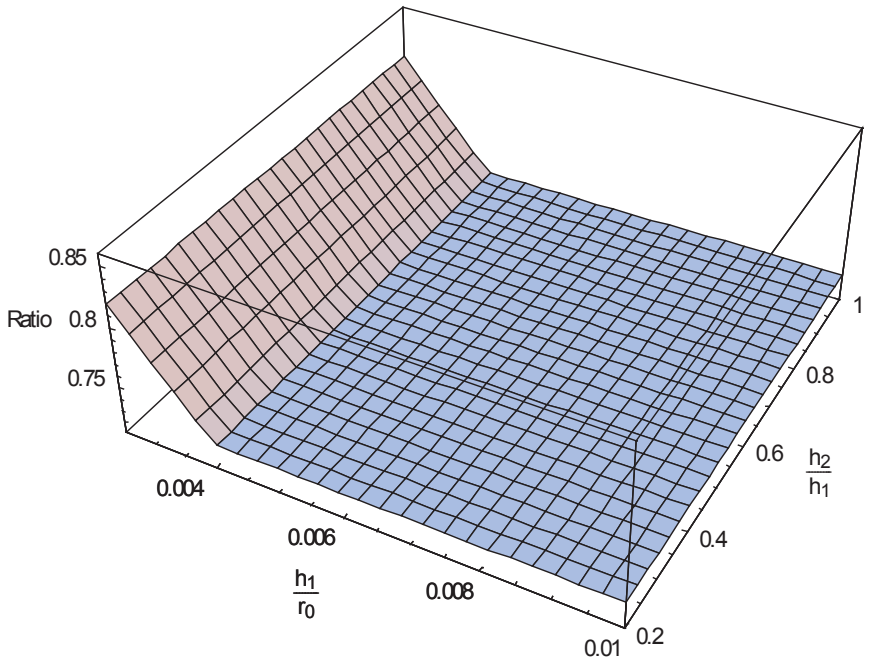

Figure 5.10: 3-D vs 2-D, Outer Shell, Steel-Water-Composite (a=0.5)

The third graph, Figure 5.11, shows the steel-water-composite results for the inner shell with $a = 0.9$, compared to the equivalent two-dimensional simulation. The three-dimensional values relative to the two-dimensional values range from a low of 75% to a high of 94%, the highest value between the two simulations, with an average match of about 85%. The trend here is clear, the match is best when the inner shell is thin and worsens as the inner shell thickness increases. If the overall trend is similar to what was seen in the steel-water-steel or steel-diesel-steel cases, Figure 5.3 and 5.7 respectively, there is probably lower limit to the match, as the slope at the highest inner shell thickness is starting to flatten out like the previous cases did.

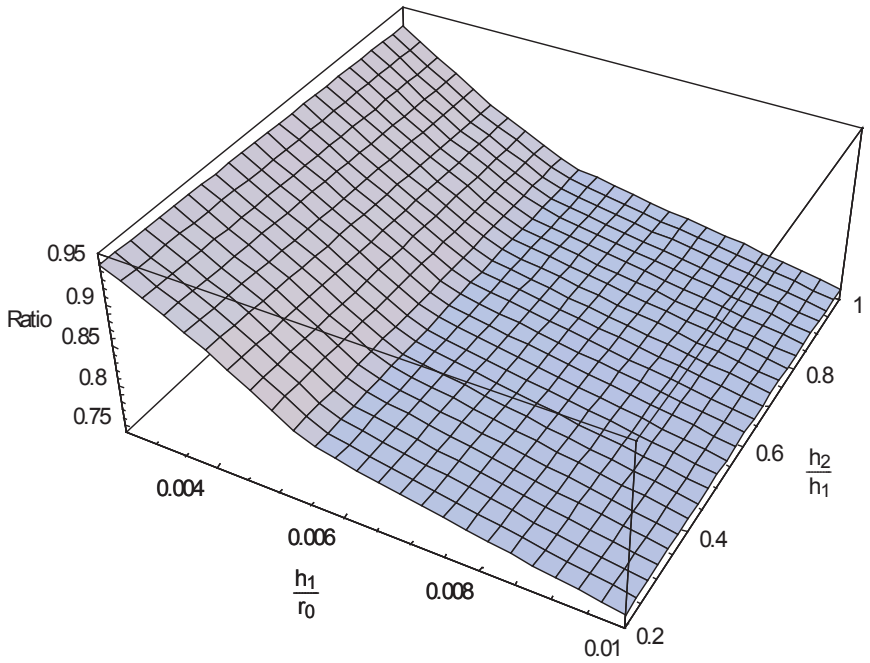

Figure 5.11: 3-D vs 2-D, Inner Shell, Steel-Water-Composite (a=0.9)

The fourth graph, Figure 5.12, shows the steel-water-composite results for the outer shell with $a = 0.9$, compared to the equivalent two-dimensional simulation. In this case the three-dimensional values relative to the two-dimensional values range from 77% to 83%, with an average of about 80%. Unlike the equivalent shell from the steel-water-steel and steel-diesel-steel cases, Figures 5.4 and 5.8 respectively, the results show a clear trend with respect to the inner shell thickness. The match between the two simulations is initially high when the inner shell is thinnest but worsens as the inner shell is increased in thickness, though the effect is not particularly large, the range of values on this graph being quite small. Additionally, the match between the three-dimensional and two-dimensional results does not appear to be notably affected by changes to the outer shell in this case; the graph indicating minimal changes in the match as the outer shell is increased in thickness.

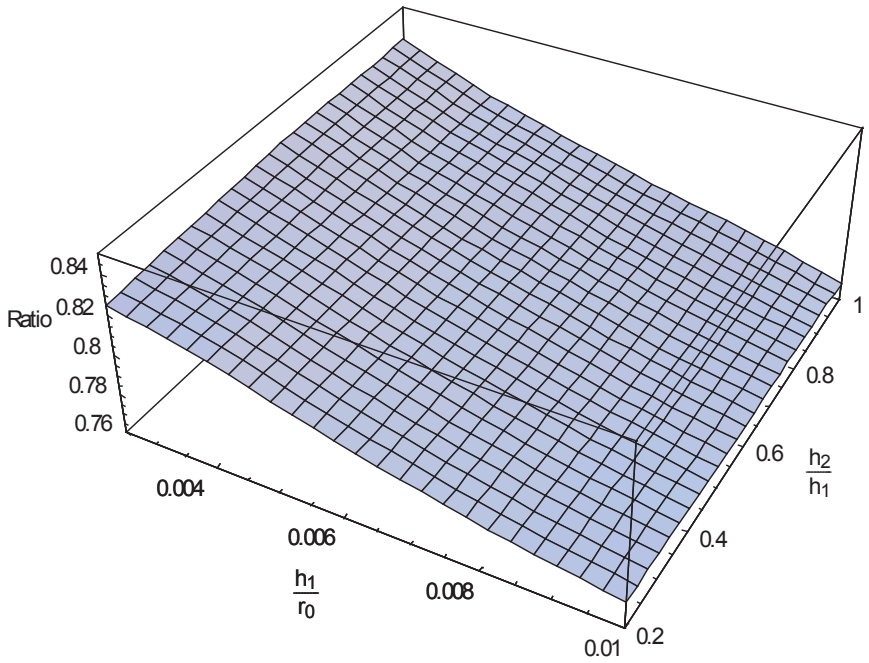

Figure 5.12: 3-D vs 2-D, Outer Shell, Steel-Water-Composite (a=0.9)

Chapter 6

Conclusions

The three-dimensional model of the twin-hulled, submerged, fluid-filled structure was able to simulate a variety of different conditions. While more computationally expensive than an equivalent two-dimensional simulation, the three-dimensional model had no problem with any of the variables considered. The results across all variable cases were consistent; the model behaved as expected given changing shell thicknesses, internal fluids, shell composition, and inter-hull space. The comparisons performed between the modified cases and the baseline models helped to isolate the individual effects that these variables had, and give some understanding to how they interact with each other.

Additionally, for all cases, the three-dimensional results match up well with those from equivalent two-dimensional simulations. All stress values were directly compared between the two models, with the differences between the two limited to a maximum of just over 30%. This value actually appeared to be a limit of sorts in many of the shell comparisons, as the match between three-dimensional and two-dimensional results approached this value multiple times before starting to improve as different variables were used.

The most notable contribution of this particular work to the established literature is the addition of a full three-dimensional workup, including results, of the twin-hulled version of the shell-shockwave problem. Additionally, as most of the previous literature focuses on a two-dimensional version of the problem, the addition of a direct comparison between these results, and equivalent two-dimensional results, is another important addition.

6.1 Parametric Analysis

For the parametric analysis, each case was first plotted against the shell thickness to create the first comparisons. The results here are consistent across all cases. Maximum stress and normal displacement greatly decrease for both internal and external shells when the internal shell thickness is increased. Additionally, for steel-water-steel and steel-diesel-steel cases, the stresses and normal displacements slightly decrease as the external shell thicknesses are increased. This isnt true for the steel-water-composite cases, however, which see very small changes as the external shell thickness is increased.

The first variable that was examined on its own was the internal fluid, the change in this case was the replacement of water as the inner shell fluid with diesel, a lighter, less dense fluid that is more limiting to sound. Slight increases in the stress and normal displacements across both the inner and outer shells for the majority of the variable combinations were observed, consistent with the use of a lighter fluid that absorbs less energy. The displacement changes were fairly minor, most limited to within 5% or so. Much more notable were two very big differences in the stress responses. When the spacing between the inner and outer shell was large, the change in internal fluid resulted in an increase of the external shell stress of between 10% to 18%. This fits with the lighter diesel fuel absorbing less of the incoming energy, but in this case also providing less support to the external shell. The other notable stress response was the internal shell when the inter-hull space was greatly reduced. In this case the inner shell response varied both positively and negatively with shell thickness, from -10% when the shells were thin to +11% when the shells were thick. Here the role of the diesel alternated, possibly damping the stress due to it occurring as a result of wave superposition in some cases, while failing to absorb as much of the impact in others.

The second variable analysed was the material composition of the outer shell, the change in this case replacing the steel outer shell with a much lighter shell made from a carbon composite material. The differences between the two models were quite predictable and consistent across geometries and thicknesses, with the outer shell essentially offering less protection and absorbing less of the incoming energy. The inner shell stresses and normal displacements increased in all cases, with the

stress and displacement increases peaking at around 10% and 15% when the inter-hull space was large to around 30% and 22% when the inter-hull space was small. These increases were, predictably, largest when the external shell in each model was thickest. The fact that the results for the small inter-hull model were larger makes sense, considering the external shell is likely playing a bigger role in the interaction when the distance between the two is so small. External shell behavior was quite different than what had been seen previously, but make sense given the change in material. The stress observed in the outer shell of the composite model was essentially an order of magnitude lower than that observed in the steel, with decreases in the range of -90% to -80% in both the large and small inter-hull space geometries. The normal displacements of the composite shells were also largely the same across both geometries, with only a slight increase when the shells are closer together. In both cases, the difference in displacements gets larger as the external shell is considered to be thicker.

The third variable analysed was the effect of the change to the inter-hull geometry, which was done by comparing each small inter-hull model to its corresponding large inter-hull model which act as the baselines. The results from these comparisons indicated that each stress and normal displacement configuration has its own pattern with respect to shell thickness, with few similarities across shells. What was common, however, was that each case, steel-water-steel, steel-diesel-steel, and steel-composite-steel affected each trend in generally the same way. For all stresses and normal displacements, shrinking the space between shells resulted in an increase in both stresses and normal displacements. The steel-water-steel case acted as the moderate case and indicated the initial trend. Each steel-diesel-steel graph had slightly reduced relative values across all thicknesses compared to the steel-water-steel case, and the steel-water-composite cases would give slightly higher values, with few exceptions.

6.2 Three-Dimensional vs Two-Dimensional Comparisons

The three-dimensional and two-dimensional models were compared by taking the maximum stress results for each shell in the three-dimensional results and dividing it by the corresponding result from a two-dimensional model that used the same variables. The two-dimensional model used the same setup, but with mathematical simplifications to consider the problem as only a cross section, rather than as a cylinder. All of the values for the three-dimensional study were lower than those of the two-dimensional values, but within about 30% for all values. How well the results matched between the two models varied somewhat unpredictably with shell thickness, but were consistent across shells for each of the variable cases. Different patterns emerged for each shell, some having trends with shell thickness and across different cases, with others being harder to decipher.

The inner shell stresses for the large inter-hull cases all followed a similar pattern with respect to the inner shell thickness. How well the two models match would initially decrease as shell thickness was increased, before reaching a low point and the trend reversing. Thus, in general, with the exception of low values for inner shell thickness, the two model values match better the thicker the inner shell is. The low point, however, shifts within each variable case, with the steel-diesel-steel low point being closer to the thinnest values than the other two cases, and thus better matching the two-dimensional model at moderate to high inner shell thicknesses. The overall ranges for this shell have high points between 85% to 90% and lows of about 72%, with averages around 80%, indicating that the three-dimensional results, on average, have a decent match to the two-dimensional results, but with a higher variance.

The outer shell stresses for the large inter-hull cases show similar patterns in the steel-water-steel and steel-diesel-steel cases, and a slightly different pattern for the steel-water-composite case. All three show a comparatively low match between the three-dimensional results and the two-dimensional results at all thickness values, ranging between 70% and 80% in each case, with average values of about 75%. The steel-water-steel and steel-diesel-steel cases vary more with respect to thickness and do not follow any definite trend with respect to shell thicknesses. The steel-water-composite case, however, shows a pattern similar to what was seen in the stress for that shell, with a maximum at the lowest shell thickness, and minimal change at other

thickness values. Overall, the three-dimensional values for the outer shell stresses when the inter-hull space is large just do not match as well to the two-dimensional values as some of the other shells do, but show less overall variance.

The inner shell stresses for the small inter-hull cases show very similar patterns in each case. In these cases, the three-dimensional and two-dimensional results are more similar at low thickness values, but the match worsens as the shells are increased in thickness. The steel-water-steel and steel-water-composite cases show the highest variance, with the match between the two models varying from over 90% when the inner shells are thin to between 70% and 75% when the shells are thick, with averages between 80% and 85%. The steel-diesel-steel case does not vary as much, and shows some improvement in the match as the shells approach their thickest values. The match in this case varies between a high of just over 80% to a low of 70%, averaging about 75%. Overall, the three-dimensional values for this shell tend to be further from the corresponding two-dimensional values the higher the shell thicknesses that are considered, and tend to have more overall variance.

The outer shell stresses for the small inter-hull cases show similar patterns in the steel-water-steel and steel-diesel steel cases. with a very different pattern for the steel-water-composite case. The overall match between the three-dimensional results and the corresponding two-dimensional results averages to be around 80% in each of these cases, ranging between 85% and 75%, depending on the shell thicknesses. The first two cases, steel-water-steel and steel-diesel-steel do not show any particular trend with respect to shell thickness, while the third case, steel-water-composite, shows a decline in the match between the three and two-dimensional model as the inner shell thickness increases. These results suggest that the overall variance in the difference between the three and two-dimensional results for this shell is smaller, and the average match is decent, so while it may be difficult to predict, it doesn't vary as much as some of the others do with respect to shell thicknesses.

6.3 Summary of Results

A brief summary of the results is as follows:

- Parametric Analysis
  - Shell Thickness
    - Increased inner shell thickness reduced stress and normal displacements on both shells
    - Increased outer shell thickness slightly reduced stress and normal displacements on both shells in steel and diesel cases
    - Composite case did not see this stress reduction as a result of increased outer shell thickness
  - Diesel Internal Fluid
    - Inner shell sees both increases and decreases in stress, dependant on shell thickness when the internal fluid is changed
    - Inner shell normal displacement is changed minimally
    - Outer shell stress and normal displacement increase, more when the inter-hull space is large
  - Composite External Shell
    - Internal stress and normal displacements increase
    - Increased external shell thickness no longer causes decrease in stress and normal displacements
    - External shell stress is an order of magnitude lower than steel cases
    - External shell normal displacement is greater than steel case, especially at thicker shell values

  - Decreased Inter-hull Space
    * Inner shell stress in steel and diesel cases see both increases and decreases at different shell thicknesses
    * Inner shell stress in composite case increases
    * Inner shell normal displacements increase
    * Outer shell stresses greatly increase at lower shell thicknesses, and slightly increase at high shell thicknesses
    * Outer shell normal displacements increase, more at lower shell thicknesses

- Two-Dimensional Comparisons
  - Shells had similar patterns of how well the two-dimensional and three-dimensional results agreed
  - Three-dimensional results always lower than two-dimensional results, with a lower limit of about 70%
  - Inner shell stress saw wider ranges of difference between the two shells, dependant on shell thicknesses
  - Outer shell stress had smaller ranges of difference than inner shells; difference, on average, greater than inner shell
  - Outer shell stress did not trend in any particular way with increased shell thicknesses

6.4 Future Work

Having completed the parametric analysis, there is still work to do with the three-dimensional model. This analysis successfully provided a wide range of three-dimensional results for multiple variables, but, for the most part, avoided going into greater detail with any variable besides shell thickness.

If further analyses are performed, a narrower focus on individual variables would be one way to proceed. From a design standpoint, the material composition of the shells seems a likely variable to explore in greater detail. Given the model is meant to simulate a submarine, it would be appropriate to consider a cross section of different materials used in marine construction as potential shell materials. Alternatively, using real materials as a guideline, fictitious materials could be used to better highlight the overall trends in behaviour as different qualities, such as density, are varied incrementally.

Another variable that could easily be examined in greater detail is the shell spacing. Here, two different shell geometries were considered as part of the parametric analysis, but it would be entirely possible to examine the shell spacing in much more gradual increments to see if any particular patterns of behavior emerge. The need to compute response functions for each geometry mean that extremely fine variations in spacing wouldnt be a desirable approach, but an analysis using a modest number of different geometries is possible.

A final consideration for future work would involve the way that the different cases are examined. For this study, in order to easily compare the many different cases, the different variables were analyzed according to their effect on the maximum stress and normal displacement of each shell. However, the effect each variable had on the timings and locations of these maxima could be an important consideration from a design standpoint. This would most easily be done when the focus is on individual variable effects, rather than as part of a study involving a wide variety of variables.

Bibliography

[1] Ahyi, A. C., Pernod, P., Gatti, O., Latard, V., Merlen, A., Uberall, H., 1998. Experimental demonstration of the pseudo-Rayleigh (A_0) wave. Journal of the Acoustical Society of America 104, 2727-2732.

[2] Ahyi, A. C., Cao, H., Raju, P. K., Uberall, H., 2005. Re-radiation of acoustic waves from the A_0 wave on a submerged ealstic shell. Journal of the Acoustical Society of America 118, 124-128.

[3] Bryson, A.E., Gross, R.W.F., 1961. Diffraction of strong shocks by cones, cylinders, and spheres. Journal of Fluid Mechanics 10, 1-16.

[4] Carrier, G.F., 1951. The interaction of an acoustic wave and an elastic cylindrical shell. Technical Report No. 4, Brown University, USA.

[5] Chambers, G., Sandusky, H., Zerilli, F., Rye, K., Tussing, R., Forbes, J., 2001. Pressure measurements on a deforming surface in response to an underwater explosion in a water-filled aluminum tube. Shock and Vibration 8, 1-7.

[6] Cole, R.H, 1948. Underwater Explosions. Dover Publications, New York.

[7] Derbesse, L., Pernod, P., Latard, V., Merlen, A., Decultot, D., Touraine, N., Maze, G., 2000. Acoutsic scattering from complex elastic shells: visualization of S_0, A_0 and A waves. Ultrasonics 38, 860-863.

[8] Drikakis, D., Ofengeim, D., Timofeev, E., Voionovich, P., 1997. Computation of non-stationary shock-wave/cylinder interaction using adaptive-grid methods. Journal of Fluids and Structures 11, 665-691.

[9] Eidelman, S., Yang, X., Lottatl, I., 1993. Numerical simulation of shock wave reflection and diffraction in a dusty gas. Proceedings of the 19th International Symposium on Shock Waves, Marseille, France, pp. 56-60.

[10] Forrestal, M.J., 1968. Response of an elastic cylindrical shell to a transverse, acoustic pulse. Journal of Applied Mechanics 35, 129-141.

[11] Geers, T. L., 1969. Excitation of an elastic cylindrical shell by a transient acoustic wave. Journal of Applied Mechanics 36, 459-469.

[12] Geers, T.L., 1971. Residual potential and approximate methods for three-dimensional fluid-structure interaction problems. Journal of the Acoustical Society of America 49, 1505-1510.

[13] Geers, T.L., 1974. Shock response analysis of submerged structures. Shock and Vibration Bulletin 44, supp. 3, pp. 17-32.

[14] Geers, T.L., 1978. Doubly asymptotic approximations for transient motions of submerged structures. Journal of the Acoustical Society of America 64, 1500-1508.

[15] Geers, T.L., Zhang, P., 1994a. Doubly asymptotic approximations for submerged structures with internal fluid volumes: formulation. Journal of Applied Mechanics 61, 893-899.

[16] Geers, T.L., Zhang, P., 1994b. Doubly asymptotic approximations for submerged structures with internal fluid volumes: evaluation. Journal of Applied Mechanics 61, 900-906.

[17] Gitterman, Y. and Shapira, A., 2000. Audio-visual and hydroacoustic observations of the Dead Sea calibration experiment. Proceedings of the 22nd Annual DOD/DOE Seismic Research Symposium: Planning for Verification of and Compliance with the Comprehensive Nuclear-Test-Ban Treaty.

[18] Glass, I.I., Kaca, J., Zhang, D.L., Glaz, H.M., Bell, J.B., Trangenstein, J.A., Collins, J.P., 1989. Diffraction of planar shock waves over half-diamond and semicircular cylinders: an experimental and numerical comparison. Proceedings of the 17th International Symposium on Shock Waves and Shock Tubes, Bethlehem, Pennsylvania, USA, pp. 246-251.

[19] Haywood, J. H., 1958. Response of an elastic cylindrical shell to a pressure pulse. Quarterly Journal of Mechanics and Applied Mathematics 11, 129-141.

[20] Heilig, G., 1999. Shock-induced flow past cylinders with various radii. Proceedings of the 22nd International Symposium on Shock Waves, Imperial College, London, UK, 1099-1104.

[21] Heilig, W., 1987. The influence of wall- and shock curvature on shock reflection processes. Proceedings of the 16th International Symposium on Shock Tubes and Wave, Aachen, Germany, pp. 543-549.

[22] Hermann, D., Weblau, F.P., Adomeit, G., 1987. Measurements of heat transfer and vortex shedding frequency of cylinders in shock tube cross flow. Proceedings of the 16th International Symposium on Shock Tubes and Waves, Aachen, Germany, pp. 822-830.

[23] Huang, H., 1970. An exact analysis of the transient interaction of acoustic plane waves with a cylindrical elastic shell. Journal of Applied Mechanics 37, 1091-1099.

[24] Huang, H. and Wang, Y. F., 1970. Transient interaction of spherical acoustic waves and a cylindrical elastic shell. Journal of the Acoustical Society of America 48, 228-235.

[25] Huang, H., Wang, Y.F., 1971. Early-times interaction of spherical acoustical waves and a cylindrical elastic shell. Journal of the Acoustical Society of America 50, 885-891.

[26] Huang, H., 1975. Scattering of spherical pressure pulses by a hard cylinder. Journal of the Acoustical Society of America 58, 310-317.

[27] Huang, H., 1979a. Transient response of two fluid-coupled cylindrical elastic shells to an incident pressure pulse. Journal of Applied Mechanics 46, 513-518.

[28] Huang, H., 1979b. Transient response of two fluid-coupled sphercal elastic shells to an incident pressure pulse. Journal of the Acoustical Society of America 65, 881-887.

[29] Iakovlev, S., 2002. Interaction of a spherical shock wave and a submerged fluid-filled circular cylindrical shell. Journal of Sound and Vibration 225, 615-633.

[30] Iakovlev, S., 2004. Influence of a rigid co-axial core on the stress-strain state of a submerged fluid-filled circular cylindrical shell subjected to a shock wave. Journal of Fluids and Structures 19, 957-984.

[31] Iakovlev, S., 2006. External shock loading on a submerged fluid-filled cylindrical shell. Journal of Fluids and Structures 22, 997-1028.

[32] Iakovlev, S., 2007. Submerged fluid-filled cylindrical shell subjected to a shock wave: fluid-structure interaction effects. Journal of Fluids and Structures 23, 117-142.

[33] Iakovlev, S., 2008a. Interaction between a submerged evacuated cylindrical shell and a shock wave. Part I: Diffraction-radiation analysis. Journal of Fluids and Structures 24, 1077-1097.

[34] Iakovlev, S., 2008b. Interaction between a submerged evacuated cylindrical shell and a shock wave. Part II: Numerical aspects of the solution. Journal of Fluids and Structures 24, 1098-1119.

[35] Iakovlev, S., 2009. Interaction between an external shock wave and a cylindrical shell filled with and submerged into different fluids. Journal of Sound and Vibration 322, 401-437.

[36] Iakovlev, S., Gaudet, J., Dooley, G. MacDonald, B., 2010. Hydrodynamic fields induced by the shock response of a fluid-filled submerged cylindrical shell containing a rigid co-axial core. Journal of Sound and Vibration 329, 3359-3381.

[37] Iakovlev, S., Santos, H.A.F.A., Williston, K., Murray, R., Mitchell, M., 2013. Non-stationary radiation by a cylindrical shell: numerical modeling using the Reissner-Mindlin theory. Journal of Fluids and Structures 36, 50-69.

[38] Iakovlev, S., Furey, C., Pyke, D., Lefieux, A., 2015. Shock response of a system of two submerged co-axial cylindrical shells coupled by the inter-shell fluid. Journal of Fluids and Structures. Pending publication. http://dx.doi.org/10.1016/j.jfluidstructs.2014.12.011

[39] Jappinen, T. and Vehvilainen, K., 2006. Extreme littoral UNDEX - explosions under ice. Proceedings of the 77th Shock and Vibration Symposium, Monterey, USA.

[40] Jialing, L., Hongli, N., 1997. Study on propagation of blast wave over cylinder in a channel bend. Proceedings of the 21st International Symposium on Shock Waves, Great Keppel Island, Australia, pp. 104-107.

[41] Junger, M.C. and Feit, D., 1972. Sound, structures, and their interaction. MIT Press, Cambridge, USA.

[42] Lax, J.A., Sette, W.J., and Gooding, R.C., 1953. Additional calculations on the response of a uniform cylindrical shell to a pressure pulse. 6th Conference on Progress in Underwater Exxplosions Research. Report 155-1.

[43] Love, A.E.H., 1927. A Treatise on the Mathematical Theory of Elasticity. Cambridge University Press, Cambridge, London.

[44] Mair, H.U., 1999a. Review: Hydrocodes for structural response to underwater explosions. Shock and Vibration 6, 81-96.

[45] Mair, H.U. 1999b. Benchmarks for submerged structure response to underwater explosion. Shock and Vibration 6, 169-181.

[46] Mindlin, R. D. and Bleich, H. H., 1953. Response of an elastic cylindrical shell to a transverse step shock wave. Journal of Applied Mechanics 20, 189-195.

[47] Murray, W.W., 1955. Interaction of a spherical acoustic wave with a beam of circular cross section. Underwater Explosion Research Division Report I-55, Norfolk Naval Shipyard, Portsmouth, Virginia, USA.

[48] Oakley, J.G., Puranik, B. P., Anderson, M. H., Peterson, R. R., Bonazza, R., Weaver, R. P., and Gittings, M. L., 1999. An investigation of shock-cylinder interaction. Proceedings of the 22nd International Symposium on Shock Waves, Imperial College, London, UK, 941-946.

[49] Oakley, J.G., Anderson, M.H., Wang, S. Bonazza, R., 2001. Shock loading of a cylinder bank with imaging and pressure measurements. Proceedings of the 23rd International Symposium on Shock Waves, Fort Worth, Texas, USA, pp. 589-595.

[50] Ofengeim, D., Drikakis, D., 1997. Simulation of blast wave propagation over a cylinder. Shock Waves 7, 205-317.

[51] Payton, R.G., 1960. Transient interaction of an acoustic wave with a circular cylindrical elastic shell. Journal of the Acoustical Society of America 32, 722-729.

[52] Peralta, L.A., Raynor, S., 1964. Initial response of a fluid-filled elastic, circular, cylindrical shell to a shock wave in acoustic medium. Journal of the Acoustical Society of America 36, 476-488.

[53] Sandusky, H., Chambers, P., Zerilli, F., Fabini, L., Gottwald, W., 1999. Dynamic measurements of plastic deformation in a water-filled aluminum tube in response to detonation of a small explosives charge. Shock and Vibration 6, 125-132.

[54] Sigrist, J.-F., Broc, D., and Laine, C., 2007. Fluid-structure interaction effects modeling for the modal analysis of a nuclear pressure vessel. Journal of Pressure Vessel Technology 129, 1-6.

[55] Stultz, K.G.Jr., Atkatsh, R. S., Chan, K. K., 1994. Single hull versus double hull design shock response of underwater vessels. Proceedings of the 65th Shock and Vibration Symposium, San Diego, CA, October 31 November 3, 1994, pp. 209-218.

[56] Sugiyama, H., Arai, T., Nagumo, H. Sueki, H., Izumi, M., Takayama, K. 1989. An experimental and numerical study of the shock wave-induced flows past a circular cylinder in a dusty-gas shock tube. Proceedings from the 17th International Symposium on Shock Waves and Shock Tubes, Bethlehem, Pennsylvania, USA, pp. 258-263.

[57] Sun, M., 1998. Numerical and experimental studies of shock wave interaction with bodies. Ph.D. Thesis, Tohoku University, Japan.

[58] Takano, Y. Hayashi, K., and Goto, T., 1997. A computational procedure for interactions of shock waves with solid materials in liquid. Proceedings of the 21st International Symposium on Shock Waves, Great Keppel Island, Australia, pp. 1039-1044.

[59] Tukayama, K., 1987. Holographic interferometric study of shock wave propagation in two-phase media. Proceedings of the 16th International Symposium on Shock Tubes and Waves, Aachen, Germany, pp. 52-62.

[60] Takayama, K., 1993. Optical flow visualization of shock wave phenomena (Paul Vieille Memorial Lecture). Proceedings of the 19th International Symposium on Shock Waves, Marseille, France, pp. 8-16.

[61] Wardlaw, A.B., Jr. and Luton, J. A., 2000. Fluid-structure interaction mechanisms for close-in explosions. Shock and Vibration 7, 265-275.

[62] Yang, J.Y., 1985. Computation of nonstationary shock wave diffraction from curved surfaces. Proceedings of the 15th International Symposium on Shock Waves and Shock Tubes, Berkeley, California, USA, pp. 399-405.

[63] Yang, J.Y., Liu, Y., 1987. Computation of shock wave reflection by circular cylinders. AIAA Journal 25, 683-689.